INTERACTIONS BETWEEN COLLOIDAL PARTICLES AND SOLUBLE POLYMERS

H. J. Ploehn and
W. B. Russel

Department of Chemical Engineering
Princeton University
Princeton, New Jersey 08544

I. Introduction

Interactions between soluble polymer and colloidal particles control the behavior of a large number of chemical products and processes and, hence, their technological viability. These dispersions have also attracted considerable scientific interest because of their complex thermodynamic and dynamical behavior—stimulated by the synthesis of novel polymers, improved optical and scattering techniques for characterization, and a predictive capability emerging from sophisticated statistical mechanical theories. Thus, the area is active both industrially and academically as evidenced by the patent literature and the frequency of technical conferences.

Polymers in colloidal systems function in a variety of ways depending on their molecular structure and concentration, the nature of the solvent, and the characteristics of the particles. Three primary types of situations exist for *homopolymers*:

(1) *Adsorption.* When each segment can adsorb reversibly onto a particle with energy comparable to kT, the chain assumes a configuration (Fig. 1b) quite different from the random coil in bulk solution (Fig. 1a). At equilibrium, bound and free segments rapidly interchange within the adsorbed chains, but bound and free chains exchange much more slowly.

(2) *Depletion.* Without adsorption the chain receives no compensation for the configurational degrees of freedom lost in approaching the surface. Hence, the center of mass generally remains a coil radius away from the surface, and the segment density at the surface falls below that in the bulk solution (Fig. 1c).

ADVANCES IN CHEMICAL ENGINEERING, VOL. 15

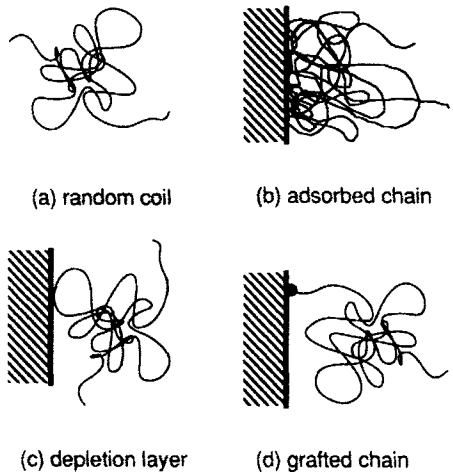

FIG. 1. Conformation of homopolymer chains in solution: (a) Bulk solution; (b) adsorbing; (c) nonadsorbing; (d) terminally anchored.

(3) *Grafting.* A chain which does not adsorb can be tethered to the surface by one end, e.g., through a chemical reaction. The rest of the molecule then extends toward the bulk solution (Fig. 1d).

The widespread development of copolymers provides several interesting combinations of these modes of interaction:

(1) *Random copolymers* composed of strongly adsorbing and nonadsorbing groups assume different configurations than adsorbing homopolymers, e.g., with the size of loops determined by the distance between adsorbing groups rather than the balance between configurational and enthalpic contributions to the free energy (Fig. 2a). Most modern polymeric flocculants have such structures (Rose and St. John, 1985).

(2) *Diblock copolymers* consisting of soluble and insoluble parts (Fig. 2b) act much as grafted chains once they are adsorbed on the surface. However, the thermodynamics of the initial solution, consisting primarily of micelles, and the conformation of the insoluble blocks on the surface affect the coverage in ways not well understood (e.g., Munch and Gast, 1988; Marques *et al.*, 1988; Gast, 1989). Many dispersants or polymeric surfactants are synthesized in this way (Reiss *et al.*, 1987).

(3) Grafting hydrophobic groups onto the ends of water soluble chains forms *triblock copolymers*, which associate to form a gel in solution and adsorb reversibly onto hydrophobic portions of particle surfaces (Fig. 2c). Molecules of this sort, carefully tailored to balance the hydrophobic and

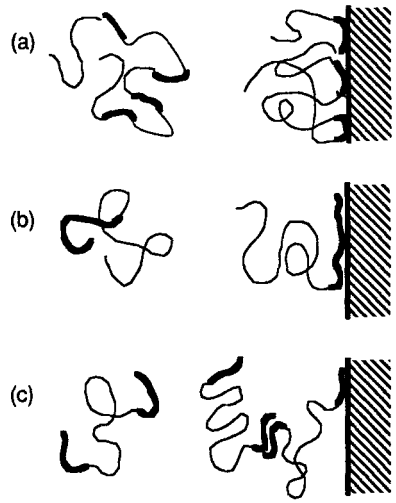

FIG. 2. Conformation of AB copolymers in solution: (a) Random copolymer; (b) diblock copolymer; (c) triblock copolymer.

hydrophilic functions, comprise the associative thickeners hailed as a revolutionary advance in the coatings industry (Sperry *et al.*, 1987).

Even these simple classifications of the interactions between polymer and colloidal particles present a wide variety of possibilities, suggesting the importance of understanding the effect of the macromolecular and particle characteristics on specific macroscopic processes. Unfortunately, the linkage is incomplete in most cases; however, considerable qualitative understanding has evolved relating the interparticle potential to the behavior of colloidal systems. In addition, direct measurements of forces between surfaces exposed to or treated with well-characterized polymers have begun to define the phenomena and provide quantitative data for testing theories. Thus, we address the more limited issue of quantifying this potential, as affected by the various modes of interaction. Then in the final section of this review, we discuss the effects on both the quiescent state of colloidal dispersions, i.e., stabilization, flocculation, phase separation, and dynamics such as the rheology.

This review is intended to complement those of Cohen Stuart *et al.* (1986) and de Gennes (1987). The former details experimental techniques available for probing polymer–particle interactions and the lattice, i.e., mean field, theories that predict, via numerical solutions, segment-density profiles and interaction potentials. The latter constructs a simple and elegant picture of the same phenomena through scaling theories developed for semidilute solutions.

Here we steer a middle course, emphasizing analytical results extracted from the mean-field theories, in context with the lattice and scaling approaches, and explaining the relationship to macroscopic phenomena. Our treatment draws on Russel *et al.* (1989) in some places.

II. Polymer Solution Thermodynamics

A. General Features

The preceding section illustrates the variety of phenomena that may be observed in polymer–colloid–solvent mixtures. Polymer dissolved in a colloidal suspension is in some ways similar to ionic solutes responsible for electrostatic effects. Interactions between colloidal particles and polymer generate nonuniform distributions of polymer throughout the solution. Particle–particle interactions alter the equilibrium polymer distribution, producing a force in which sign and magnitude depend on the nature of the particle–polymer interaction. The major difference between polymeric and ionic solutions lies in the internal degrees of freedom of the polymer. Thus, a complete treatment of particle–polymer interactions requires detailed consideration of the thermodynamics of polymer solutions.

A large body of theoretical (Flory, 1953; Yamakawa, 1971; Lifshitz *et al.*, 1978; de Gennes, 1979; Freed, 1987) and experimental (Brandrup and Immergut, 1975) results demonstrates that many of the properties of polymers in solution display universal behavior as a consequence of the molecules' chainlike architecture. Measurements on a length scale comparable to the size of the polymer chain are insensitive to the details of atomic arrangements or interactions. Polymer properties that depend primarily on gross molecular structure include the radius of gyration (R_g) and the second virial coefficient (A_2) in the series expansion of the solution osmotic pressure in powers of polymer concentration. Under many conditions R_g and A_2 vary as KM^a where M is the polymer molecular weight. In general, K and a differ for R_g and A_2, and depend on the characteristics of the materials. Nonetheless, universal theories successfully predict many solution properties over a wide range of conditions, suggesting the functional relationships (such as power-law) scaling) among key dimensionless groups formed from the parameters characterizing the solution.

Universal models of polymer solutions attempt to describe a variety of large-scale properties with a minimum number of phenomenological parameters. Some theories (Flory, 1969) predict these parameters through microscopic models of bond geometry and interactions, and difficult but

unavoidable procedure when the characteristic length scale in the solution is comparable to the bond length. In bulk polymer, for example, molecular interactions influence many macroscopic properties (Bovey, 1982) and necessitate detailed models. Fortunately, most of the features relevant to interactions between colloidal particles and soluble polymer can be predicted by theories that fix a few phenomenological parameters through independent measurements. These polymer solution theories only require the polymer concentration, the contour length of the molecule, a measure of its flexibility, and a minimal characterization of interactions among different parts of the molecule.

Universality allows the detailed, monomer-level description of the polymer to be replaced by a simpler, equivalent model. The most common random-walk model idealizes the polymer molecule as a freely jointed chain of n segments of length l. If the segments were aligned, the chain would be fully extended with a mean-square end-to-end distance $\langle r^2 \rangle = (nl)^2$. Thermodynamically, this state is highly improbable. The most likely configuration when segments do not interact is a random walk with $\langle r^2 \rangle_0 = nl^2$ where the subscript 0 denotes ideality. The real molecule and this idealized chain must have the same contour length and mean-square end-to-end distance. With l_b and m_b as the average bond length and molecular weight per bond, this leads to

$$\frac{M}{m_b} l_b = nl \tag{1}$$

and

$$\langle r^2 \rangle_0 \equiv \frac{C_\infty M}{m_b} l_b^2 = nl^2, \tag{2}$$

where C_∞ is the characteristic ratio defined by the first equality in Eq. (2). Values of l_b, m_b, and C_∞ have been measured for many systems (Brandrup and Immergut, 1975); some examples are given in Table I. The segment length l measures the chain flexibility in such one-parameter models of ideal polymer solutions.

In real molecules, segments on distant portions of the chain do interact because of their physical volume and short range attractions such as van der Waals forces. The excluded volume parameter

$$v \equiv \int [1 - e^{-V(r)/kT}]\, dr, \tag{3}$$

derived from the mean (solvent-mediated) interaction potential $V(r)$ between a pair of segments separated by r, represents the effective volume that one

TABLE I

PROPERTIES OF POLYMER IN SOLUTION[a]

	$l_{\phi b}$ (nm)	$m_{\phi b}$ (10^{-3} kg/mol)	$\tilde{v}$ (10^{-3} m^3/kg)	C_∞	l (nm)	m (10^{-3} kg/mol)	$w^{1/2}/l^3$
Poly(oxyethylene)	0.148	14.7	0.79	4.1	0.60	60	0.3
Poly(12-hydroxy-stearic acid)	0.150	20	—	6.1	0.91	122	—
Poly(dimethyl siloxane)	0.162	37	0.98	5.2	0.84	192	0.5
Polystyrene	0.154	52	0.95	9.5	1.46	494	0.2

[a] Taken from Brandrup and Immergut (1975).

segment excludes to all others. The ideal or "theta" state occurs at a temperature $T = \theta$ at which $v = 0$. Expanding Eq. (3) around $T = \theta$ gives

$$v \approx Kl^3\left(1 - \frac{\theta}{T}\right), \tag{4}$$

where the constant K may be positive or negative depending on the variation of $V(r)$ with T. For $K > 0$, (4) indicates that $T > \theta$ in good solvents ($v > 0$), while $T < \theta$ in poor solvents ($v < 0$). Theoretical treatments of an isolated chain (e.g., Yamakawa, 1971) indicate that the chain approximates an ideal random walk when $-1 < vn^{1/2}/l^3 < 1$, but that excluded volume "swells" the chain such that $\langle r^2\rangle \approx n^{6/5}l^{4/5}v^{2/5}$ when $vn^{1/2}/l^3 > 1$. In poor solvents (Moore, 1977a; Lifshitz *et al.*, 1978), chains contract so that $\langle r^2\rangle \approx n^{2/3}l^2$, but a complete treatment of this coil–globule transition requires consideration of more than pair interactions. The two phenomenological parameters, l and v, provide an adequate description of the behavior of dilute solutions for $v > 0$ and appear in the dimensionless universal groups $\langle r^2\rangle/nl^2$ and $vn^{1/2}/l^3 = vn^2/\langle r^2\rangle_0^{3/2}$, such that $\langle r^2\rangle/nl^2 = f(vn^{1/2}/l^3)$, in most two-parameter theories (Yamakawa, 1971).

As the segment density ρ increases from the dilute limit (or as coils collapse for $v < 0$), higher-order interactions (three-body, four-body, . . .) become important. The fraction of space excluded by chains may be expressed by the expansion $\rho v/2 + \rho^2 w/3 + \cdots$, where v, w, . . . are the corresponding many-body cluster integrals. As ρ increases, an accurate representation of solution properties requires either more phenomenological parameters or closure approximations, which express the higher-order interactions in terms of v *and* w. The simplest closure assumes that segment interactions can be represented by a mean field averaged over some region of space. Such mean-field theories are most accurate for concentrated solutions in which higher-order interactions eliminate pair correlations.

Beyond the *dilute* limit lies a range of concentrations in which the solution properties are adequately characterized by n, l, v, and w. The *semidilute* regime begins when the average polymer concentration becomes comparable to that within an isolated coil, i.e., when chains begin to overlap and intermolecular interactions become important. As concentration increases further, the intermolecular interactions dominate the intramolecular interactions, marking the transition from semidilute to *concentrated* systems. Within the semidilute regime, Daoud and Jannink (1976) and Schaefer (1984) map several distinct domains of qualitatively different behavior on a temperature–concentration (T–c) diagram.

A schematic T–c diagram is shown in Fig. 3 for fixed values of n, l, and w. Note that the excluded volume v is related to T through Eq. (4), and the polymer volume fraction φ is related to mass concentration c and chain number density ρ/n through

$$\varphi = \tilde{v}c = \frac{\tilde{v}M\rho}{nN_A}, \tag{5}$$

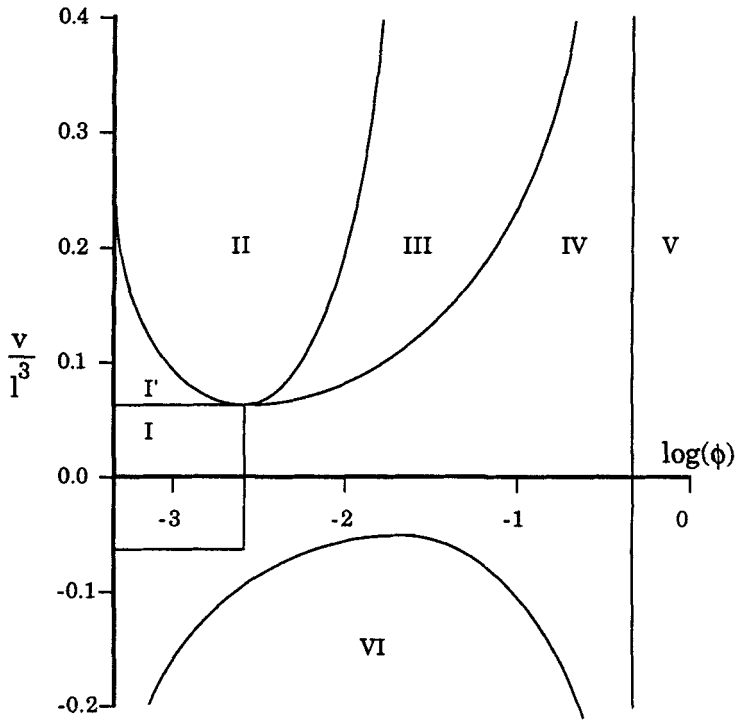

FIG. 3. Schematic temperature–concentration (T–c) diagram. The dimensionless excluded volume v/l^3 is related to T by Eq. (4); φ is proportional to c via Eq. (5). The various regimes are described in the text.

where $\tilde{v}$ is the polymer specific volume, and N_A is Avogadro's number. In region I, chains assume isolated, ideal random walks ($\langle r^2 \rangle_0 \approx nl^2$). Intrachain-excluded volume swells isolated chains ($\langle r^2 \rangle \approx n^{6/5} l^{4/5} v^{2/5}$) in region I'. Region V denotes the concentrated regime where higher-order interactions ($\geq$ three-body) become important. On the poor-solvent side of the diagram, phase separation of the polymer—solvent mixture occurs in region VI. The most significant regions for polymer—colloid interactions, labeled II, III and IV, have been designated (Schaefer, 1984) as the semidilute-good, -marginal, and -theta regimes, respectively.

Within the semidilute-good regime, chains swell because of intrachain excluded volume, but also they overlap and interact. The resulting entangled network of chains has a correlation length ξ as introduced by Edwards (1966). On length scales greater than ξ, random interchain interactions screen intrachain-excluded volume, and chains are ideal, but excluded volume still causes the osmotic pressure to increase nonlinearly with φ. As φ increases, ξ decreases and chains relax toward the ideal state. In the semidilute-marginal regime, excluded volume only weakly perturbs chain configurations so that chains are essentially ideal on all length scales. As φ increases still further, or as v decreases, three-body interactions dominate two-body terms, producing the semidilute-theta regime.

The crossover curves between each pair of regions, detailed by Schaefer (1984), should be interpreted as approximate delimiters rather than sharp boundaries. Within each region, different physical phenomena control the solution's thermodynamic behavior, and so different theoretical approaches have developed. Scaling theory (de Gennes, 1979) predicts trends which agree with experimental data for semidilute-good solutions. Renormalization-group theory (Freed, 1987) supplements scaling theory by providing numerical coefficients and extending predictions beyond the semidilute-good regime within a universal framework. For semidilute-marginal and -theta solutions, mean-field theories have a long history (Yamakawa, 1971) and take a variety of forms. Of these, the self-consistent field (SCF) method has proven most useful for modelling polymer solutions as well as polymer interfaces.

B. Scaling Theory

The concepts of scaling theory are based on the analogy between polymer chain statistics and the properties of fluids and magnets near critical conditions (de Gennes, 1972, 1979, 1987; Des Cloizeaux, 1975). Although most expositions introduce critical phenomena in the context of magnetic materials, the phenomenology of liquid–gas phase transitions is equally valid. In any homogeneous phase, the temperature T and pressure P determine the

fluid's properties, such as the density ρ, compressibility $(\partial\rho/\partial P)_T$, and heat capacities C_P and C_V, through a suitable equation-of-state. On the boundary between two phases, however, the fluid properties are not uniquely determined. The liquid–gas phase boundary, represented by a T, P curve on a phase diagram, ends at the critical point (T_c, P_c), where the densities of the two phases become equal to ρ_c. Near the critical point, large fluctuations of the local density $\rho(\mathbf{r})$ from the mean value ρ are observed. Correlations of the fluctuations, measured by neutron scattering through the Fourier transform,

$$G(q) = \int \langle [\rho(\mathbf{r}) - \rho][\rho(\mathbf{0}) - \rho] \rangle e^{-i|\mathbf{q}\cdot\mathbf{r}|}\, d\mathbf{r},$$

with $\langle \cdots \rangle$ denoting an average over all possible configurations (states) of the system, are found to be peaked at $q = 0$ with the width of the peak defined through

$$\xi^{-2} \equiv -\frac{1}{2G(0)}\left[\frac{d^2G}{dq^2}\right]_{q=0}.$$

Physically, ξ represents the correlation length of the density fluctuations near the critical point. Many measurements demonstrate that for T near T_c,

$$\xi \approx |T - T_c|^{-\nu}, \tag{6}$$

where ν is a critical exponent. Measurements for a variety of systems (liquid–gas phases, liquid mixtures, alloys, magnetic materials) invariably indicate $\nu \approx \frac{3}{5}$, demonstrating the universality of ν.

For polymer solutions, de Gennes (1972) first identified $|T - T_c|$ with $1/n$ and with the root–mean–square end-to-end distance for an isolated chain. Thus, an expression analogous to Eq. (6) is

$$\langle r^2 \rangle^{1/2} \approx n^{\nu} l, \tag{7}$$

valid for dilute solutions in the limit $n \to \infty$. For ideal chains, $\nu = \frac{1}{2}$ results from the classic analyses of random walks (e.g., Chandrasekhar, 1943). The value $\nu \approx \frac{3}{5}$ for good solvents (0.588 is the most accurate value indicated) has been verified theoretically (Flory, 1953; Edwards, 1965; Yamakawa, 1971; Freed, 1987), numerically (Domb, 1963, 1969), and experimentally (Flory, 1969).

The concentration dependence follows through heuristic arguments (de Gennes, 1979) or formal mathematical definitions (Des Cloizeaux, 1975; Kosmas and Freed, 1978). The crossover from dilute to semidilute behavior in good solvents occurs at a segment density $\rho^* \approx n/\langle r^2 \rangle^{3/2} \approx n^{-4/5} v^{-3/5} l^{-6/5}$. For $\rho > \rho^*$, the solution resembles an entangled network with a correlation length $\xi(\rho)$, which is independent of n. At the crossover, the correlation length

must vary continuously so that $\xi = \langle r^2 \rangle^{1/2}$ at $\rho = \rho^*$. In terms of $\varphi \equiv \rho l^3$ [not the φ defined in Eq. (5)], scaling theory derives $\xi(\varphi)$ by forming the dimensionless groups $\xi/\langle r^2 \rangle^{1/2}$ and $\rho/\rho^* = \varphi/\varphi^*$, and postulating the functional relation

$$\frac{\xi(\varphi)}{\langle r^2 \rangle^{1/2}} \approx f(\varphi/\varphi^*) \approx \left[\frac{\varphi}{\varphi^*}\right]^m \tag{8}$$

for φ/φ^* large (Freed, 1987). Using

$$\langle r^2 \rangle^{1/2} \approx n^{3/5} v^{1/5} l^{2/5}$$

and

$$\varphi^* \approx n^{-4/5} v^{-3/5} l^{9/5},$$

the value $m = -\frac{3}{4}$ gives ξ independent of n as

$$\xi(\varphi) \approx \varphi^{-3/4} v^{-1/4} l^{7/4} \tag{9}$$

for $\varphi > \varphi^*$. Data by Daoud *et al.* (1975) and Wiltzius *et al.* (1983) shown in Figs. 4 and 5 confirm this behavior. Further comparisons of scaling-theory predictions and neutron-scattering measurements for moderate ranges of φ and T are presented by Cotton *et al.* (1976) in terms of a $T - c$ diagram as proposed by Daoud and Jannink (1976).

The osmotic pressure Π is the thermodynamic function most accessible to experimental measurement. Dilute solutions of chains exhibit ideal behavior

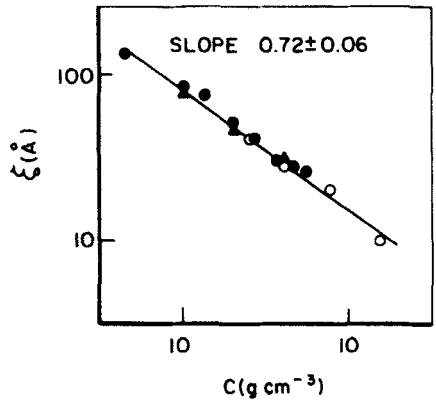

FIG. 4. Correlation length as a function of polymer concentration measured by neutron scattering by Daoud *et al.* (1975). Closed symbols denote polystyrenes of two different molecular weights in deuterated benzene; open symbols denote deuterated polystyrenes of two molecular weights in carbon disulfide.

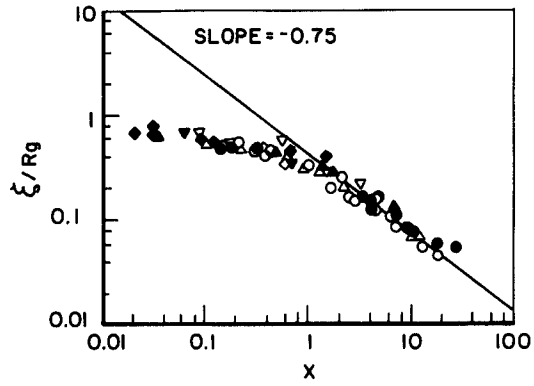

FIG. 5. Correlation length, scaled on R_g, as a function of reduced concentration $X \approx c/c^*$ as measured through static light-scattering by Wiltzius *et al.* (1983). Symbols denote various molecular weight polystyrenes in toluene and methyl ethyl ketone at 25°C.

with $\Pi = \rho kT/n$. At semidilute concentrations, Π has the general form

$$\frac{\Pi}{kT} = \frac{\rho}{n} f\left[\frac{\rho}{\rho^*}, \frac{v}{l^3}, \frac{l_b}{l}\right] = \frac{\varphi}{nl^3} f\left[\frac{\varphi}{\varphi^*}, \frac{v}{l^3}, \frac{l_b}{l}\right], \tag{10}$$

with f an unknown function and $\varphi \equiv \rho l^3$. The scaling hypotheses summarized by Freed (1987) require that f depend only on large-scale variables so that

$$f\left[\frac{\varphi}{\varphi^*}, \frac{v}{l^3}, \frac{l_b}{l}\right] = f_1\left[\frac{\varphi}{\varphi^*}\right] \approx \left[\frac{\varphi}{\varphi^*}\right]^q,$$

with the power-law scaling again assumed for φ/φ^* large. With $\varphi^* \approx n^{-4/5} v^{-3/5} l^{9/5}$, Eq. (10) becomes

$$\frac{\Pi}{kT} \approx \frac{\varphi}{nl^3}\left[\frac{\varphi}{\varphi^*}\right]^q \approx \varphi^{q+1} n^{4q/5-1} l^{-3}. \tag{11}$$

Since Π must be independent of n, $q = \frac{5}{4}$ and

$$\frac{\Pi}{kT} \approx \varphi^{9/4} v^{3/4} l^{-21/4} \approx \frac{1}{\xi^3}. \tag{12}$$

Thus, Π scales as the thermal energy per correlation volume. Neutron scattering (Daoud *et al.*, 1975) and laser-light scattering (Wiltzius *et al.*, 1983) yield $\partial\Pi/\partial\varphi$ in the limit of zero scattering vector support and the scaling $\partial\Pi/\partial\varphi \ \varphi^{5/4}$ for $\varphi > \varphi^*$. Direct measurements of Π (Noda *et al.*, 1981), reproduced in Fig. 6, agree with the predicted scaling of Eq. (12).

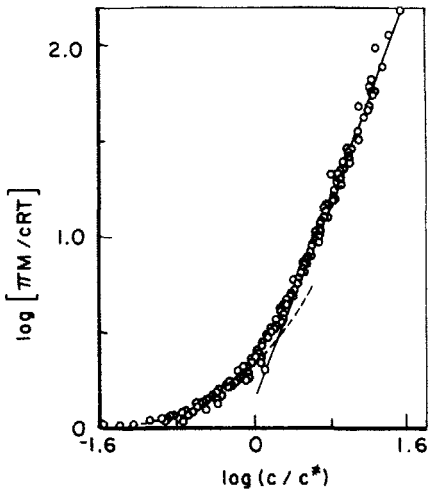

FIG. 6. Reduced osmotic pressure vs. reduced concentration, plotted on a log–log scale, measured through osmometry by Noda *et al.* (1981). Symbols denote various molecular weights of poly(α-methylstyrene) in toluene at 25°C. The solid line has a slope of 1.32.

C. RENORMALIZATION-GROUP THEORIES

The polymer–magnet analogy gives scaling theory its theoretical foundation but restricts its applicability in describing polymer solutions. Still, the formal mathematical similarity is compelling and prompted efforts (Edwards, 1975; Moore, 1977b; Moore and Al-Noaimi, 1978; Des Cloizeaux, 1980a,b,c, 1981; Oono and Freed, 1981) to apply renormalization group (RG) methods, developed for studies in condensed-matter physics, to the problems of polymer solutions. RG methods produce the asymptotic forms of solution properties with numerical prefactors and expressions in the crossover regions. By mathematically connecting the field theoretic models of polymer statistics with the concepts of universality and dimensional scaling, RG theory provides a systematic approach for predicting universal behavior throughout the dilute and semidilute regimes. The purpose here is to introduce some of the fundamental concepts and recent results; Freed's text (1987) is a far more complete and detailed reference.

Several varieties of RG theory are reviewed in extant texts (e.g., Stanley, 1971; Ma, 1976; Ziman, 1979; Freed, 1987). Although the details differ, all approaches share the basic operations of coarse-graining and scaling. Coarse-graining introduces phenomenological parameters that characterize but obviate fine details, thus simplifying the description and facilitating calculations. For example, sequences of real monomers become statistical

segments of length l. Scaling formulates a minimal set of phenomenological parameters through dimensional analysis and relates regions of the parameter space through transformations such as rotation, translation, reflection, or more complicated symmetries. Thus, the self-similarity (translational symmetry) of semidilute solutions allows ξ to be related to l. Beginning with a set of parameters characterizing one model (e.g. n, l, v, w), a sequence of scaling and coarse-graining operations leads to a new form represented by a set of renormalized parameters. Repeating the procedure generates a series of models belonging to the same *universality class* which comprise the *renormalization group*. Renormalization ends when the model becomes invariant to transformation, i.e., when an asymptotic limit is reached. Polymer properties can, in principle, be evaluated more easily in such limits.

In semidilute solutions, chain interactions are strongly coupled, producing significant density fluctuations. One successful RG technique (Edwards, 1966, 1975; Muthukumar and Edwards, 1982) renormalizes the segment length l and the segment–segment interaction $v\delta r$ into l_1 and Δr in order to define an effective single chain in an average excluded-volume field. The new segment length is defined by

$$l_1 \equiv \frac{\langle r^2 \rangle}{nl}. \tag{13}$$

The excluded-volume field $\Delta(\mathbf{r})$

$$\Delta(r) \equiv v\left[\delta(r) - \frac{1}{4\pi\xi^2 r}\exp(-r/\xi)\right] \tag{14}$$

contains the screening length ξ equivalent to the Edwards (1966) correlation length. Properties of the effective single chain are extracted by making $\Delta(r)$ self-consistent via the "method of random fields" and then solving in the asymptotic limit of highly-stretched chains (Edwards, 1966, 1975).

Edwards and co-workers (Edwards and Jeffers, 1979; Edwards and Singh, 1979) adapted these techniques to determine chain dimensions in semidilute solutions. Subsequently, Muthukumar and Edwards (1982) formulated RG expressions for the solution free-energy and derived Π explicitly in the low and high concentration limits. The general expression for the free-energy density relative to that of an infinitely dilute solution is

$$\frac{A}{VkT} = -\frac{9}{16\pi}\frac{vn\rho}{ll_1\xi} - \frac{1}{24\pi\xi^3} + v\rho^2, \tag{15}$$

where l_1 and ξ satisfy

$$l_1^3\left[\frac{1}{l} - \frac{1}{l_1}\right] = \frac{\alpha v\xi}{l^2} \tag{16}$$

and

$$\frac{1}{\xi^2} = \frac{6v\rho}{ll_1\left[1 + \dfrac{27v\xi}{8\pi l^2 l_1^2}\right]}, \tag{17}$$

where α is a numerical coefficient. For $\rho \to 0$ and $n \to \infty$, Muthukumar and Edwards find

$$\frac{\Pi}{kT} = \frac{\rho}{n} + \frac{40\pi}{243}\left[\frac{16\pi\alpha^3}{9}\right]^{1/4} v^{3/4} l^{3/2} \rho^{9/4}, \tag{18}$$

with the $\rho^{9/4}$ dependence confirming the scaling-theory result. In the limit $\rho \to \infty$,

$$\frac{\Pi}{kT} = \frac{\rho}{n} - \frac{5\sqrt{6}}{32\pi}\frac{(v\rho)^{3/2}}{l^2} + v\rho^2, \tag{19}$$

conforming to the ρ^2 dependence expected for semidilute-marginal solutions where pair interactions dominate the solution free-energy (Schaefer, 1984). The osmotic pressure at intermediate concentrations follows from the free energy through solution of Eqs. (16) and (17) for l_1 and ξ and partial differentiation of Eq. (15). Fixing the coefficient α requires a measurement of $\langle r^2 \rangle$ at a known value of v; then

$$l_1^{5/2}\left[\frac{1}{l} - \frac{1}{l_1}\right] = \frac{\alpha v (nl)^{1/2}}{2\sqrt{6\pi l^2}}, \tag{20}$$

which, along with Eq. (13), gives α.

Another RG analysis (Des Cloizeaux, 1980a,b, 1981; Oono and Freed, 1981; Oono *et al.*, 1981; Ohta and Oono, 1982) produces a closed-form expression for Π. With one independent measurement to fix A_2 in the dilute limit, Ohta and Oono (1982) define $X \equiv \frac{16}{9}(M/N_A)A_2\rho$ as the universal concentration variable (Wiltzius *et al.*, 1983) and derive

$$\frac{\Pi}{\rho kT} = 1 + \frac{X}{2}\exp\left\{\frac{1}{4}\left[\frac{1}{X} + \left(1 - \frac{1}{X}\right)\ln(X)\right]\right\}, \tag{21}$$

with the scaling-theory trend ($\Pi \approx X^{9/4}$) emerging as X grows large. Comparisons with the data of Noda *et al.* (1981) (Fig. 6), from Ohta and Oono (1982) (Fig. 7), and from Wiltzius *et al.* (1983) (Fig. 8) demonstrate the validity of Eq. (21), at least for dilute and semidilute conditions. Since the Muthukumar and Edwards expression, Eq. (18), pertains to semidilute and concentrated conditions, the two are complementary.

RG theories are currently being extended into the semidilute-marginal and -theta regimes. Results (Freed, 1985; Bawendi *et al.*, 1986) remain limited and

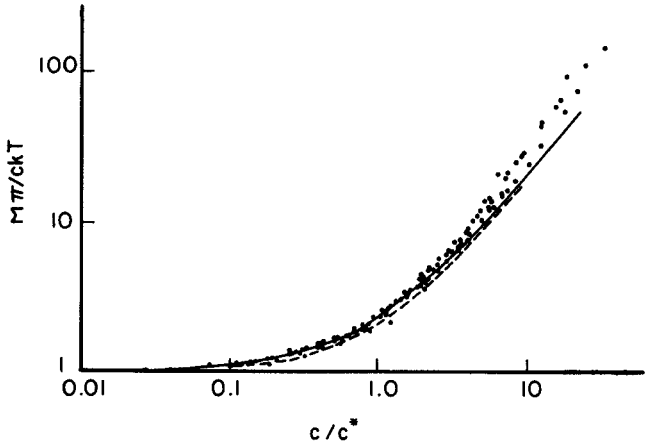

FIG. 7. $\Pi/\rho kT$ vs. reduced concentration plotted on a log–log scale. Symbols denote the data of Noda *et al.* (1981) as in Fig. 6. Solid curve, which has been shifted horizontally to fit the data, is the prediction of Eq. (21). Reproduced from Ohta and Oono (1982).

restricted to the vicinity of $T = \theta$ where $v \approx 0$ but $w > 0$. The complexity of calculations involving three-body interactions is daunting (Freed, 1987, Chap. 11), but may eventually lead to thermodynamic properties. At present, RG theory provides the best hope of describing polymer solutions within a unified, universal framework.

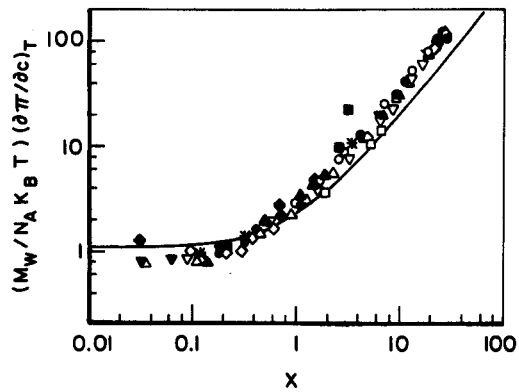

FIG. 8. Dimensionless reciprocal compressibility vs. reduced concentration plotted on a log–log scale, measured through static light-scattering by Wiltzius *et al.* (1983). Symbols denote data for various molecular weight polystyrenes in toluene and methyl ethyl ketone at 25°C. The solid curve is the prediction derived from Eq. (21); the proportionality of X to c is fixed by an independent measurement so the curve requires no adjustable parameters.

D. Flory Mean-Field Theories

The first mean-field theories, the lattice models, are typified by the Flory–Huggins model. Numerous reviews (see, e.g., de Gennes, 1979; Billmeyer, 1982; Forsman, 1986) describe the assumptions and predictions of the theory; extensions to polydisperse and multicomponent systems are summarized in Kurata's monograph (1982). The key results are reiterated here.

Space is discretized into a lattice of sites occupied by either segments or solvent molecules. Each site has z nearest neighbors. The number of Flory–Huggins segments per chain, $r = \tilde{v}M/V_s$, equals the ratio of polymer ($\tilde{v}M$) and solvent (V_s) molar volumes. Thermodynamic properties are computed by filling a unit volume of the lattice with a total of ρ/r chains of r segments and ρ_s solvent molecules. As a chain is placed in the lattice, the probability of inserting the ith segment is $(z-1)(1-p_i)$, since $(z-1)$ sites are available adjacent to segment $i-1$ (z neighbors minus one site occupied by segment $i-2$), and $1-p_i$ is the probability of a particular adjacent site being vacant. Flory (1942) and Huggins (1942) replace the local p_i with a mean $\langle p_i \rangle$ averaged over the lattice, creating the mean field. Thus, the theory is restricted to concentrated solutions in which density fluctuations and correlations are unimportant.

Manipulation of combinatorial statistics leads to the Flory–Huggins free energy of mixing (per unit volume)

$$\frac{\Delta f_M}{VkT} = \frac{\rho}{n}\ln(\varphi) + \rho_s \ln(1-\varphi) + \rho_s \varphi \chi \tag{22}$$

where χkT is the enthalpy of mixing a segment with an excess of solvent. The Gibbs and Helmholtz free energies of mixing both equal Δf_M since $\Delta V_M \equiv 0$. With $\varphi = \rho/(\rho + \rho_s)$ and $\Pi \equiv -[\partial(\Delta f_M V)/\partial V]_T$, a simple calculation produces

$$\frac{\Pi V_s}{N_A kT} = -[\ln(1-\varphi) + (1-1/r)\varphi + \chi\varphi^2] \tag{23}$$

$$= \frac{\varphi}{r} + (1-2\chi)\frac{\varphi^2}{2} + \frac{\varphi^3}{3} + \cdots, \tag{24}$$

allowing identification of $v/l^3 \approx (1-2\chi)$.

In practice, the Flory–Huggins theory fails to predict many features of polymers solutions, either qualitatively or quantitatively, but remains widely used because of its simplicity. The Flory parameter χ, assumed to be constant, often increases with φ. Furthermore, χ, an interaction-energy scaled on kT, often exhibits a more complicated temperature dependence than $1/T$ (Flory, 1970). Such behavior stems from energetic effects, such as directional polar

interactions, which preferentially orient segments. Reinterpretation of χ as a composite of enthalpic and entropic factors (Flory, 1970) rationalizes these variations; Eq. (22) then provides a convenient means of correlating data, but the exercise does little to suggest improvements of the theory. As a mixture theory, the analysis also ignores pure component properties.

Corresponding-states theory (Prigogine, 1957; Flory, 1970) incorporates features of the pure component properties and liquid structure in the mixture equation-of-state, producing nonzero values of ΔV_m and contributing enthalpic and entropic terms beyond those in Flory–Huggins theory. The theory assumes that all pure components and mixtures obey the same universal equation-of-state, e.g., (Flory, 1970)

$$\frac{\tilde{\Pi}\tilde{V}}{\tilde{T}} = \frac{\tilde{V}^{1/3}}{\tilde{V}^{1/3} - 1} - \frac{1}{\tilde{V}\tilde{T}} \tag{25}$$

where $\tilde{\Pi}$, $\tilde{V}$, and $\tilde{T}$ are Π, V, and T reduced with parameters fixed by measurements for pure components. Further theoretical efforts, often employing lattice fluid-models (e.g., Sanchez and Lacombe, 1978), postulate mixing rules that combine the pure component parameters in mixture reduction parameters. The corresponding-states approach is generally successful in predicting mixture properties and phase behavior but requires a significant investment to determine pure component properties.

Another effort (Dickman and Hall, 1986) aims to remove the artificiality of lattice geometry by transposing the concepts of Flory–Huggins theory to continuous space. Calculations for athermal solvents ($\chi = 0$) indicate that the resulting "generalized" Flory theory predicts $\Pi/\rho kT$ in agreement with computer-simulation data for short chains of hard disks and spheres, whereas the lattice-based Flory–Huggins theory gives a severe underestimate. The Dickman–Hall theory has not yet been extended to other values of χ, however.

E. Self-Consistent Mean-Field Theories

Like all mean-field theories, SCF theories replace the detailed, configuration-dependent interaction potentials with a mean potential averaged over the distribution of molecular configurations. Unlike other mean-field theories, SCF theory explicitly calculates the mean field by accounting for the polymer chain statistics. This field, in turn, controls the distribution of polymer configurations: Hence the term "self-consistent."

The classic SCF analyses (Edwards, 1965; de Gennes, 1969, 1979; Freed, 1972; Helfand, 1975c) define the number of configurations available to a subchain of $s \leq n$ contiguous segments which begins at $\mathbf{r}'$ and ends at $\mathbf{r}$ as

$G(\mathbf{r}, \mathbf{r}'; s)$. For a complete chain of n segments, integrating over $\mathbf{r}$ and $\mathbf{r}'$ gives the configuration integral

$$W = \iint G(\mathbf{r}, \mathbf{r}'; n)\, d\mathbf{r}\, d\mathbf{r}', \tag{26}$$

which acts as the partition function for individual chains. The normalized function G/W is a probability density.

The configuration of a polymer chain is analogous to the path $\mathbf{r}(s)$ of a diffusing particle with the segment rank s replacing time. At equilibrium, configurations follows the Boltzmann distribution

$$G(\mathbf{r}, \mathbf{r}'; s) = \exp\left[-\int \beta U[\mathbf{r}(s')]\, ds' \right] \tag{27}$$

where $\beta = 1/kT$ and the potential $U(\mathbf{r})$ per segment accounts for all interactions along the contour of the chain. A suitable definition of U as a "potential of mean force" (Freed, 1972), or, in other words, a mean field, decouples the many-body problem of segment interactions so that the chain propogates as a Markov process (van Kampen, 1981). Consequently, addition of another segment to a chain of $s - 1$ segments produces

$$G(\mathbf{r}, \mathbf{r}'; s) = \frac{1}{4\pi l^2} \int G(\mathbf{r} + l\mathbf{n}, \mathbf{r}'; s-1) \exp\left[-\int_{s-1}^{s} \beta U[\mathbf{r}(s')]\, ds' \right] d\mathbf{n}, \tag{28}$$

where $\mathbf{n}$ is the unit vector from segment s to $s - 1$. If U varies slowly on the scale of l, then

$$\int_{s-1}^{s} \beta U[\mathbf{r}(s)]\, ds \approx \beta U(\mathbf{r}) \tag{29}$$

so that

$$G(\mathbf{r}, \mathbf{r}'; s) = \frac{e^{-\beta U(\mathbf{r})}}{4\pi l^2} \int G(\mathbf{r} + l\mathbf{n}, \mathbf{r}'; s-1)\, d\mathbf{n}. \tag{30}$$

Expanding $G(\mathbf{r} + l\mathbf{n}, \mathbf{r}'; s - 1)$ in a Taylor series in $\mathbf{r}$ and s, integrating, and rearranging gives the SCF equation

$$\frac{\partial G}{\partial s} = \frac{l^2}{6} \nabla^2 G + [1 - e^{\beta U(\mathbf{r})}] G, \tag{31}$$

with the initial condition

$$G(\mathbf{r}, \mathbf{r}'; 0) = \delta(\mathbf{r} - \mathbf{r}'). \tag{32}$$

Equation (31) describes phenomena (Chandrasekhar, 1943; Weiss and Rubin, 1983) ranging from the Brownian motion of colloidal particles to stellar

evolution. For polymer molecules, the first term in Eq. (31) accounts for the connectivity of the chain, the second for the tendency of entropy to disperse the segments, and the third for all long-range interactions.

Since the chain statistics are governed by a Markov process, the chain may be divided into two independent subchains of lengths s and $n - s$. The probability of finding the sth segment at $\mathbf{r}$ for a chain that begins at $\mathbf{r}'$ and ends at $\mathbf{r}''$ is $G(\mathbf{r}, \mathbf{r}'; s)G(\mathbf{r}'', \mathbf{r}; n - s)/e^{-\beta U(\mathbf{r})}$; the denominator remedies the overcounting of the junction segment. Integrating over the endpoint positions and all contour locations where subchains may intersect yields

$$\varphi(\mathbf{r}) = \frac{e^{\beta U(\mathbf{r})}}{n} \int_0^n \iint G(\mathbf{r}, \mathbf{r}'; s)G(\mathbf{r}'', \mathbf{r}; n - s)\, d\mathbf{r}'\, d\mathbf{r}''\, ds. \tag{33}$$

Once the SCF $U = U[\varphi(\mathbf{r})]$ is specified, Eqs. (31) and (33), and the necessary boundary, initial, and normalization conditions form a closed "self-consistent" set of equations.

Solutions for dilute ideal chains with $U \approx 0$ are particularly simple. Since segments do not interact, only internal configurations are important. With $\mathbf{r}' = 0$, Eq. (31) becomes

$$\frac{\partial G}{\partial s} = \frac{l^2}{6r^2} \frac{\partial}{\partial r}\left[r^2 \frac{\partial G}{\partial r} \right],$$

with $G(r, 0; 0) = \delta(r)$ and $G(\infty, 0; s) = 0$ as the boundary and initial conditions. The solution

$$G = \frac{3}{(2\pi l^2 s)^{3/2}} \exp\left[-\frac{3r^2}{2l^2 s} \right] \equiv G_0$$

indicates a Gaussian chain for which

$$\langle r^2 \rangle_0 = \frac{1}{W} \int r^2 G(r, 0, n)\, dr = nl^2,$$

as required.

The osmotic pressure calculation remains simple for all dilute solutions. Statistical mechanics gives the Helmholtz free-energy

$$A = -kT \ln(Q) \tag{34}$$

as a function of the canonical partition function Q. For $n_p \equiv \rho V/n$ chains in a volume V at high dilution,

$$Q \approx \frac{[VW]^{n_p}}{n_p!} \tag{35}$$

(McQuarrie, 1976). After using Stirling's approximation, Eqs. (34) and (35)

yield

$$\frac{An}{\rho VkT} = \ln(\rho) - 1 - \ln(W) \tag{36}$$

as the free energy per chain. The free energy therefore depends on the internal state of the isolated chain, but the osmotic pressure

$$\frac{\Pi n}{\rho kT} = -\frac{Vn}{\rho kT}\left(\frac{\partial A}{\partial V}\right)_T = 1 \tag{37}$$

does not.

In concentrated solutions, U is a constant independent of position; Eq. (31) is again linear with the solution

$$G = G_0 \exp\{s[1 - \exp(\beta U)]\}, \tag{38}$$

demonstrating that chains are ideal. Between the dilute and concentrated limits, however, Q may not be factored into translational and internal parts (V and W) as in Eq. (34). Edwards' (1965) single-chain analysis is the foundation for all many-chain SCF theories. Expressions for Q take the form of functional integrals (Freed, 1972; Helfand, 1975c) which depend on many-body interactions and cannot be evaluated analytically.

Statistical mechanical manipulations of the functional integral representation of Q are necessary for inhomogeneous systems (Helfand, 1975c; Hong and Noolandi, 1981). Minimization of the free energy fixes the equilibrium spatial distribution of polymer and solvent. Edwards' "random field" technique (1965) leads to

$$U(\mathbf{r}) = \frac{\partial}{\partial \rho}[f(\rho, \rho_s) - \rho\mu_p^b - \rho_s\mu_s^b] - \frac{kT}{n}\ln(\rho/\rho_b) \equiv \Delta\mu_p, \tag{39}$$

where $\rho(\mathbf{r})$ and ρ_s are the segment and solvent densities, μ_p^b and μ_s^b are the respective chemical potentials in the bulk solution where $\rho \to \rho_b$, and $f(\rho, \rho_s)$ is the local free-energy density of a (perhaps hypothetical) mixture of composition ρ, ρ_s. Thermodynamically, $U(\mathbf{r})$ is the local excess chemical potential of the polymer; the logarithm term insures that U is invariant with respect to the choice of segment length (Hong and Noolandi, 1981). For a homogeneous solution, $U \to 0$ so that Eq. (39) provides no new information. Now the closed self-consistent set of Eqs. (31), (33), and (39) give the properties of a nonuniform solution in terms of the local segment interactions represented in $f(\rho, \rho_s)$. The segment equation-of-state must come from another source, such as the Flory–Huggins theory. Although its utility is limited in bulk solutions, the SCF method plays a central role in theories of surface tension and polymer adsorption.

III. Randomly Adsorbing Homopolymer

A. Introduction

In many systems of practical interest, polymer chains adsorb onto surfaces through contacts distributed randomly along the contour of the chain. These contacts result from attractive forces between polymer segments and the surface, generally attributed to van der Waals forces, hydrogen bonding, or other material-specific interactions. Measurements of polymer–surface interactions are relatively few in number (Killmann *et al.*, 1977; Brebner *et al.*, 1980a,b; Cohen Stuart *et al.*, 1984a,b; Killmann and Bergmann, 1985, Van der Beek and Cohen Stuart, 1988). In spite of this, theories of random homopolymer adsorption have progressed remarkably by treating the energy of adsorption of a single segment as a phenomenological parameter. Random adsorption of individual segments and the concomitant impact on the overall configurations of adsorbed chains distinguished these systems from the related cases of terminally anchored chains and depletion layers created by nonadsorbed polymer.

Unlike terminally anchored polymer, both ends of a randomly adsorbed chain extend from the surface into solution; multiple interior points along the contour of the chain contact the surface. This architecture has generated its own terminology: Sequences of segments lying on the surface are "trains," nonadsorbed sequences with adsorbed segments at both ends are "loops," and sequences that leave the surface and never return are "tails." These structures are easily visualized and provide a conceptual link between the statistics of chain configurations and experimentally observable quantities. Furthermore, train, loop, and tail statistics measure the relative importance of competing physical phenomena: The loss of chain configurational entropy due to the impenetrable surface and interactions with other chains relative to energetic effects resulting from polymer–polymer, polymer–solvent, and polymer–surface interactions.

Such interactions control the structure of an adsorbed polymer layer. The equilibrium state of a system, including a surface, adsorbed and free polymer, and the solvent, of course, correspond to a minimum in the total free energy. The impenetrable adsorbing surface eliminates many of the configurations that the chain could assume in bulk solution. In addition, each adsorbed segment loses a translational degree of freedom. The resulting decrease in configurational entropy increases the total free energy and is unfavorable. Repulsion between segments on the same or different chains further reduces the number of available configurations and decreases the entropy. Despite this, adsorption still occurs when the energy decrease associated with

segment–surface contacts compensates for the entropy loss. The balance between configurational entropy loss (due to the surface and interchain interactions) and energy gain (from adsorption) is central to the understanding of polymer adsorption.

The free energy is minimized to varying degrees by the formation of trains, loops, and tails, subject to the constraints of overall chain structure. For example, trains have low energies but also have low entropies; loops and tails effectively preserve entropy and promote segment–solvent contact but forego the adsorption energy at the surface. The polymer molecular weight and concentration in bulk solution and the solvent quality all affect the equilibrium amount of adsorbed polymer and the distribution of trains, loops, and tails within the adsorbed layer.

Recent models of polymer adsorption incorporate all these considerations, whereas early theories generally invoked one or more assumptions which limited their applicability. The most common approximations included the neglect of interchain interactions (i.e., isolated chain adsorption), restriction to infinite molecular weights, predetermination of the statistical distribution of loops and tails, and a priori specification of the polymer density profile. Nonetheless, the early theories provide the foundation for all succeeding work, treating the important physical phenomena individually and providing insights that might be overlooked today. Comprehensive reviews of early adsorption theories exist elsewhere (Stromberg, 1967; Silberberg, 1971; Vincent, 1974; Eirich, 1977; Tadros, 1982, 1985; Takahashi and Kawaguchi, 1982); we limit our treatment to those results that bear on contemporary analyses.

The development of theory for polymer adsorption parallels that for polymer solutions, since the two problems share the same physics (except for the effect of adsorption) on length scales comparable to the segment length. Several complementary approaches have emerged, including scaling theory, renormalization group theory, and self-consistent mean-field theory, to describe the layer structure in terms of parameters characterizing the universal aspects of polymer chains. Each idealizes the relevant physics, but the approximations and, hence, the ranges of validity differ as discussed later. In addition, recent experimental results will be presented and compared with theoretical predictions.

B. Early Adsorption Theories

1. *Individual Ideal Chains*

The development of models began in earnest (around 1950) when a growing body of experimental data suggested that macromolecular adsorption could not be described by concepts applied successfully to low molecular weight

adsorbates. Jenckel and Rumbach (1951), for instance, observed adsorbed amounts corresponding to roughly 10 monolayers of segments. They reasoned that interactions were too weak in their dilute system to cause phase separation or multilayer adsorption; thus, the polymer must adsorb in alternating sequences of trains and loops. The first theoretical analysis based on this idea appeared in a series of papers by Simha, Frisch, and Eirich (Frisch *et al.*, 1953; Simha *et al.*, 1953; Frisch and Simha, 1954, 1956, 1957; Frisch, 1955). Polymer configurations are represented as ideal (Gaussian) random walks in a discrete three-dimensional lattice bounded by an impenetrable planar surface. Random walks reaching lattice sites on the surface are reflected back into the solution, a boundary condition motivated by the fundamental work of Chandrasekhar (1943).

However, Silberberg (1962b), DiMarzio (1965), and DiMarzio and McCrackin (1965) criticized the use of the reflecting boundary condition for overcounting allowable configurations. They argued in favor of the "adsorbing" boundary condition, i.e., discounting any configuration reaching a hypothetical lattice point *behind* the surface. Silberberg (1962a) also objected to decoupling the calculation of polymer configurations from the thermodynamic considerations which determine the equilibrium adsorbed amount and observed that "the discussion of the isolated macromolecule should be reformulated, and the shape of the polymer introduced as a variable into the full thermodynamic treatment."

Silberberg then addressed the equilibrium configuration of an isolated adsorbed macromolecule by dividing the chain into m_i loops of length i and $\tilde{m}_j$ trains of length j. The total number of segments in the chain is $n = \sum i m_i + \sum j \tilde{m}_j$, and, neglecting tails, $\sum m_i = \sum \tilde{m}_j$. This allows the partition function for the polymer to be expressed in terms of m_i, $\tilde{m}_j$, and the functions $\psi(i)$ and $\tilde{\psi}(j)$, specifying the number of possible configurations for loops and trains of lengths i and j, respectively. By assuming the loop and train size distributions to be sharply peaked at $i = P_B$ and $j = P_S$ [a serious restriction subsequently eliminated by Hoeve *et al.* (1965)] and choosing reasonable forms for $\psi(P_B)$ and $\tilde{\psi}(P_S)$, Silberberg minimized the free energy subject to the constraint of fixed chain length. The resulting simultaneous equations yielded P_B and P_S and the bound fraction of segments as $p = P_S/(P_B + P_S)$.

The configurational statistics derived from the model depend on the coordination numbers of the lattice and the energy of replacing an adsorbed solvent molecule with a segment, χ_s. The most notable result was a sharp transition from small p to $p \approx 1$ at low χ_s, the first indication of a critical energy χ_{sc} distinguishing depletion from adsorption. Silberberg (1962b) concluded that polymer random walks "can continue in [the surface] in two out of three dimensions, and that a small reduction in energy per segment can compensate largely for the entropy loss in the third."

Hoeve *et al.* (1965) carried this concept forward by varying the lattice geometry to account for chain flexibility and using correct combinatorial factors in the partition function with no a priori assumptions regarding the size distributions of loops and trains. In the limit of very stiff chains, the bound fraction becomes discontinuous: $p = 0$ for $\chi_s < \chi_{sc}$ and $p = 1$ *for* $\chi_s > \chi_{sc}$. Some flexibility broadens the transition, but a critical adsorption energy always exists below which $p = 0$. They also found (1) broad train and loop size distributions with no maxima, (2) average loop lengths that increase with decreasing flexibility and adsorption energy and become infinite at the critical energy (for infinite chain lengths), and (3) average train lengths that increase with increasing flexibility and adsorption energy. Later work by Silberberg (1967) confirmed these results.

Roe (1965, 1966) and Rubin (1965) completed the description of the dependence of bound fraction and average loop and train sizes on adsorption energy, chain flexibility, and molecular weight for isolated macromolecules. Clear distinctions emerged among adsorption energies greater than, equal to, or less than the critical energy. For $\chi_s < \chi_{sc}$, $\nu = np$ (the number of adsorbed segments per chain) and is independent of the chain length n; at $\chi_s = \chi_{sc}$, $\nu \simeq n^{1/2}$ (also shown in Simha *et al.*, 1953); and for $\chi_s > \chi_{sc}$, $\nu \simeq n$, implying a constant bound fraction. The bound fraction never falls to zero for finite chain lengths, but a well-defined transition, dependent on the lattice geometry or the chain flexibility, still exists at the critical energy. The variation of the average loop and train lengths with adsorption energy are the same as found earlier by Hoeve *et al.* (1965). Although the train length does not vary significantly with chain length, the loop length does: For $\chi_s < \chi_{sc}$, loop length is independent of n for $n > 100$, but for $\chi_s > \chi_{sc}$, loop length is proportional to $n^{1/2}$.

Roe's analysis (1965), the first to allow for tails, is highly significant. First, the average tail length decreases with stronger adsorption, as expected. For $n > 1000$ segments, the tail length exceeds the loop length by an order of magnitude and increases in proportion to the chain length. Below the critical adsorption energy, the root–mean–square distance of segments from the surface is proportional to the radius of gyration, $(nl^2/6)^{1/2}$; above the critical energy, the thickness is only a few segments. Loops dominate the segment density profiles for $\chi_s > \chi_{sc}$, while tails are more important for $\chi_s \leq \chi_{sc}$. In fact, near the critical energy, about 70% of all segments are in tails and "the thickness of [the adsorbed] layer ... is largely determined by the size of the dangling polymer chain ends, rather than by the size of the loop, as was frequently assumed."

This conclusion can easily be rationalized. Chandrasekhar (1943; Hoeve, 1965; Hesselink, 1969) has shown that for long tails of i segments, the number of possible configurations is $(2\pi i)^{-1/2}2^i$, while the number of possible loop configurations is $(2\pi i)^{-1/2}2^i i^{-1}$. Thus, configurational entropy alone favors

tails over loops. Near the critical adsorption energy, the attractive surface binds the chain but does not distort it significantly from its ideal state. Thus, tails dominate. Stronger adsorption overcomes the entropic effects and flattens the chain onto the surface. Then tails can be neglected for isolated macromolecules without excluded volume effects.

2. *Equilibrium and Excluded Volume*

In practice, macromolecules almost never adsorb in isolation. Although the adsorption energy per segment may be low, the number of adsorbing segments per chain results in the deposition of many chains, even from dilute bulk solutions. Hence, two intimately related problems must be addressed: Determination of the equilibrium adsorption as a function of bulk solution concentration (the adsorption isotherm) and assessment of the effects of excluded volume and solvency. Silberberg (1962b) laid the foundation for subsequent developments by demonstrating two key concepts: (1) The adsorption energy equals the energy required to replace an adsorbed solvent molecule with a segment and (2) a mixing parameter that includes entropic and energetic contributions adequately characterizes solvent–segment contacts.

Simha *et al.* (1953), Silberberg (1962b, 1968), and Hoeve, *et al.* (1965; Hoeve, 1966) addressed the problem of equilibrium, predicting adsorption isotherms in at least qualitative agreement with experimental data. On a linear scale, the adsorbed amount grows very steeply with polymer volume fraction and then levels off in a "pseudoplateau." The adsorbed amount increases with chain length, reaching a limit of about one monolayer of segments for long chains adsorbed from dilute solutions.

In retrospect, the early adsorption models identified most of the significant aspects of the adsorption problem. The relationship between adsorption energy and average chain configuration was explored extensively. The assumptions necessary for the calculations, however, limited the utility of these models in predicting the behavior of real systems and, hence, their credibility. Improved analyses of excluded volume and equilibrium required a more comprehensive mathematical framework.

C. Lattice Models and Matrix Methods

Lattice models play a central role in the description of polymer solutions as well as adsorbed polymer layers. All of the adsorption models reviewed so far assume a one-to-one correspondence between lattice random-walks and polymer configurations. In particular, the general scheme was to postulate the train–loop or train–loop—tail architecture, formulate the partition function, and then calculate the equilibrium statistics, e.g., bound fraction, average loop

and train sizes, and segment density distribution (Roe, 1966; Hoeve, 1965). In some cases, the adsorbed macromolecules were equilibrated with bulk solution, but the analyses usually focussed on isolated chains with at least one segment on the surface.

The work of DiMarzio and Rubin (DiMarzio, 1965; Rubin, 1965; DiMarzio and Rubin, 1971) began the development of a related but more powerful approach. Rather than calculating microstructural details from a presumed architecture, Rubin's matrix method concentrates on the effect of local interactions on the propagation of the chain, thereby deriving the statistical properties of the random walk and the structure of the entire chain. This formalism is the foundation for several subsequent models, so some details are reviewed here. The notation is transposed into a form consistent with the contemporary models discussed below.

The space near the adsorbing surface is discretized into layers of lattice sites numbered $i = 1, 2, \ldots m$ with layers 1 and m being adsorbing planar surfaces and $m \to \infty$ corresponding to two isolated surfaces. Each lattice site has Z nearest neighbors with Z_0 of these in the same layer. Far from the surface, all random walks have the same *a priori* probability, but adsorption changes the statistical weights of configurations near the surface.

Let $P(i, s)$ be the unnormalized probability that the sth step of a polymer random walk ($s + 1$ segments) ends at a lattice site in layer i. The preceeding step $s - 1$ must reside in one of the layers $i - 1$, i, or $i + 1$, suggesting the recurrence relation

$$P(1, s) = \lambda_0 \exp(\chi_s) P(2, s-1) + \lambda_1 \exp(\chi_s) P(1, s-1), \qquad i = 1$$

$$P(i, s) = \lambda_1 P(i+1, s-1) + \lambda_0 P(i, s-1) + \lambda_1 P(i-1, s-1), \quad i \geq 2 \qquad (40)$$

where $\lambda_1 = \frac{1}{2}(Z - Z_0)/Z$ and $\lambda_0 = Z_0/Z$ are the fractions of nearest neighbors in adjacent layers or the same layer, respectively. The term $\exp(\chi_s)$ in Eq. (40) enhances the probability of configurations contacting the surface. In matrix form, the equation

$$\mathbf{P}(s) = \mathbf{W}(\chi_s)\mathbf{P}(s-1) = [\mathbf{W}(\chi_s)]^s \mathbf{P}(0) \qquad (41)$$

relates $\mathbf{P}(s)$, the column vector with elements $P(i, s)$, $i = 1, \ldots, \infty$, to $\mathbf{P}(0)$, the vector of starting probabilities $[\mathbf{P}(0)]^T \equiv [e^{\chi_s}, 1, 1, \ldots]$, through $\mathbf{W}$, a matrix of transition probabilities

$$\mathbf{W} \equiv \begin{bmatrix} \lambda_0 e^{\chi_s} & \lambda_1 e^{\chi_s} & & & \\ \lambda_1 & \lambda_0 & \lambda_1 & & \\ & \lambda_1 & \lambda_0 & \lambda_1 & \cdots \\ & & \vdots & & \end{bmatrix}. \qquad (42)$$

Structural characteristics of adsorbed chains, such as the mean distance of chain ends from the surface and the fraction of segments in each layer, derive from $P(i,s)$. The partition function and thermodynamic properties depend on the eigenvalues of **W** (Flory, 1969). In the limit $n \to \infty$, calculation of thermodynamic functions simplifies because one eigenvalue, denoted by Λ, dominates the free energy per segment,

$$a = -kT\ln(\Lambda), \tag{43}$$

and the entropy per segment,

$$s = k\frac{\partial}{\partial\chi_s}\left[\chi_s \ln(\Lambda)\right]. \tag{44}$$

Locating a second adsorbing surface at layer $i = m$ indicates $a = a(m)$; the force between the surfaces

$$-\frac{da(m)}{dm} = a(m) - a(m+1) = -kT\ln\left[\frac{\Lambda(m)}{\Lambda(m+1)}\right] \tag{45}$$

is negative for attraction.

DiMarzio and Rubin's predictions (Rubin, 1965; DiMarzio and Rubin, 1971) confirm earlier results (Hoeve *et al.*, 1965; Silberberg, 1967; Roe, 1965, 1966) and provide new ones. The entropy per segment is zero for $\chi_s < \chi_{sc}$, but decreases considerably as chains lose configurational freedom upon adsorption for $\chi_s > \chi_{sc}$. The force between surfaces is monotonically repulsive for $\chi_s < \chi_{sc}$ and increases as χ_s decreases. For $\chi_s > \chi_{sc}$, monotonic attraction is predicted, although its strength at fixed separation passes through a maximum and then falls as χ_s increases. These predictions, however, do not allow for exchange of polymer with the bulk solution.

The most significant aspect of this work is the opportunity for extension afforded by the matrix formalism. DiMarzio (1965) and Rubin (1965) suggested incorporating excluded volume by multiplying each row of **W** by a factor $e^{\beta U(i)}$ where $U(i)$, the potential energy of segments in layer i, includes the energy of segment–segment, segment–solvent, and segment–surface interactions. In turn, the spatial distributions of these interactions depend on the overall configuration of chains in the adsorbed layer to be calculated from **W**. The coupling between the configuration probability and the hypothetical potential field is the central idea in contemporary SCF models discussed in the next section.

Other lattice models are noteworthy as well. Roe (1974), for instance, developed a statistical mechanical formulation for an adsorbed layer capable of exchanging polymer and solvent with the bulk solution. The grand canonical ensemble, first introduced by DiMarzio and Rubin (1971),

ensures an equilibrium distribution of polymer and solvent. Segment–solvent contacts, each having an energy characterized by the Flory–Huggins parameter χ, are counted within a mean-field approximation based on a random distribution of segments and solvent in each layer. The purely configurational part of the partition function closely follows Flory's derivation of the entropy of mixing polymer with solvent in bulk solutions, thereby consistently describing excluded volume in adsorbed layers and in bulk solutions.

In addition to the assumptions inherent in the Flory–Huggins theory, Roe and others introduced another approximation. In general, the distribution of segments depends on spatial position as well as contour location or rank within the chain. Roe (1974) neglected the latter dependence, making all segments equivalent to middle segments and precluding the treatment of tails and other end effects. This approximation was obscured by Roe's focus on volume fractions rather than chain configurations. The models of Helfand (1975a, 1976; Weber and Helfand, 1976) for bulk polymer interfaces rely directly on statistical analysis of configuration probability while incorporating the Flory–Huggins theory for chain entropy. Likewise, Levine *et al.* (1978) treated solvency and excluded volume by analogy with polymer-solution theory within the matrix formalism of DiMarzio and Rubin (1971). These efforts also ignore the influence of segmental rank within the chain on the spatial distribution of segments, a limitation overcome in contemporary adsorption models discussed later.

D. Scaling and Renormalization Group Theories

1. *Self-Similarity*

Several complementary approaches, roughly paralleling those for polymer solutions, have emerged for modelling polymer adsorption. The introduction of scaling concepts (de Gennes, 1981) has stimulated considerable discussion (Fleer *et al.*, 1988) concerning the applicability of this method relative to traditional mean-field theories. Renormalization group theory may help resolve this question, but the technique has only recently yielded results (Eisenriegler, 1985; Nemirovsky and Freed, 1985).

The scaling analysis of long flexible chains in a good solvent in contact with a surface (de Gennes, 1981; for reviews see Cohen Stuart *et al.*, 1986; de Gennes, 1987; Fleer *et al.*, 1988) relies heavily on the solution results introduced earlier. An adsorbed layer can be pictured as a transient network of entangled chains (de Gennes, 1981) with correlation length ξ which varies with z, the distance from the surface. Since ξ and z are the only length scales in the problem, dimensional analysis requires that $\xi \approx z$, making the adsorbed layer

"self-similar." Thus, the volume fraction must satisfy $z \approx \xi[\varphi(z)] \approx l\varphi^{-3/4}$ so that

$$\varphi(z) \approx \left[\frac{z}{l}\right]^{-4/3} \tag{46}$$

results as the fundamental scaling prediction. Note that the functional form of Eq. (46) is independent of the segment–surface interaction potential.

Of course, the self-similarity of the layer has limits. The correlation length cannot exceed that in bulk solution; as z increases, $\xi \to \xi_b \approx l\varphi_b^{-3/4}$. Distances $z > \xi_b$ thus define the "distal" region where $\varphi(z)$ decays exponentially (de Gennes, 1981). The lower bound on Eq. (46) is set by a length D that depends on the adsorption energy. For $z < D$ (defining the "proximal" region), the adsorption energy influences $\varphi(z)$. Scaling analyses for the proximal region have appeared (Eisenriegler *et al.*, 1982; Eisenriegler, 1983; de Gennes and Pincus, 1983). At such small length scales, surface roughness or molecular effects may also enter (Cohen Stuart *et al.*, 1986) when adsorption is strong. Universal behavior, though, is expected in the "central" region $D < z < \xi_b$ governed by Eq. (46).

2. *Adsorbed Amount and Free Energy*

The remaining problem is to determine D or, alternately, the apparent surface volume fraction φ_s. De Gennes (1981) originally conjectured that $D \approx \xi(\varphi_s) \approx l\varphi_s^{-3/4}$, but subsequent work by Eisenriegler *et al.* (1982; Eisenriegler, 1983) leads to $D \approx l\varphi_s^{-1}$ (de Gennes and Pincus, 1983) as supported by Monte Carlo simulations and exact enumerations (Ishinabe, 1982). D (or φ_s) may now be fixed by minimizing the layer's free energy.

The free-energy density of the inhomogeneous system may be expanded in powers of $\nabla\varphi, \nabla^2\varphi, \ldots$, with the first term representing the free energy needed to create a unit volume of solution at φ from a reservoir at φ_b (Cahn and Hilliard, 1958; Cahn, 1977; Widom, 1979). Integration over z gives the surface tension γ (free energy per unit area of interface) in the form (Cahn, 1977)

$$\gamma = \gamma_d(\varphi_s) + I[\varphi_s, \varphi_b] \tag{47}$$

where γ_d accounts for segment–surface interactions and I is an integral measure of the energy penalty associated with maintaining the composition gradient of the layer. Next, γ_d is expanded as

$$\gamma_d = \gamma_0 + \gamma_1\varphi_s + O(\varphi_s^2) \approx \gamma_0 + \gamma_1\left[\frac{D}{l}\right]^{-1}, \tag{48}$$

with $\gamma_1 < 0$ for adsorption; truncation at $O(\varphi_s)$ assumes $|\gamma_1|l^2/kT = \chi_s \ll 1$, i.e., weak segment–surface interactions. Since contributions to the free energy due

to the composition gradient are greatest near the surface, de Gennes (1981; de Gennes and Pincus, 1983) assumed $I[\varphi_s, \varphi_b] \approx I(\varphi_s)$ and, with Eq. (12), integrated over a thickness comparable to D to obtain

$$I(\varphi_s) \approx \int_0^D \frac{kT}{\xi^3(\varphi_s)} dz \approx \frac{kT}{D^2}. \tag{49}$$

Combining Eqs. (47)–(49) and minimizing with respect to D yields

$$\frac{D}{l} \approx \left[\frac{|\gamma_1| l^2}{kT}\right]^{-1} = \chi_s^{-1}, \tag{50}$$

indicating that $D > l$ for $\chi_s < 1$.
Integrating Eq. (46) gives the adsorbed amount of polymer as

$$\Gamma \equiv \int_0^\infty \frac{\varphi(z)}{l^3} dz \approx \frac{1}{l^2}\left[\frac{l}{D}\right]^{1/3} \approx \frac{1}{l^2}\left[\frac{|\gamma_1| l^2}{kT}\right]^{1/3} \tag{51}$$

in units of monolayers (i.e., number of segments per segment area). For γ_1 not too small, Γ is $O(1)$ and independent of φ_b and n; mean-field theories predict qualitatively similar behavior for $v > 0$ and $n \to \infty$, where scaling is valid.

A subsequent analysis (de Gennes, 1982) provides the scaling form of the interaction potential between planar adsorbed layers at separation h and highlights the question of equilibrium. For $h \gg D$ and full equilibrium, i.e., polymer in the gap freely exchanging with the bulk solution,

$$\varphi(h/2) \approx \left[\frac{l}{h}\right]^{4/3}$$

and

$$\Pi(h/2) \approx \frac{kT\varphi^{9/4}}{l^3} \approx \frac{kT}{h^3}$$

from Eq. (46) and Eq. (12). Variations of Eq. (47), $\delta\gamma/\delta h$, include contributions from the change of integration limits in $I[\varphi_s, \varphi_b]$ and from variations in the profile $\varphi(z)$. Neglecting the latter, de Gennes finds an attractive interaction potential

$$\frac{\Delta A(h)}{l^2} \approx -\int_h^\infty (h'/2)\, dh' \approx \frac{-kT}{h^2}.$$

On the other hand, holding the adsorbed amount Γ constant introduces a constraint that is incorporated in the minimization of γ through a Lagrange multiplier. Although the details of the original analysis (de Gennes, 1982) are not completely correct (de Gennes and Pincus, 1983), the resulting repulsion $\Delta A(h)/l^2 \approx kT/h^2$ is universal for $h \gg D$ and this "restricted" equilibrium

condition that allows relaxation of chains within the layer but no exchange with the bulk solution. Scaling analyses do not predict attraction and repulsion in the same potential curve.

3. *Comparison with Scattering Measurements*

Neutron-scattering experiments allow a direct test of Eq. (46) for polymer layers on an adsorbent having a high surface area-to-volume (S/V) ratio. The tendencies of the adsorbent, solvent, and polymer to scatter neutrons (also known as the "contrast" relative to background noise) are adjusted through the isotopic compositions of the components. Scattering theory (Cebula *et al.*, 1978; Auvray and Cotton, 1987; Cosgrove *et al.*, 1987a) relates the measured intensity to "structure factors" which characterize the density profiles in the system.

Matching the contrasts of the adsorbent and solvent enables detection of the structure factor S_{pp} for polymer–polymer correlations within the adsorbed layer, defined by

$$S_{pp}(q) \equiv 2\pi\left[\frac{S}{V}\right] q^{-2} \left| \int_0^\infty \langle \varphi(z) \rangle e^{iqz}\, dz \right|^2 + \tilde{S}_{pp}, \tag{52}$$

where $q = 4\pi/\lambda \sin(\theta/2)$, λ is the neutron wavelength, θ is the scattering angle, $\langle \varphi \rangle$ denotes the average of φ over directions parallel to the surface, and $\tilde{S}_{pp}$ is a contribution due to fluctuations of φ about $\langle \varphi \rangle$. The data of Auvray and Cotton (1987) (Fig. 9), for poly(dimethylsiloxane) (PDMS) adsorbing on silica

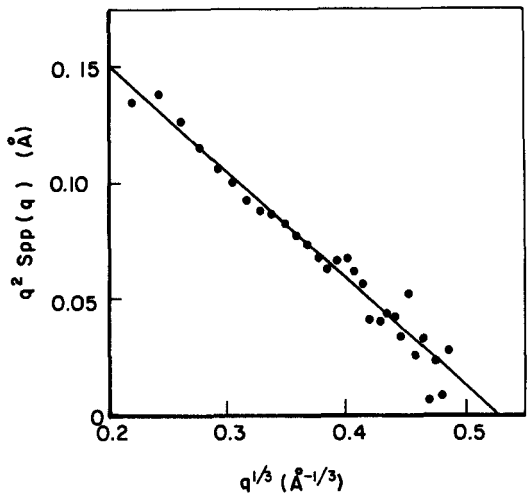

FIG. 9. Structure factor for polymer–polymer correlations plotted as $q^2 S_{pp}(q)$ vs. $q^{1/3}$, for PDMS adsorbing on silica from cyclohexane (Auvray and Cotton, 1987).

in cyclohexane, confirms the scaling prediction

$$S_{pp}(q) \approx (ql)^{1/3}, \tag{53}$$

derived from Eqs. (46) and (52) by Auvray and de Gennes (1986). Concentration fluctuations, which produce $\tilde{S}_{pp} \approx (ql)^{2/3}$, are not observed on the large length scales (small q values) probed by the experiment.

Adjusting the contrast difference between the adsorbent and the solvent away from zero (Cebula *et al.*, 1978) reveals the structure factor

$$S_{pg}(q) = 2\pi\left[\frac{S}{V}\right] q^{-3} \int_0^\infty \langle \varphi(z) \rangle \sin(qz)\, dz \tag{54}$$

for adsorbent–polymer correlations. Combining Eq. (54) and Eq. (46) yields

$$S_{pg}(q) \approx (ql)^{-8/3} \tag{55}$$

as the scaling prediction; Fig. 10 hows the corresponding data of Auvray and Cotton (1987). For several reasons, unambiguous measurement of S_{pg} is difficult and entails considerable experimental error (Auvray and Cotton,

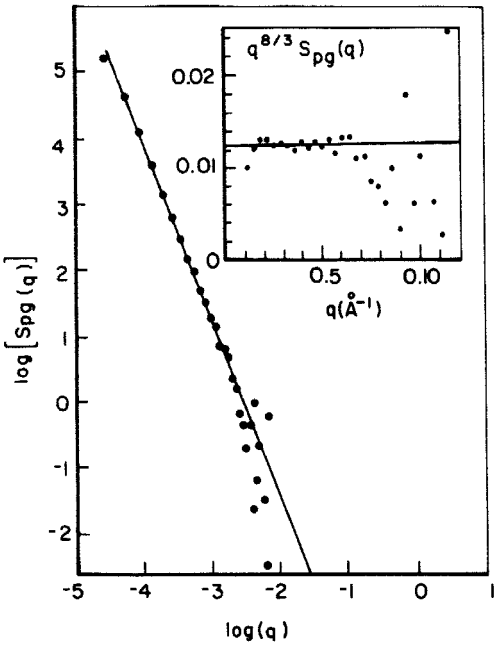

FIG. 10. Structure factor for polymer–adsorbent correlations plotted on a log–log scale, and as $q^{8/3}S_{pg}(q)$ vs. q in the inset, for PDMS adsorbing on silica from cyclohexane (Auvray and Cotton, 1987).

1987; Cosgrove *et al.*, 1987b); still, the data apparently exhibit the $q^{-8/3}$ trend.

Other neutron-scattering data, for poly(ethylene oxide) (PEO) adsorbing on deuterated polystyrene latex in water (Cosgrove *et al.*, 1987a,b), clearly *do not* show scaling behavior. Schaefer's (1984) analysis indicates that solutions of very flexible polymers, such as PDMS, have a large semidilute-good regime in which scaling is valid, whereas solutions of slightly stiffer and much shorter chains, such as PEO, are more aptly modelled by mean-field theory for moderate φ. Thus the T-c diagrams, though qualitative, do suggest a rationalization of these two sets of otherwise conflicting polymer adsorption data.

4. *Renormalization Group Approaches*

Recent efforts have capitalized on analogies with other critical phenomena in applying RG methods to polymer adsorption and depletion. Eisenriegler *et al.* (1982) consider isolated chains in both theta and good solvents but only for adsorption energies near the critical value. Eisenriegler (1983, 1984, 1985) extended the analysis to semidilute solutions contacting a surface with an arbitrary affinity for segments. Explicit functional forms for $\varphi(z)$, $\varphi(0)$, and Γ emerge, although the crossover behavior between theta and good solvent conditions is not detailed. In general, Eisenriegler's results verify the scaling predictions, most notably Eq. (46), and introduce several new predictions including the scaling form of the surface tension.

Freed's criticism (1987) of the magnet analogy, which also applies to scaling theory, concerns the inability of these methods to predict the molecular weight dependence of properties such as the mean layer thickness. Nemirovsky and Freed (1985) calculated layer properties via the "conformation–space" RG method developed for polymer solutions (Freed, 1987). The chain partition function and moments of the vector between chain ends, evaluated for theta and good solvent conditions, provide the crossover behavior for surface affinities ranging from strong repulsion to moderate attraction. However, the complexity of the analysis, especially the notation, makes assessment of the results difficult. Other efforts (Douglas *et al.*, 1986, 1987) are primarily concerned with polymer interacting with penetrable surfaces.

E. The Scheutjens-Fleer Lattice Model

1. *Motivation and Formulation*

Each of the lattice models reviewed in the previous section introduces important concepts but fails to describe adsorbed layers satisfactorily over a

wide range of conditions. The most complete synthesis to date is the model of Scheutjens and Fleer (SF) (Scheutjens and Fleer, 1979, 1980, 1985; Fleer and Scheutjens, 1986; see also the discussion following Levine *et al.*, 1978). The SF model implements DiMarzio and Rubin's (1971) suggestion that the probability of each step in the chain's random walk should depend on a local potential field which accounts for all interactions. This mean field is averaged parallel to the surface and neglects correlations between segments. Like Roe's model (1974), the SF model resides in the grand canonical ensemble, permitting the exchange of polymer and solvent with bulk solution. Their free energy minimization with respect to a function measuring the probability of chain configurations is equivalent to Helfand's (1975c) method for establishing the "self-consistent" mean field.

The many reviews of the SF model (Tadros, 1982, 1985; Takahashi and Kawaguchi, 1982; Fleer and Lyklema, 1983; Cohen Stuart *et al.*, 1986; Fleer *et al.*, 1988; Fleer, 1988) reflect both the importance of polymer adsorption and the ability of the SF model to predict many features of adsorbed layers for wide ranges of polymer molecular weight, bulk solution concentration, solvent quality, and adsorption energy.

As in earlier lattice models, the solution is divided into layers of lattice sites parallel to the surface, labeled $i = 1, 2, \ldots$, having fractions λ_1 of nearest neighbors in each adjacent layer and $\lambda_0 = 1 - \lambda_1$ in the same layer, respectively. As in Flory–Huggins solution theory (see section II.D), all sites are occupied by either a solvent molecule or a chain segment, and every chain contains r sequential segments numbered $s = 1, 2, \ldots, r$. A function $P(i, s)$ specifies the unnormalized probability that any subchain of $s \leq r$ contiguous segments ends in layer i. In the bulk, all configurations are equivalent so that $P(i, s) \to 1$ as $i \to \infty$. The "initial" condition $P(i, 1)$ represents the probability of finding a subchain of length 1, i.e., individual segments, in layer i. Following the development of DiMarzio and Rubin (1971), $P(i, s)$ is constructed recursively from

$$P(i, s) = P(i, 1)[\lambda_1 P(i - 1, s - 1) + \lambda_0 P(i, s - 1) + \lambda_1 P(i + 1, s - 1)] \quad (56)$$

beginning with $P(i, 1)$. The term in brackets is the probability that a subchain of $s - 1$ segments ends at a site adjacent to the sth segment; multiplication by $P(i, 1)$ accounts for the likelihood of finding a segment at the site of interest.

Although DiMarzio and Rubin (1971) assumed $P(i, 1) \equiv 1$ for $i > 1$, the actual value depends on the mean field $U(\varphi_i)$ through

$$P(i, 1) \equiv e^{-\beta[U(\varphi_i) - U(\varphi_b)]} \quad (57)$$

where φ_i and φ_b indicate the segment volume fractions in layer i and in bulk solution. The appropriate form of $U(\varphi_i)$ minimizes the free energy of the layer and, therefore, produces the equilibrium distribution of chain configurations.

The form derived by Scheutjens and Fleer (1979) depends on the Flory–Huggins expression for the free energy of a solution [Eq. (22)]. The Helfand (1975b) SCF [Eq. (39)] can incorporate any equation-of-state; indeed, supplementing Eq. (22) by a term accounting for adsorption energy and substituting into Eq. (39) produces

$$\beta U(\varphi_i) = -\ln(1-\varphi_i) - 2\chi\langle\varphi_i\rangle - \delta_{i,1}(\chi_s + \lambda_1\chi), \tag{58}$$

as derived by Scheutjens and Fleer (1979). Note that $\chi_s > 0$ for adsorption and $\delta_{i,1} = 1$ if $i = 1$, and $\delta_{i,1} = 0$ if $i > 1$;

$$\langle\varphi_i\rangle \equiv \lambda_1\varphi_{i-1} + \lambda_0\varphi_i + \lambda_1\varphi_{i+1} \tag{59}$$

accounts for nonlocal segment–solvent interactions. Equation (57) then provides

$$P(i,1) = \frac{1-\varphi_i}{1-\varphi_b}\exp[\delta_{i,1}(\chi_s + \lambda_1\chi) + 2\chi(\langle\varphi_i\rangle - \varphi_b)] \tag{60}$$

as the initial condition for Eq (56).

Now, the system of equations must be closed by relating φ_i to $P(i, s)$. Since every segment within a chain of total length r also belongs to two "subchains" of lengths s and $r - s + 1$, the volume fraction is proportional to the joint probability of the two subchains meeting in layer i summed over all contour locations within the chain,

$$\varphi_i = \frac{\varphi_b}{P(i,1)r}\sum_{s=1}^{r} P(i,s)P(i,r-s+1), \tag{61}$$

where the denominator eliminates the double counting of the junction segment. Note that as $i \to \infty$, $\varphi_i \to \varphi_b$ as required.

Given the lattice parameters λ_1, λ_0 and the physical parameters r, φ_b, χ, and χ_s, Eqs. (56), (60), and (61) form a closed system that, when solved numerically, completely describes an adsorbed polymer layer. From φ_i, simple calculations give the adsorbed amount

$$\varphi_{ads} = \sum_{i=1}^{\infty}[\varphi_i - \varphi_b], \tag{62}$$

the surface coverage φ_1, the bound fraction $p = \varphi_1/\varphi_{ads}$, and higher moments of φ_i corresponding to various integral measures of the layer thicknesses. The statistics of trains, loops, and tails (including their relative numbers, length distributions, etc.) follow from $P(i, s)$ with minor computational effort. Evaluation of the partition function produces the surface tension of the layer. Calculation of the hydrodynamic thickness (Cohen Stuart *et al.*, 1984c) requires an additional constitutive relation for the permeability of the

adsorbed layer as a function of φ_i plus solution of the equations governing creeping flow. Placement of a second adsorbing surface at $i = m$ allows the formation of bridge sequences and alters the distribution of trains, loops, and tails. The interaction potential between the surfaces simply equals the difference between the surface tensions at separations of m and $m = \infty$.

2. *Structure of Adsorbed Layers*

Extensive results have been presented in the numerous papers and reviews cited earlier. In general, φ_i decreases steeply within a few layers near the surface followed by a gradual asymptote to φ_b. Fig. 11 (Scheutjens and Fleer, 1980) shows a typical plot of $\log(\varphi_i)$ vs. i, which highlights interesting features away from the surface. Apparently, φ_i decays as the sum of two exponentials with characteristic decay lengths that differ for low and high i. Segments in loops dominate near the surface but become less important as i increases. The density of tail segments reaches a maximum near the surface and dominates the profile at large i. Segments in nonadsorbed chains (not shown) are depleted near the surface; $\varphi_i \to \varphi_b$ at roughly $i \approx r^{1/2}$. Comparisons of predicted profiles and those obtained through neutron scattering (Cosgrove *et al.*, 1987b) indicate qualitative agreement of the general features.

The distribution of segments in trains, loops, and tails depends on all of the experimental variables. Typically, as χ_s increases, the fraction of segments in trains increases while the fractions in loops and tails decrease. The opposite trends are noted as φ_b and r increase, although the competition *between* loops and tails is more complex. For example, Fig. 12 (Cohen Stuart, 1980) shows that as r grows, most segments reside in loops and tails, although the tail fraction falls slightly at high r. In most cases of practical interest, from 10% to

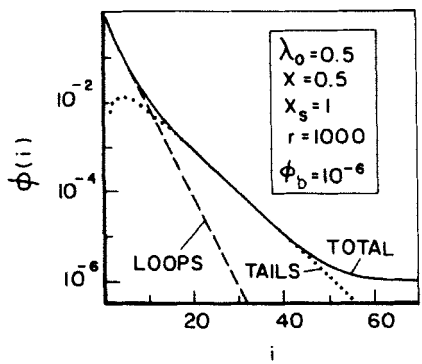

FIG. 11. Polymer volume-fraction profiles calculated by Scheutjens and Fleer (1980) and plotted as $\log(\varphi_i)$ vs. i. Parameters are given in the inset.

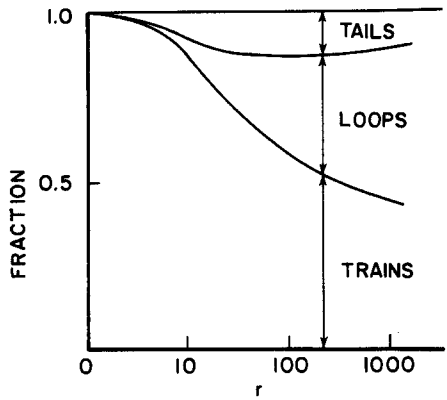

FIG. 12. Percentages of segments contained in trains, loops, and tails as a function of chain length, r, for a typical (but unspecified) set of parameters (Cohen Stuart, 1980).

25% of the segments in adsorbed chains are in tails; this value can rise as high as 67% for bulk polymer in contact with a surface.

At low values of φ_b, adsorption isotherms (φ_{ads} vs. φ_b) from the SF model rise steeply to an apparent plateau. A gradual rise in φ_{ads} continues as $\log(\varphi_b)$ increases over several decades. Most experimental adsorption isotherms for monodisperse polymer (Takahashi and Kawaguchi, 1982; Cohen Stuart *et al.*, 1986) exhibit the same trends.

Several reviews (e.g., Takahashi and Kawaguchi, 1982; Cohen Stuart *et al.*, 1986) discuss the extensive experimental data and the predictions of the SF model for the variation of φ_{ads} with polymer molecular weight. In general φ_{ads} increases linearly with $\log(r)$ for adsorption from a theta solvent, but is less in a good solvent, and appears to be limited at high r. Proper selection of parameters in the model produces excellent agreement with experimental data (Fig. 13) for both φ_{ads} and p.

Two measures of the layer thickness have been widely reported (Takahashi and Kawaguchi, 1982; Cohen Stuart *et al.*, 1986). The root–mean–square layer thickness, defined through

$$t_{rms}^2 \equiv \frac{1}{\varphi_{ads}} \sum_{k=0}^{\infty} i^2 \varphi_i, \tag{63}$$

can be compared with the thickness measured by ellipsometry. For theta solvents, Scheutjens and Fleer (1979) find $t_{rms} \approx r^{1/2}$, in agreement with other theories (Section II,C) and considerable experimental data. Experiments reveal $t_{rms} \approx r^{0.4}$ in good solvents, in accordance with the theory, but indicate

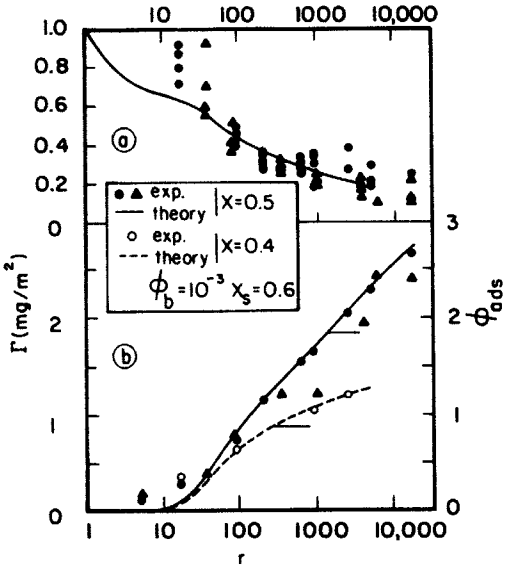

FIG. 13. Comparison of measured and calculated bound fraction (a) and adsorbed amount (b) as functions of chain length, r. The left ordinate in (b) applies to experimental points: Full circles and open circles denote PS/silica/cyclohexane and PS/silica/CCl_4 (vander Linden and van Leemput, 1978); triangles denote PS/silica/cyclohexane (Kawaguchi *et al.*, 1980). The right ordinate applies to values calculated by Fleer and Scheutjens (1982a) for $\lambda_0 = 0.5$, $\chi = 0.50$ (full curves) and $\chi = 0.40$ (dashed curve); other parameters are given in the inset.

greater layer thicknesses than in a theta solvent, though the SF model predicts the opposite.

The hydrodynamic thickness, t_{hd}, is most significant for colloidal particles bearing adsorbed polymer. Theoretical calculations (Cohen Stuart *et al.*, 1984c; Anderson and Kim, 1987) model the adsorbed layer as a porous medium with spatially-varying permeability and assume that the flow of solvent through the adsorbed layer does not perturb the layer structure. The predictions of the SF model and data for the PEO–polystyrene latex–water system (Figs. 14 and 15) (Cohen Stuart *et al.*, 1984c) agree very well and indicate $t_{hd} \approx r^{0.8}$. The results vary little with χ and χ_s but require specification of the hydrodynamic drag associated with each segment. Reasonable values (e.g., a segmental drag equal to that of a sphere of comparable size) produce qualitatively correct behavior.

3. *Interactions Between Layers*

The interaction between adsorbed polymer layers is an important component of the total potential between colloidal particles. For collisions between

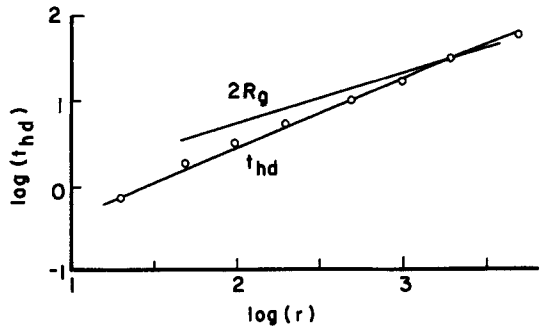

FIG. 14. Dimensionless hydrodynamic thickness vs. chain length, on a log–log scale as calculated from the SF model (Cohen Stuart *et al.*, 1984c) for $\chi_s = 1, \chi = 0.45, \varphi_b = 10^{-4}, \lambda_0 = 0.5$, and friction per segment equivalent to a Stokes sphere of diameter $l/36$. The isolated coil diameter $2R_g = 0.17n^{0.6}$ is also shown.

polymer-coated particles, several timescales are important (de Gennes, 1982) for polymer adsorption, rearrangement of the chains on the surface, and desorption during a collision. Desorption during the short interval of a collision seems unlikely, suggesting that φ_{ads} remains constant. Scheutjens and Fleer (1985; Fleer and Scheutjens, 1982b, 1986) contrasted interaction potentials for the cases of full and restricted equilibrium.

The free energy of the two surface system is calculated from the partition function expressed in terms of Flory–Huggins solution theory. The Helmholtz free energy per site, relative to pure solvent, and at constant φ_{ads} is

$$\frac{A}{kT} = \frac{2\gamma}{kT} + \frac{\mu_p}{rkT} \sum_{i=1}^{m} \varphi_i \tag{64}$$

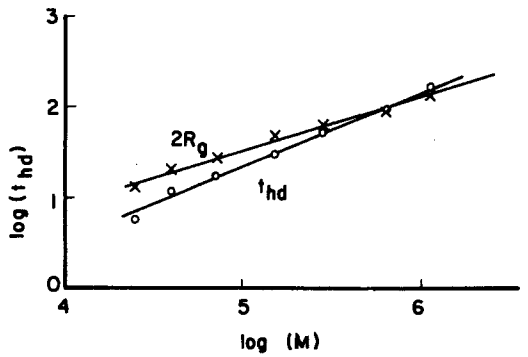

FIG. 15. Hydrodynamic thickness (in nm) vs. M, on a long–log scale, for PEO adsorbing on PS latex from water as measured by Cohen Stuart *et al.* (1984c). The isolated coil diameter is also shown.

with

$$\frac{2\gamma}{kT} = \sum_{i=1}^{m} \left\{ (1 - 1/r)(\varphi_i - \varphi_b) + \ln\left[\frac{1 - \varphi_i}{1 - \varphi_b}\right] + \chi[\varphi_i \langle \varphi_i \rangle - \varphi_b^2] \right\} \quad (65)$$

as the surface energy. Holding φ_{ads} constant implies that the chains' chemical potential

$$\frac{\mu_p}{kT} = 1 - \varphi_b^* - r(1 - \varphi_b^*) + \ln(\varphi_b^*) + r\chi(1 - \varphi_b^*)^2 \quad (66)$$

must vary with gap width m. The quantity

$$\varphi_b^* \equiv \frac{\sum_{i=1}^{m} \varphi_i}{\sum_{i=1}^{m} P(i, r)} \quad (67)$$

is the polymer volume fraction in a hypothetical bulk solution in equilibrium with the solution in the gap. The dimensionless interaction potential energy for restricted equilibrium,

$$V(m) = \frac{1}{kT}[A(m) - A(\infty)], \quad (68)$$

includes both the surface energy and the change in the chemical potential.

Interaction potentials for full equilibrium are always monotonically attractive. Restricted equilibrium (Fig. 16) produces more interesting behavior, with the character depending primarily on φ_{ads} and χ. Variations of χ_s and r certainly influence the results, but low concentrations of long chains or high concentrations of short chains give roughly the same adsorbed amount and interaction potential. At high φ_{ads}, the layers repel each other monotonically, suggesting "steric" stabilization; low φ_{ads} produces an attraction, perhaps due to "bridging." Figure 17 shows the maximum depth of the attraction as a function of φ_{ads} and χ.

Fleer and Scheutjens (1986) calculate the variation of the distribution of trains, loops, tails, and bridges with separation of the two surfaces. As one might expect, compression of the layers enhances the fractions of segments in trains and bridges at the expense of loops and tails. However, the existence and strength of attraction and repulsion have not been correlated with the fractions of segments in the various chain configurations.

Force measurements between polymer-coated mica surfaces exhibit many of the features predicted by the SF model. The force measurement technique characterizes the interaction between polymer layers and provides an indirect

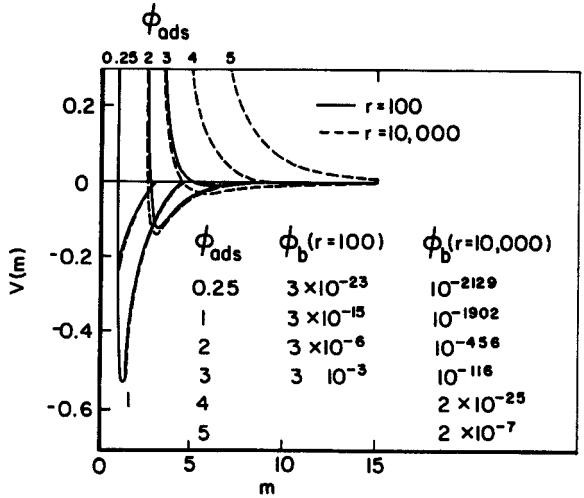

FIG. 16. Interaction potential energy between adsorbed layers vs. separation under conditions of restricted equilibrium as calculated by Scheutjens and Fleer (1985). Various adsorbed amounts are achieved for two chain lengths by varying bulk solution concentration when the surfaces are well separated; the necessary φ_b for each curve are given in the table. Other parameters include $\chi_s = 1$, $\chi = 0.5$, and $\lambda_0 = 0.5$.

measure of layer thickness. The apparatus, originally developed by Tabor and Winterton (1969), has been used extensively for investigation of van der Waals forces *in vacuo*, electrostatic forces in aqueous media, and hydration and structural forces due to ordering of solvent molecules near the surfaces. A

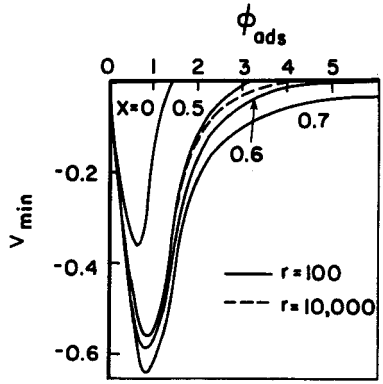

FIG. 17. Depth of the attractive minimum vs. adsorbed amount for various χ parameters and two chain lengths, as calculated by Scheutjens and Fleer (1985). No minimum implies that only repulsion is predicted.

review of these studies as well as references are provided by Russel (1987) together with references providing details of the construction and operation of the apparatus.

In all cases, the surfaces are molecularly smooth sections of cleaved mica in a crossed cylinder configuration within a thermostatted bath containing the solution of interest. The separation between the cylinders is measured with high accuracy through multiple beam interferometry. Both cylinders are attached to micrometer-driven mounts, but one of the surfaces is connected through a system of springs. Knowing the force constants of the springs, one can calculate the force between the surfaces from their separation.

In good solvents with high adsorbed amounts, PEO layers repel each other monotonically (Klein and Luckham, 1984a,b; Luckham and Klein, 1985). For strong adsorption, but low φ_{ads}, attraction is observed. To demonstrate this, Almog and Klein (1985) imposed diffusional resistances to restrict the amount of polystyrene adsorbing from cyclopentane. The attractive minima in the resultant force curves (Fig. 18) are deepest for low φ_{ads} and eventually disappear as more polymer is allowed to adsorb. Since dispersion forces are negligible in this case, only bridging can account for attraction. Similar behavior occurs with weak adsorption in slightly better-than-theta solvents (Israelachvili *et al.*, 1984). In poor solvents (Klein, 1982, 1983), strong attraction can be ascribed to the preference of segments for other segments rather than solvent. The same features, for all solvent conditions, have been predicted by the SF model (Figs. 16 and 17) (Scheutjens and Fleer, 1985; Fleer and Scheutjens, 1986).

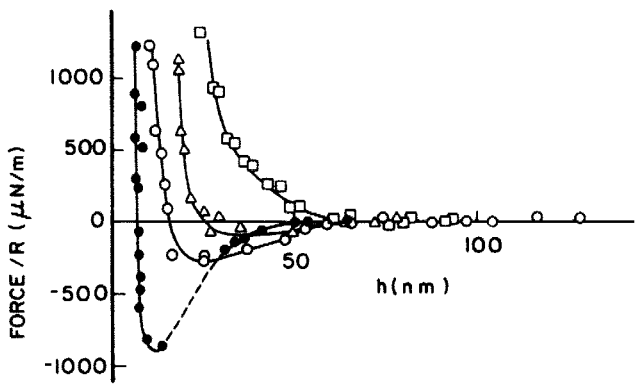

FIG. 18. Interaction potential energy (converted to a potential between planes) vs. separation between two mica surfaces bearing adsorbed polystyrene (2×10^6 g/mol) in cyclopentane, a good solvent (Almog and Klein, 1985). Full circles, open circles, triangles, and squares correspond to increasing adsorbed amounts achieved by incubating the surfaces at close separation for increasing intervals of time.

4. *Conclusions*

The SF model succeeds for several reasons. First, the model treats a wide range of experimental conditions without a priori assumptions about the configuration of the polymer molecules in the adsorbed layer, enumerating the statistical distribution of trains, loops, and tails to highlight the influence of particular configurations, especially tails, on experimentally observable quantities. The results indicate a relative surplus of chain ends far from the surface and depletion of ends near the surface. This conclusion agrees with earlier results of Chandrasekhar (1943) and Hesselink (1969, 1971), that adsorbed chains prefer long-tail–short-loop configurations rather than short-tail–long-loop configurations. These "end effects" significantly affect t_{hd} (Cohen Stuart *et al.*, 1984c; Cosgrove *et al.*, 1984) and forces between interacting adsorbed polymer layers (Scheutjens and Fleer, 1985; Fleer and Scheutjens, 1986). Extensions to polydisperse polymer and polyelectrolyte adsorption have been made and are reviewed by Fleer (1988).

On the other hand, the SF model is limited in several respects. The finite-difference form of the model facilitates numerical solution but obscures some of the underlying physics. The artificial discretization of space, necessitating the selection of λ_0 and λ_1 to characterize the lattice geometry, may not accurately reflect the reality of continuous space. Although the lattice parameters have little qualitative influence on the results (Domb, 1963), the quantitative changes significantly affect comparisons with experimental data. On a more practical level, the lattice model calculations become time consuming for long chains, especially for $n > 1000$.

F. Self-Consistent Field Theory

1. *Motivation and Formulation*

The SCF [Eq. (31)] forms the basis for many theories of polymers at surfaces (Dolan and Edwards, 1974, 1975; Jones and Richmond, 1977; Levine *et al.*, 1978; Joanny *et al.*, 1979; de Gennes, 1979) and bulk polymer interfaces (Helfand and Sapse, 1975, 1976; Helfand, 1975b,c; Helfand and Wasserman, 1976; Hong and Noolandi, 1981). In fact, the recursion relation in Eq. (56) of the SF model is simply a finite-difference form of Eq. (31); expanding $P(i+1, s-1)$, $P(i, s-1)$, and $P(i-1, s-1)$ in i and s, rearranging, and using the identity in Eq. (57) demonstrates the equivalence. The versatility and predictive ability of the SF model suggests trying to circumvent that model's limitations and extract more physical insight by reverting to the partial differential in Eq. (31). The field equation formulation allows the use of any equation-of-state, brings to bear a variety of solution techniques, and permits extensions to important related problems.

The complete formulation includes Eqs. (31)–(33); the SCF of Eq. (39); an equation-of-state relating the local free-energy density to the volume fraction; and boundary conditions at the surface and in bulk. Unfortunately, the discussion of Section II demonstrates that no single solution theory accurately describes the thermodynamic properties for all concentrations and temperatures. Thus, specialization to particular solution models is necessary.

In addition, the local free energy density must include the energy of segmental adsorption at the surface. While lattice models simply award an additional energy χ_s to segments in the surface layer, continuum models require an assumption about the range of the potential. Ploehn *et al.* (1988; Ploehn and Russel, 1989) employ a "sticky surface" model (Baxter, 1969) featuring an infinitely deep and narrow attractive well which produces a finite population of segments at $z = 0$. This idealization makes $U(\mathbf{r})$, $G(\mathbf{r}, \mathbf{r}'; s)$, and $\varphi(\mathbf{r})$ discontinuous at the surface $\mathbf{r}_0 = (x, y, 0)$, but expressible as sums of continuous and discontinuous surface functions, i.e.,

$$\begin{aligned} \int G(\mathbf{r}, \mathbf{r}'; s)\,d\mathbf{r}' &\equiv G_c(\mathbf{r}, s) + \delta(\mathbf{r} - \mathbf{r}_0)G_s(s) \\ e^{-\beta U(\mathbf{r})} &\equiv e^{-\beta U_c(\mathbf{r})} + \delta(\mathbf{r} - \mathbf{r}_0)e^{-\beta U_s} \\ \varphi(\mathbf{r}) &\equiv \varphi_c(\mathbf{r}) + \delta(\mathbf{r} - \mathbf{r}_0)\varphi_s. \end{aligned} \tag{69}$$

In this formulation, the starting point of a chain is integrated out for convenience.

The Flory–Huggins equation-of-state (22) provides simple expressions for the SCFs (Helfand, 1975c; Helfand and Sapse, 1975, 1976; Scheutjens and Fleer, 1979; Hong and Noolandi, 1981; Ploehn *et al.*, 1988),

$$\begin{aligned} \beta U_c &= -\ln\frac{(1 - \varphi_c)}{(1 - \varphi_b)} - 2\chi(\varphi_c - \varphi_b), \qquad z \geq 0, \\ \beta U_s &= -\chi_s - \ln\frac{(1 - \varphi_s)}{(1 - \varphi_b)} - 2\chi(\varphi_s - \varphi_b), \qquad z = 0 \end{aligned} \tag{70}$$

but computer simulations suggest that the former severely underestimates the osmotic pressure of chains in a continuum (Okamoto, 1975; Croxton, 1979; Dickman and Hall, 1986), at least for athermal ($\chi = 0$) solutions. For this reason, Ploehn and Russel (1989) formulated an equation-of-state which produces greater repulsion between segments.

Supplementing the entropic repulsion of the Carnahan–Starling (1969) equation with a "van der Waals" attraction leads to the SCF (Ploehn and

Russel, 1989)

$$\beta U_c = -16\alpha(\varphi_c - \varphi_b) + \frac{\varphi_c(8 - 9\varphi_c + 3\varphi_c^2)}{(1-\varphi_c)^3} - \frac{\varphi_b(8 - 9\varphi_b + 3\varphi_b^2)}{(1-\varphi_b)^3} \quad (71)$$

for positions $\mathbf{r} \neq \mathbf{r}_0$. Segments and solvent constrained to the surface interact as two-dimensional entities. Augmenting the equation-of-state of Baram and Luban (1979) for hard discs with a van der Waals-type attraction and extracting the SCF via Eq. (39) gives (Ploehn and Russel, 1988)

$$\beta U_s = -\chi_s + B_0 \ln(1-\varphi_s) + \frac{B_1\varphi_s}{1-\varphi_s} + \sum_{i=2}^{4} B_i(\varphi_s)^{(i-1)}$$

$$- B_0 \ln(1-\varphi_b) - \frac{B_1\varphi_b}{1-\varphi_b} - \sum_{i=2}^{4} B_i(\varphi_b)^{(i-1)} \quad (72)$$

for $\mathbf{r} = \mathbf{r}_0$, where $B_0 = 3.46700$, $B_1 = 5.37944$, $B_2 = 3.67599(1-2\alpha) - 1.91244$, $B_3 = 0.28413$, and $B_4 = 0.016178$. Thus results for two equations-of-state can be compared to assess the influence of the details of segment interactions on the overall layer structure.

The formulation of a proper surface boundary condition is a delicate matter, as noted by DiMarzio (1965) and de Gennes (1969). Lattice models simply require that $P(i, s) \equiv 0$ for layers $i < 0$, a form proven correct by DiMarzio (1965). In continuum models, chains intersecting the surface undergo both "reflection" and "adsorption," the relative amount of each depending on the energy of contact at the surface. The result is a mixed boundary condition expressed by de Gennes (1969) as

$$\frac{1}{G}\frac{\partial G}{\partial z}\bigg|_{z=0} = -k_{ads}(T) \quad (73a)$$

for $\varphi(0) \ll 1$. For stronger adsorption, the mixed boundary condition becomes a nonlinear function of $\varphi(0)$. For example, the recursion [Eq. (56)] of the SF lattice-model applies at the surface $i = 1$ with $P(0, s) \equiv 0$. Expanding $P(2, s-1)$ and $P(1, s-1)$ in Taylor series in i and s produces

$$\frac{P(1,s)}{P(1,1)} = (1-\lambda_1)\left[P - \frac{\partial P}{\partial s}\right] + \lambda_1 \frac{\partial P}{\partial i} \quad (73b)$$

as the continuous space form of their surface boundary condition. Ploehn *et al.* (1988) derived from Eq. (31) a general treatment of the surface region, which reduces to

$$G_c + \delta(z)G_s = e^{-\beta U}\left\{\left[\frac{1}{2} + \frac{1}{4}\mathbf{k}\cdot\nabla\right]\left(G_c - \frac{\partial G_c}{\partial s}\right) + \frac{1}{2}\left(G_s - \frac{\partial G_s}{\partial s}\right)\right\} \quad (74)$$

for $z \ll 1$. Integrating over a small interval of $O(\varepsilon)$ in z and retaining only the $O(1)$ terms, with the condition that G_c and $e^{-\beta U_c}$ vary smoothly at $z = 0$, provides the surface boundary condition

$$G_c e^{\beta U_c} = \frac{1}{2}(K_A + 1)\left[G_c - \frac{\partial G_c}{\partial s}\right] + \frac{1}{4}\mathbf{k} \cdot \nabla G_c,$$

$$G_s = K_A G_c(\mathbf{r}_0, s), \tag{75}$$

with $\mathbf{k}$ a unit vector normal to the surface and

$$K_A \equiv e^{-\beta[U_* - U_c(\mathbf{r}_0)]} \tag{76}$$

defining a partition coefficient relating segments densities at and near the surface. Since Eq. (33) requires

$$\varphi_s = K_A \varphi_c(\mathbf{r}_0), \tag{77}$$

all of the surface functions are defined in terms of their continuous counterparts. The similarity of Eqs. (75) and (73b) alludes to the relationship between adsorption energy (inherent in K_A) and chain flexibility (embodied in the lattice parameter λ_1), as demonstrated earlier by Hoeve *et al.* (1965).

Simple manipulations show that G_c and φ_c satisfy

$$\frac{\partial G_c}{\partial s} = \tfrac{1}{6}\nabla^2 G_c + [1 - e^{\beta U_c}]G_c \tag{78}$$

and

$$\varphi_c(\mathbf{r}) = \frac{c}{Z_A \exp(-\beta U_c)} \int_0^n G_c(\mathbf{r}, s) G_c(\mathbf{r}, n - s)\, ds \tag{79}$$

for $z > 0$; c is a proportionality constant, and Z_A is the configuration integral (defined later). Far from an adsorbing surface, chains have an equal probability of ending anywhere; hence

$$G_c(\infty, s) = 1 \tag{80}$$

merges G_c into the bulk solution. In addition, $\varphi_c(\infty) \to \varphi_b$ and $U_c \to 0$ so that Eq. (79) yields $c = \varphi_b Z_A / n$. In a sense, this procedure includes a chain configuration from bulk solution in the partition function for the adsorbed layer and implies "full" equilibrium between free and adsorbed chains.

Under some conditions, though, an adsorbed layer may not be in full equilibrium with bulk solution. For "restricted" equilibrium, the adsorbed amount of polymer is held constant; adsorbed chain configurations are assumed to be optimally distributed, but only solvent is free to move between the layer and bulk solution. Since Z_A normalizes $G(\mathbf{r}, s)G(\mathbf{r}, n - s)e^{\beta U(\mathbf{r})}$, integration of Eq. (79) with Eq. (69) over $\mathbf{r}$ gives $c = \varphi_{ads}/n$ where φ_{ads} is the

constant adsorbed amount of polymer (defined later). It is convenient to define a new constant $\varphi_b^* \equiv \varphi_b$ for full equilibrium, and $\varphi_b^* \equiv \varphi_{ads}/Z_A$ for restricted equilibrium so that $c = \varphi_b^* Z_A/n$ in all cases.

2. *Ground State Solutions*

Various techniques enable approximate solutions of the closed system of equations; here we specialize for one dimensional variations of layer structure in the direction normal to the surface. Regarding the SCF as an external field, de Gennes (1969, 1979) treated Eq. (78) as a "pseudo-linear" equation de Gennes, 1969, 1979) and expanded G_c in eigenfunctions,

$$G_c(z, s) = \sum_{j=0}^{\infty} g_j(z) \exp(\lambda_j s) \tag{81}$$

with λ_j as the eigenvalues. For large n, the $j = 0$ (ground state) term dominates; this "ground state approximation,"

$$G_c(z, s) = g(z) \exp(\lambda_0 s), \tag{82}$$

is the basis of several analytical solutions (Jones and Richmond, 1977; Joanny *et al.*, 1979; Ploehn *et al.*, 1988).

Further progress requires linearizing $e^{\beta U(z)}$ as

$$e^{\beta U_c} \approx 1 + v\varphi_c + \frac{w}{2}\varphi_c^2, \tag{83}$$

with φ_b assumed to be small so that $\exp[\beta U_c(\varphi_b)] \approx 1$. Retention of the $O(\varphi^2)$ term permits application of Eq. (83) in theta solvents for which $v = 0$. The Flory–Huggins form, [Eq. (70)], yields $v = 1 - 2\chi$, and $w = 2(1 - 2\chi + 2\chi^2)$; the SCF Eqs. (71)–(72) produce $v = 8(1 - 2\alpha)$ and $w = 2[47 + 128\alpha(\alpha - 1)]$. Note that Eqs. (70)–(72) are not expanded at $z = 0$ so that φ_s and φ_c cannot exceed unity there.

Combining Eqs. (79) and (82) gives

$$\frac{\varphi_c(z)}{\varphi_b^*} = \exp(\beta U_c) g^2(z) \exp(\lambda_0 n), \tag{84}$$

and substituting Eqs. (82)–(84) into Eq. (78) produces a nonlinear ordinary differential equation for φ_c. Its solution (Ploehn *et al.*, 1988),

$$\varphi_c(z) = \frac{4\lambda_0 c_i e^{\gamma z}}{(c_i e^{\gamma z} - v/2)^2 - \frac{2}{3}\lambda_0 w} = \frac{4\lambda_0 c_i e^{-\gamma z}}{(c_i - (v/2)e^{-\gamma z})^2 - \frac{2}{3}\lambda_0 w e^{-2\gamma z}}, \tag{85}$$

includes $\gamma = (24\lambda_0)^{1/2}$ as the reciprocal of the profile's decay length and c_i as an integration constant that must be determined from Eq. (70). A normalization condition to be discussed later fixes λ_0.

Unfortunately, the ground state approximation dictates a spatial distribution of segments along the contour of the chain, i.e.,

$$\frac{\varphi_c(z, s)}{\varphi_b^*} \equiv \frac{1}{n} G_c(z, s) G_c(z, n - s) \exp[\beta U_c(z)]$$

$$= \frac{1}{n} g^2(z) \exp(\lambda_0 n) \exp[\beta U_c(z)], \tag{86}$$

which is *independent* of s. As in the lattice models of Roe (1974) and Levine *et al.* (1978), all segments are equivalent. Thus, the ground state solution in Eq. (85) ignores end effects and precludes the prediction of tails. Although the segment density profile yields some of the layer's qualitative features, the calculated values of φ_{ads}, t_{rms}, and t_{hd} fall short of the corresponding experimental quantities.

3. *Matched Asymptotic Expansion*

A more realistic representation of an adsorbed layer recognizes the fundamental differences between the layer structure close to and far from the surface. Such distinctions appear naturally in scaling theory through the proximal and central regions (de Gennes, 1981). In the context of mean-field theory, Scheutjens *et al.* (1986) demonstrated that two eigenfunctions in the solution of Eq. (78) are necessary and sufficient to describe end effects: The ground state eigenfunction dominates near the surface, while the second eigenfunction accounts for bulk solution configurations.

Ploehn and Russel (1989) developed a matched asymptotic solution of Eq. (73) equivalent to a two-eigenfunction approximation for G_c. Near the surface, $\varphi(z)$ is $O(1)$ and Eq. (81) is presumably accurate; adsorption and interchain interactions distort chain configurations so that the characteristic length is l. Far from the surface, chains are ideal and the characteristic length scales as $n^{1/2}l \gg l$. The widely separated length scales enable the "inner" ground state solution to be matched asymptotically to an "outer" solution, yielding a uniform approximation for all z.

Rescaling z and s so that $x = z/n^{1/2}$ and $t = s/n$ converts Eq. (78) to

$$\frac{\partial G_c}{\partial t} = \frac{1}{6} \frac{\partial^2 G_c}{\partial x^2} + n[1 - \exp(\beta U_c)] G_c. \tag{87}$$

Then expanding G_c in a regular perturbation series as

$$G_c = G_0 + \frac{1}{n} G_1 + \cdots, \tag{88}$$

and the SCF as $n(1 - e^{\beta U_c}) \simeq -nv(\varphi_c - \varphi_b)$ produces a hierarchy of

independent partial differential equations, one for each power of $1/n$. Assuming that $nv(\varphi_c - \varphi_b) \ll 1$ reduces the lowest order equation to the diffusion equation,

$$\frac{\partial G_0}{\partial t} = \frac{1}{6}\frac{\partial^2 G_0}{\partial x^2}, \tag{89}$$

expressing the ideal behavior of the outer region at this level of approximation. Homogeneity of the bulk solution requires $G_0(x, 0) = 1$ and $G_0(\infty, t) = 1$. Rescaling Eq. (75) and substituting in Eq. (88) shows that $G_0(0, t) = 0$.

Laplace transforms easily produce

$$G_0(z, s) = \operatorname{erf}\left[\frac{z\sqrt{6}}{2\sqrt{s}}\right] \tag{90}$$

as the outer solution; the scaling cancels since Eq. (89) is a similarity solution. The sum of G_0 and the inner (ground state) solution G_{gs} derived from Eqs. (82)–(85), minus any common terms that appear in the appropriate limits of each, then constitutes a uniformly valid approximation. However, $G_0 \to 0$ as $z \to 0$, and $G_{gs} \to 0$ as $z \to \infty$, so the common terms are zero, leaving

$$G_c(z, s) = g(z)\exp(\lambda_0 s) + \operatorname{erf}\left[\frac{z\sqrt{6}}{2\sqrt{s}}\right] \tag{91}$$

as the matched solution.

The integral in Eq. (79) can be evaluated analytically through Laplace transforms. Recognizing Eq. (79) as a convolution leads to

$$\mathscr{L}\left\{\frac{\varphi_c^*}{\varphi_b^*}\right\} = \tilde{G}_c^2(z, \eta),$$

with $\tilde{G}_c(z, \eta) = \mathscr{L}\{G_c(z, n)\}$. Substituting in the transform of Eq. (91) and inverting yields

$$\varphi_c(z) = \varphi_b^* \mathscr{L}^{-1}\{\tilde{G}_{gs}^2 + 2\tilde{G}_{gs}\tilde{G}_0 + \tilde{G}_0^2\}$$

with

$$\tilde{G}_{gs} = \frac{g(z)}{\eta - \lambda_0}, \qquad \tilde{G}_0 = \frac{1}{\eta}[1 - e^{-z(6\eta)^{1/2}}].$$

The corresponding volume fraction $\varphi_c(z)$ consists of three terms arising from configurations with two, one, or zero sequences of segments originating in the inner region. The first term is exactly the ground state solution, representing segments contained in loops. The second and third terms

correspond to segments contained in tails and nonadsorbed chains. Labelling the individual contributions to φ_c as φ_L, φ_T, and φ_N gives

$$\varphi_c(z) = \varphi_L(z) + \varphi_T(z) + \varphi_N(z) \tag{92}$$

with

$$\varphi_L(z) = \frac{4\lambda_0 c_i e^{-\gamma z}}{\left(c_i - \frac{v}{2}e^{-\gamma z}\right)^2 - \frac{2}{3}\lambda_0 w e^{-2\gamma z}}$$

$$\frac{\varphi_T(z)}{\varphi_b^*} = \frac{2g(z)}{n\lambda_0}\left\{e^{n\lambda_0}\left[1 - \frac{1}{2}(e^{-(6\lambda_0)^{1/2}z})\right]\operatorname{erfc}\left[\frac{z\sqrt{6}}{2\sqrt{n}} - (n\lambda_0)^{1/2}\right]\right. \tag{93}$$

$$\left. + e^{(6\lambda_0)^{1/2}z}\operatorname{erfc}\left[\frac{z\sqrt{6}}{2\sqrt{n}} + (n\lambda_0)^{1/2}\right] - \operatorname{erf}\left[\frac{z\sqrt{6}}{2\sqrt{n}}\right]\right\},$$

[$G(z)$ from Eq. (84) with φ_c replaced by φ_L and $\exp(\beta U_c) \approx 1$] and

$$\frac{\varphi_N}{\varphi_b^*} = 1 - 2\left[1 + \frac{3z^2}{n}\right]\operatorname{erfc}\left[\frac{z\sqrt{6}}{2\sqrt{n}}\right] + 2\left[\frac{6}{\pi n}\right]^{1/2} z\, e^{-3z^2/2n}$$

$$+ \left[1 + \frac{12z^2}{n}\right]\operatorname{erfc}\left[\frac{z\sqrt{6}}{\sqrt{n}}\right] - 2\left[\frac{6}{\pi n}\right]^{1/2} z\, e^{-6z^2/n}.$$

Finally, the solution must be normalized in order to determine λ_0. The adsorbed amount (on a per surface basis),

$$\varphi_{ads} \equiv \int_0^\infty [\varphi_c(z) - \varphi_N(z)][1 + \delta(z)K_A]\, dz$$

$$\equiv \frac{\varphi_b^*}{n}\int_0^\infty \int_0^n [G_{gs}(z, s)G_{gs}(z, n - s) + G_{gs}(z, s)G_0(z, n - s)$$

$$+ G_0(z, s)G_{gs}(z, n - s)][1 + \delta(z)K_A]\, ds\, dz, \tag{94}$$

includes only chains having at least one segment on the surface. Alternately, a count of chain ends multiplied by n gives φ_{ads} since every chain has an end:

$$\varphi_{ads} = \varphi_b^* \int_0^\infty [G(z, n) - G_0(z, n)]\, dz \tag{95a}$$

gives this tally. For full equilibrium, λ_0 and φ_{ads} must satisfy Eqs. (94) and (95a).

The configuration integral for adsorbed chains is defined as

$$Z_A \equiv \int_0^\infty [G(z, n) - G_0(z, n)]\, dz = \int_0^\infty G_{gs}(z, n)[1 + \delta(z)K_A)\, dz \tag{95b}$$

so that nonadsorbed chains are not included. Under restricted equilibrium conditions, $\varphi_b^* = \varphi_{ads} n/Z_A$ and Eq. (95a) is an identity; however, Eq. (94) can be taken as another equation for Z_A. Thus Eqs. (94) and (95b) are solved for λ_0 and Z_A when φ_{ads} is held constant.

4. *Results for Isolated Layers*

Apart from two constants, c_i and λ_0, found as the zeroes of two nonlinear algebraic equations, the volume fraction profiles expressed in Eq. (93) are analytical and easily evaluated. Typical profiles shown in Fig. 19 (Ploehn and Russel, 1989) roughly correspond to 5.3×10^3 kg/mol polystyrene adsorbing from cyclohexane at $T = \theta$ with $\chi_s = 1.0$. Scaling φ on φ_b and plotting on a logarithmic scale magnifies the details at low φ relative to the linear scale in the inset. Distance from the surface is scaled with the radius of gyration of an ideal chain, $R_g = (nl^2/6)^{1/2}$.

The volume fraction falls off sharply over $0 \leq z \leq \frac{1}{3}R_g$ and is dominated by the exponential decay of segments contained in loops. In the interval $0.80R_g < z < 1.80R_g$, φ decays more slowly with tail segments making up

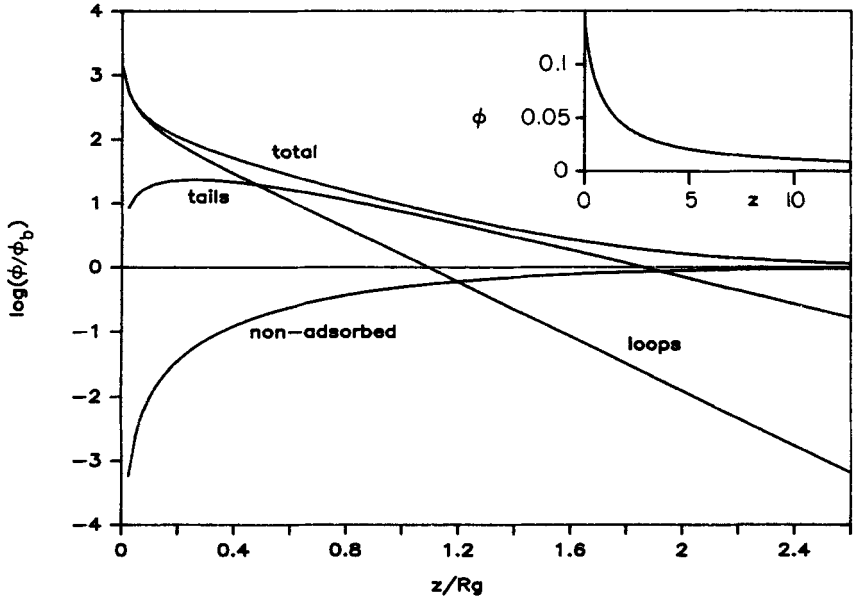

FIG. 19. Polymer volume fraction profiles, plotted as $\log[\varphi(z)/\varphi_b]$ vs. z/R_g, as calculated by Ploehn and Russel (1989) using the SCF given by Eqs. (71) and (72). The profiles for all segments (total), loops, tails, and nonadsorbed segments correspond to φ, φ_L, φ_T, and φ_N given by Eqs. (92) and (93). The total profile plotted on a linear scale is shown in the inset.

most of the total. As found by Scheutjens and Fleer (1980), the tail profile has a maximum and then falls off exponentially, but with a much longer decay length than the loop profile. Beyond about 2.5 R_g, nonadsorbed segments comprise most of total as the adsorbed layer merges into the bulk solution. Segments near the surface almost always belong to adsorbed chains, while segments of nonadsorbed chains are depleted there. In a sense, the surface is a "sink" for nonadsorbed chain probability and a "source" of adsorbed chain probability.

The features of $\varphi(z)$ obtained from the matched asymptotic expansion closely resemble those predicted by the SF model (Fig. 11) and measured through neutron scattering (Cosgrove *et al.*, 1987a). Clearly, mean-field models can account for the effects of adsorption energy, solvency, and excluded volume on layer structure. Effects arising from complex phenomena such as surface heterogeneity or molecular details such as polar association among segments cannot be accommodated. Such complications are suspected, for example, for PEO solutions and layers (Israelachvili *et al.*, 1980) as probed with neutron scattering by Cosgrove *et al.* (1987b); hence, behavior beyond the scope of the theories might be responsible for some of the quantitative disagreement between theory and experiment.

The adsorbed amount, defined by Eq. (94), is related to the experimental polymer adsorbance Γ (g/cm^2) through $\varphi_{ads} = \Gamma\tilde{v}/l$. Adsorption isotherms (Ploehn *et al.*, 1988; Ploehn and Russel, 1989) show a sharp initial rise of φ_{ads} followed by a plateau as φ_b increases. The plateau value of φ_{ads} is less in a good solvent than in a theta solvent. These trends are widely observed experimentally and theoretically (Takahashi and Kawaguchi, 1982; Cohen Stuart *et al.*, 1986; Fleer and Lyklema, 1983).

The predicted influence of n on φ_{ads} is compared in Fig. 20 with experimental data for adsorption of polystyrene on chrome (Takahashi *et al.*, 1980) and silica (vander Linden and van Leemput, 1978; Kawaguchi *et al.*, 1980) from cyclohexane at $T = \theta$. Curves A and B ($\chi_s = 1$ and 15) were calculated using Eqs. (71) and (72); curves C and D ($\chi_s = 1$ and 15) are based on the Flory–Huggins SCF of Eq. (70). Except for χ_s, all parameters are calculated from experimental conditions.

These results indicate that φ_{ads} increases with χ_s and n but appears to reach a limit at large n in good solvents. φ_{ads} is roughly linear in $\log(n)$ for $n < 10^4$. Selection of $\chi_s = 1.0$ produces curves (A and C) having the same qualitative features as the silica data. Although the predictions with two equations-of-state bracket the silica data, neither produces quantitative agreement over a significant range of n. Increasing χ_s to 15 (curves B and D) produces limited agreement with *different* sets of data, but loses some of the qualitative features of the data for $n < 1000$. Values of $\chi_s > 15$ are probably unrealistic.

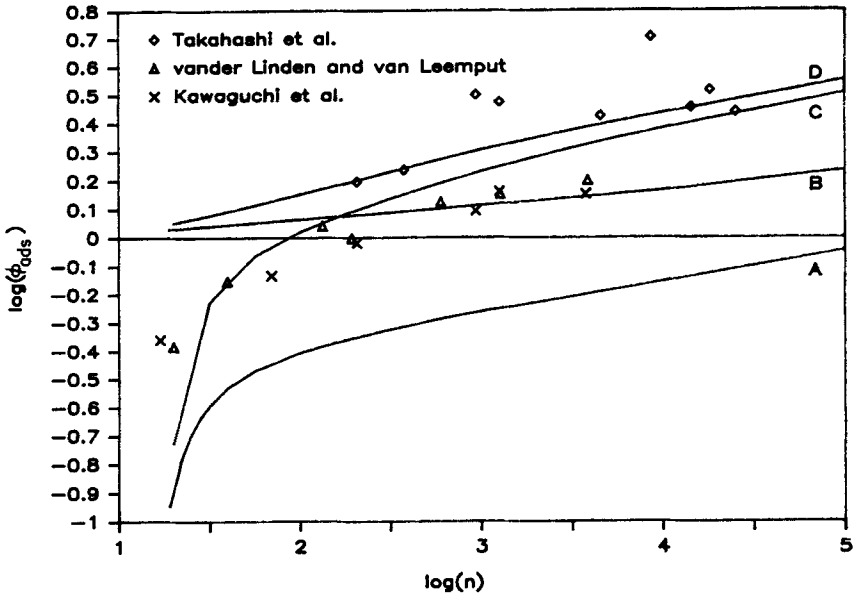

FIG. 20. Adsorbed amount vs. chain length plotted on a log–log scale. The points are measured values for PS/chrome/cyclohexane (diamonds, Takahashi *et al.*, 1980) and PS/silica/cyclohexane (triangles, vander Linden and van Leemput, 1978; crosses, Kawaguchi *et al.*, 1980). The curves are the predictions of Ploehn and Russel (1988) for $\chi = 0.5$ and $\varphi_b = 1.856 \times 10^{-4}$. Curves A and B ($\chi_s = 1$ and 15) are based on the SCF of Eqs. (71) and (72); curves C and D ($\chi_s = 1$ and 15) utilize the Flory–Huggins SCF of Eq. (70).

Ellipsometry measures the relative attenuation and phase shift of polarized light reflected from a polymer-coated surface. The Drude equations (Drude, 1889a,b, 1890; Stromberg *et al.*, 1963; McCrackin and Colson, 1964) relate the attenuation and phase shift to the average refractive index and thickness t_{el} of an equivalent homogeneous film. Interpretation of t_{el} in terms of the actual refractive index distribution or the polymer distribution $\varphi(z)$ is problematic. The ad hoc analysis of McCrackin and Colson (1964) provides

$$t_{el} = \frac{\varphi_{ads}^2}{\int_0^\infty [\varphi(z) - \varphi_b]^2 \, dz}, \tag{96}$$

and other calculations show that t_{el} is proportional to t_{rms} if various profiles for $\varphi(z)$ (e.g., Gaussian, exponential, linear) are assumed. Rigorous solutions of Maxwell's equations by Charmet and de Gennes (1983), accurate to first order

in the refractive index difference between polymer and solvent, yield

$$t_{el} = \frac{2\int_0^\infty z[\varphi_c(z) - \varphi_N(z)]\,dz}{\varphi_{ads}}, \tag{97}$$

which gives the proper thickness for a homogeneous film of finite extent.

Extensive experiments (Takahashi and Kawaguchi, 1982) show $t_{el} \approx M^a$, where $a = 0.50$ for theta solvents and $a = 0.40$ for good solvents. Figure 21 illustrates the power-law scaling for polystyrene adsorption onto chrome from cyclohexane at $T = \theta \approx 35°C$ (Takahashi *et al.*, 1980) and from CCl_4 at $T = 35°C$, a good solvent (Kawaguchi *et al.*, 1983). A least-squares fit of the two sets of data gives slopes of 0.46 and 0.44 for the theta and good solvents, respectively. Figure 21 also displays several different theoretical predictions for the variation of $\log(t_{el})$ with $\log(n)$ (Ploehn, 1988); all are based on Eq. (97). Curves A and B ($\chi = 0.4993$ and 0.452) derive from the matched asymptotic solution with the SCF in Eqs. (71)–(72). For the theta solvent

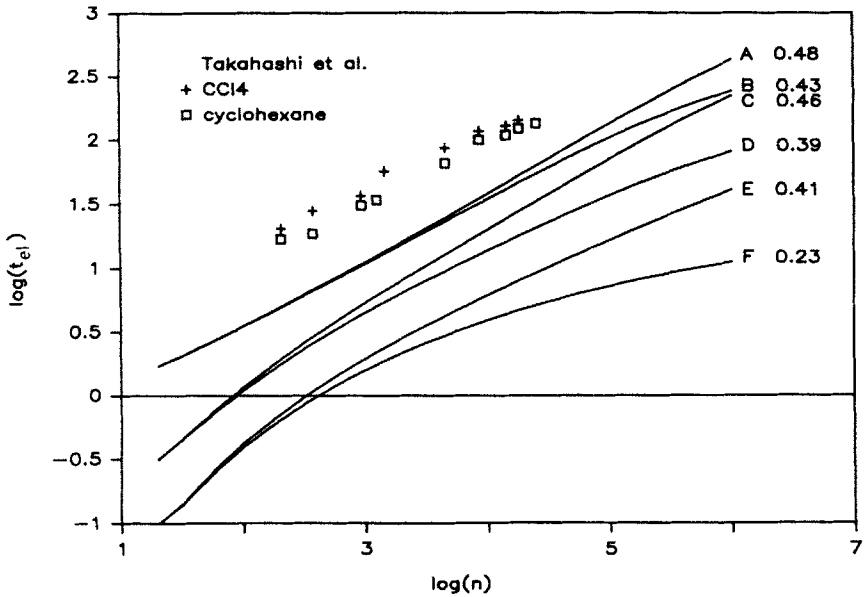

FIG. 21. Ellipsometric thickness as a function of chain length plotted on a log–log scale. The points (squares and crosses) are the data of Takahashi *et al.* (1980) for PS adsorbing onto chrome from cyclohexane or CCl_4. Curves A and B are calculated using the SCF in Eqs. (71) and (72); curves C–F utilize the SCF of Eq. (70). Curves A–D result from the matched asymptotic solution, while curves E and F are groundstate solutions. Other parameters include $\chi_s = 1$ and $\varphi_b = 2.784 \times 10^{-3}$. Numbers on the right are estimated slopes.

case (curve A), the calculated values are within a factor of 2–3 of the measurements, and the slope, 0.48, agrees, within error limits, with the experimental value. However, the predictions for the good solvent case (curve B) lie below those for the theta solvent, the opposite of the experimental trend. The calculated slope, 0.43, does match the experimental value. These predictions represent a considerable improvement over those based on the Flory–Huggins SCF in Eq. (70): Curves C and D ($\chi = 0.4993$ and 0.452) from the matched asymptotic solution and curves E and F ($\chi = 0.4993$ and 0.452) from on the ground state solution.

Figure 21 suggests some conclusions regarding the effect of individual contributions in the matched asymptotic solution and the SCF [Eqs. (71)–(72)] relative to the ground-state/Flory–Huggins field solution. First, the improvement of curves C and D over curves E and F stems from the matched asymptotic solution alone, i.e., the inclusion of tails, since the field is the same. The exponents should be regarded with some skepticism, though, since some of the lines are curved. Changing the field from Eq. (70) to Eqs. (71)–(72) produces power-law scaling, better exponents, and closer quantitative agreement with the data. Finally, the thicknesses for good and theta solvents move together, at least for low n.

The calculated hydrodynamic thickness, t_{hd}, shows similar agreement (Fig. 22) with the thicknesses measured by Cohen Stuart *et al.* (1984c) and Kato *et al.* (1981) by dynamic light scattering for adsorption of PEO on polystyrene particles suspended in water at 25°C (a very good solvent for PEO). Both groups find $t_{hd} \approx n^a$ with $a = 0.80$ (Cohen Stuart *et al.*, 1984c) or $a = 0.56$ (Kato *et al.*, 1981). The values of t_{hd} calculated by Ploehn and Russel (1989) show the same scaling ($a = 0.66$) but only half the magnitude. The frictional drag of each segment equals that of a sphere of diameter l or $2l$; the results vary relatively little with the segmental drag or χ_s.

Figure 22 also demonstrates that the hydrodynamic thickness due to segments in loops alone is considerably less than that due to all segments. Indeed, previous calculations (Cohen Stuart *et al.*, 1984c; Anderson and Kim, 1987; Scheutjens *et al.*, 1986) indicate that hydrodynamic methods probe the outer region of the adsorbed layer where tails dominate.

5. *Interactions Between Layers*

The SCF [Eq. (39)] minimizes the free energy of the interfacial system. The Helmholtz free energy per area of segment for restricted equilibrium is

$$\frac{A}{kT} = \frac{2\gamma}{kT} + \frac{\mu_p \varphi_{ads}}{nkT}, \tag{98}$$

with the surface energy (equivalent to the interaction potential for full

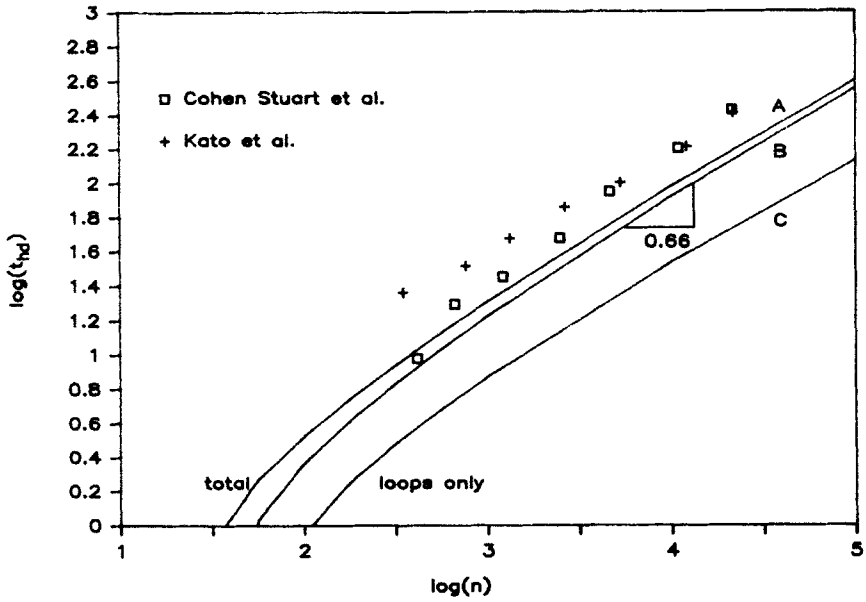

FIG. 22. Hydrodynamic thickness vs. chain length plotted on a log–log scale. The points (squares and crosses) are data for PEO/PS latex/water measured through dynamic light-scattering (squares, Cohen Stuart *et al.*, 1984c; crosses, Kato *et al.*, 1981). The curves are calculated by Ploehn and Russel (1989) using the SCF of Eqs. (71) and (72). Curves A and B denote frictions per segment equivalent to Stokes spheres of diameter l and $2l$, respectively. Curve C is the thickness based only on segments contained in loops (Stokes sphere diameter = l).

equilibrium) expressed as

$$2\gamma = -l^2 \int_0^{z_m} [\Pi_m(z) - \Pi_b]\, dz, \tag{99}$$

where z_m is the dimensionless gap half-width (infinite for a single surface), $\Pi_m(z) \equiv \Pi[\varphi(z; z_m)]$ is the osmotic pressure of a solution with volume fraction φ, and Π_b is that of bulk solution (Helfand, 1975a; Hong and Noolandi, 1981; de Gennes, 1981; Ploehn, 1988). Equation (98) is equivalent to Eq. (64) as used by Scheutjens and Fleer (1985). Since the polymer distribution is discontinuous at the surface, the osmotic pressure difference includes continuous and surface functions, e.g.,

$$\Pi_m - \Pi_b = \Pi_c - \Pi_b + \delta(z)[\Pi_s - \Pi_b], \tag{100}$$

with Π_c and Π_s provided by a polymer solution equation-of-state.

The Flory–Huggins forms of γ and μ_p are simply the continuous space analogs of Eqs. (65) and (66). Ploehn and Russel (1989) use a segment equation-of-state giving greater intersegment repulsion than the Flory–Huggins

equation. Applying the prescription of Dickman and Hall (1986) produces the *polymer* equation-of-state

$$\frac{\Pi_c v_1}{kT} = \lambda_n\left[\frac{\varphi_c(1+\varphi_c+\varphi_c^2+\varphi_c^3)}{(1-\varphi_c)^3} - 8\alpha\varphi_c^2\right] + \varphi_c/n(1-n\lambda_n)$$

$$\frac{\Pi_s v_1}{kT} = \lambda_n\left[B_0\ln(1-\varphi_s) + \frac{B_1\varphi_s}{1-\varphi_s} + (B_1 - B_0 + 1)\varphi_s + \tfrac{1}{2}B_2\varphi_s^2 + \tfrac{2}{3}B_3\varphi_s^3 + \tfrac{3}{4}B_4\varphi_s^4\right] + \frac{\varphi_s}{n}(1-n\lambda_n), \tag{101}$$

where $v_1 \equiv \tilde{v}M/nN_A$ is the volume per segment, $\lambda_n = 0.61418 + 0.45914/n$, and the B_i are defined following Eq. (72). With

$$\varphi_b^* \equiv \frac{\varphi_{ads}}{Z_A} = \frac{\varphi_{ads}}{\int_0^{z_m}[G(z,n) - G_0(z,n)]\,dz}$$

for restricted equilibrium (analogous to Eq. (67)], the chemical potential of chains confined to the gap is

$$\frac{\mu_p}{kT} = 1 + \ln(\varphi_b^*) + n\lambda_n\left[\frac{3-\varphi_b^*}{(1-\varphi_b^*)^3} - 16\alpha\varphi_b^*\right]. \tag{102}$$

Interaction potential energies for restricted equilibrium based on Ploehn and Russel's (1989) equations are given in dimensionless form as

$$V(z_m) = \frac{v_1}{l^3 kT}[A(z_m) - A(\infty)]. \tag{103}$$

Like the models of de Gennes (1982) and Scheutjens and Fleer (1985; Fleer and Scheutjens, 1986), the SCF model predicts monotonic attraction between adsorbed layers under conditions of full equilibrium. For constant φ_{ads} (restricted equilibrium), Fig. 23 shows $\Delta\gamma \equiv \gamma(z_m) - \gamma(\infty)$ (curve A) increases slightly before falling as the separation decreases; $\Delta\mu_p \equiv \mu_p(z_m) - \mu_p(\infty)$ increases upon compression (curve B), and the total potential (curve C) displays an attractive minimum as well as a steep repulsive "wall." Potentials for various φ_{ads} (Fig. 24) resemble those of Fig. 16 and those measured by Almog and Klein (1985) (Fig. 18). In contrast to the SF model, the potentials do not superimpose for the same φ_{ads} with different combinations of n and φ_b (i.e., dosage at infinite separation). The reasons for this difference are not clear at this point.

The parameters for the predictions presented in Fig. 24 are intended to duplicate the conditions used by Almog and Klein (1985) for adsorption of 6×10^5 g/mol polystyrene (the data of Fig. 18 are for 2×10^6 g/mol).

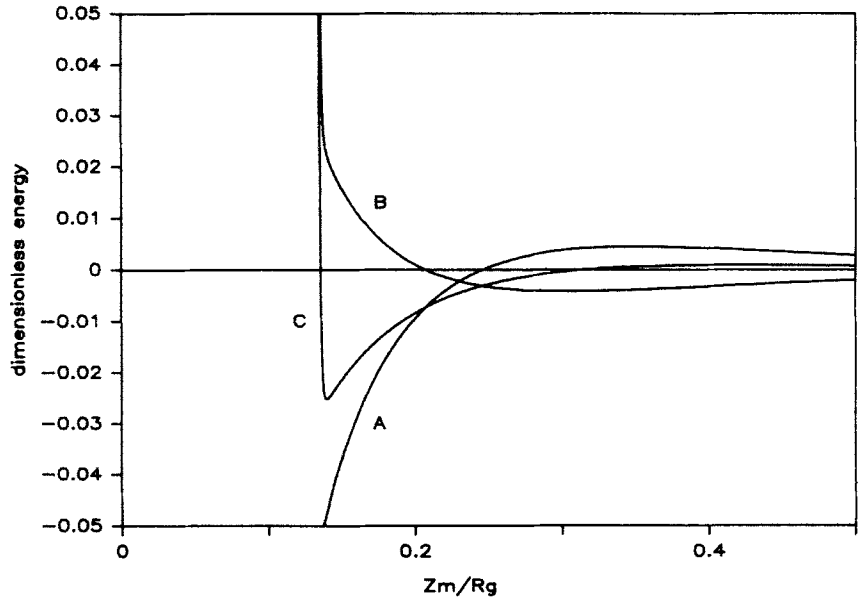

FIG. 23. Typical interaction potential energy vs. gap half-width (scaled on R_g) for restricted equilibrium (curve C) calculated by Ploehn (1988) using the Flory–Huggins SCF of Eq. (70). The components of the potential are the potential for full equilibrium, i.e., the surface tension, (curve A) and the chains' chemical potential (curve B). Parameters are $\chi_s = 1$, $\chi = 0.488$, and $n = 1129$; the dosage $\varphi_b = 1.392 \times 10^{-10}$ at large separation gives $\varphi_{ads} = 1.308$, which is held constant.

After incubating the mica surfaces at a large separation in 15 μg/ml solution, Almog and Klein reported $\Gamma = 2.5 \pm 1.5$ mg/m^2, equivalent to $\varphi_{ads} = \tilde{v}\Gamma/l = 1.58 \pm 0.95$ (Ploehn, 1988) with $\tilde{v}$ as the specific volume of the polymer given in Table I. Using $\varphi_b(\infty) = c_b\tilde{v} = 1.392 \times 10^{-5}$ (Ploehn, 1988), the matched asymptotic solution for a single surface predicts $\varphi_{ads} = 1.583$ agreeing with the measured value within experimental error. For this case, Almog and Klein measured a purely repulsive potential, but the corresponding theoretical prediction, curve B of Fig. 24, displays some attraction. However, the measured location of the repulsive wall at $2z_m l = 30$ nm, or $z_m l/R_g = (30 \text{ nm}/2)(38.5 \text{ nm}) = 0.39$ compares favorably with the predicted location.

Almog and Klein measured attractive minima as deep as 1000 μN/m; multiplying by $v_1/2\pi lkT$ (the 2π arises in converting the potential between the curved mica surfaces to that between planes) gives dimensionless potentials as large as 0.1. The same order of magnitude results from the SF model (Figs. 16 and 17) when v_1/l is taken as 1 nm^2. The matched asymptotic solution using the Flory–Huggins equation-of-state (Fig. 24) yields attractive minima of $O(0.01)$; using $v_1/l \approx 0.5$ nm^2 (Ploehn, 1988), the attractions also agree with the

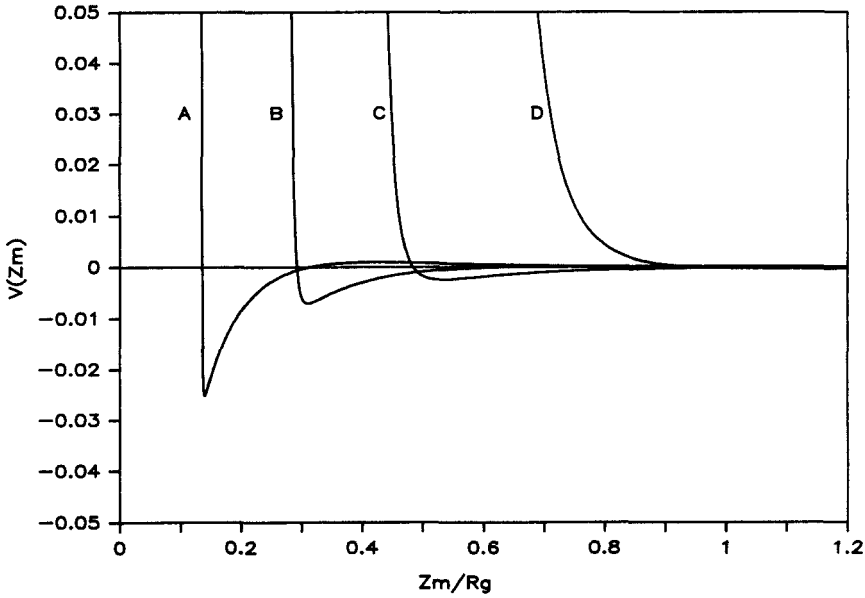

FIG. 24. Interaction potential energy vs. gap half-width (scaled on R_g) for various φ_{ads} as calculated by Ploehn (1988) using the SCF of Eq. (70). Parameters include $\chi_s = 1$, $\chi = 0.488$, and $n = 1129$. Curves A–D denote increasing dosages at large separations: $\varphi_b = 1.392 \times 10^{-10}$, 3.65×10^{-5}, 1.392×10^{-3}, and 1.392×10^{-2} correspond to $\varphi_{ads} = 1.308$, 1.583, 1.825, and 2.232, respectively.

magnitude of the measured values. However, the equation-of-state, Eqs. (71) and (72), which produces Eqs. (101) and (102) leads to potentials with much weaker attractive minima (Fig. 25) under the same conditions. The reasons for the differences between the results in Figs. 24 and 25 are entirely due to the different SCFs. The reasons for the differences between the theory and experimental data are not yet clear but are currently being investigated. The work of Evans (1989) suggests that the potential of Eq. (103) may not be appropriate for comparisons with the experimental force measurements. Rather, a work potential based on an integral of the total *stress* from infinite separation to z_m is indicated. Evans' calculations for interacting depletion layers at full equilibrium must be extended to the adsorption case with restricted equilibrium in order to resolve this important point.

One should realize that these forces, measured between macroscopic surfaces, often exceed those relevant for interacting colloidal particles. Even a small attraction between planes, say, of $O(10^{-3}\ kT/\text{nm}^2)$, translates into an attraction of $O(10kT)$ between 0.1 μm spheres separated by a distance of $O(1R_g)$. Thus the lower end of the experimental range is of primary interest.

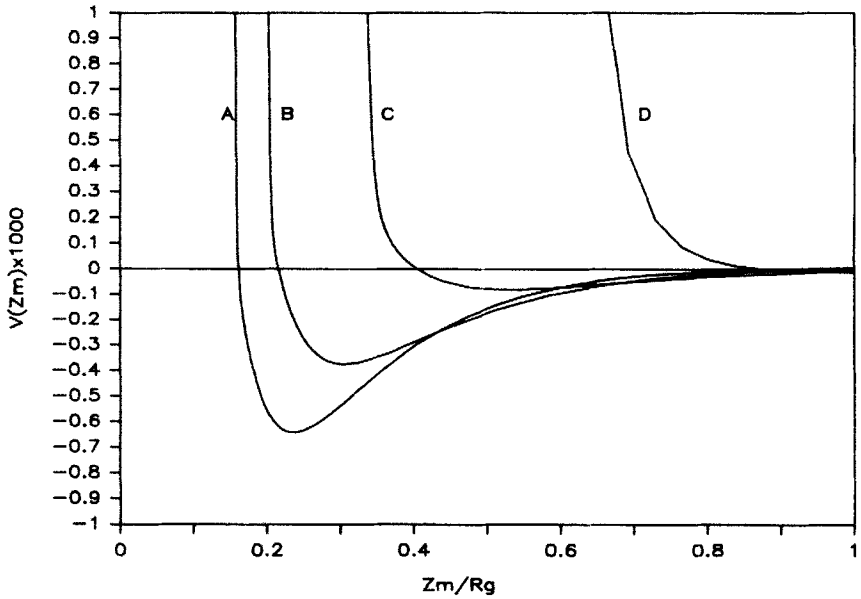

FIG. 25. Interaction potential energy vs. gap half-width (scaled on R_g) for various φ_{ads} as calculated by Ploehn (1988) using the SCF of Eqs. (71) and (72). Parameters include $\chi_s = 1$, $\chi = 0.488$, and $n = 1129$. Curves A–D denote increasing dosages at large separations: $\varphi_b = 1.000 \times 10^{-10}$, 1.392×10^{-8}, 1.392×10^{-5}, and 1.392×10^{-3} correspond to $\varphi_{ads} = 0.449$, 0.468, 0.515, and 0.613, respectively.

6. *Conclusions*

A matched asymptotic solution of the general SCF equations, a mathematical approximation of the exact numerical solution furnished by the SF model, provides analytical solutions and successfully predicts many of the qualitative features of experimental data. The SF model suffers the approximations inherent in Flory–Huggins statistics and the limitations imposed by the iterative numerical solutions, but does encompass all eigenfunctions rather than just two. The two-eigenfunction solution of Ploehn *et al.* underestimates the measured φ_{ads} and t_{el} by a considerable margin; quantitative comparisons have not yet been made with the Schuetjens–Fleer (1980) predictions. The clearest success of the Ploehn–Russel (1988) model is the prediction of t_{hd}; two eigenfunctions encompass tails that apparently dominate the hydrodynamics of adsorbed layers. Interaction potentials between adsorbed layers show the same characteristics as those measured between polymer-coated mica surfaces, although not in quantitative agreement.

Adsorption models are only as accurate as the local free-energy density that determines the SCF. A limited number of comparisons (Figs. 18, 24, and 25) between results based on the Flory–Huggins SCF, and those generated from

Ploehn and Russel's (1988) SCF, clearly show different characteristics for the adsorbed layer. Further progress depends on the evolution of accurate polymer solution theories as well as more extensive comparisons of solution and adsorption data with theoretical predictions.

G. Summary

Extensive experimentation demonstrates that polymer adsorption differs fundamentally from small molecule adsorption because of the polymer's configurational degrees of freedom. Increasingly sophisticated theories have emerged to predict the characteristics of adsorbed layers and their interactions. Early theories assumed isolated chains fixed at the surface, but recent efforts incorporate polymer excluded-volume, finite molecular weight, and equilibrium with bulk solution. Thus, quantities of practical interest, such as adsorbed amount, bound fraction, layer thicknesses, and interaction potentials, can be predicted qualitatively as functions of molecular weight, bulk solution concentration, and temperature. Improvements in quantitative comparisons between theory and experiment rely on (1) the development of new model colloidal materials and polymers with controlled microstructure and chemistry, (2) advances in experimental techniques for probing adsorbed layers, and (3) more realistic models of polymer solutions and polymer–surface interactions. Accurate prediction of large scale properties seems within reach.

IV. Terminally Anchored Polymers

A. Isolated Layers

When soluble polymers are attached by one end to a surface, the thickness of the resulting layer, L, depends on the surface density of chains σ as well as n and the excluded volume v/l^3 (de Gennes, 1980). At low densities $\sigma\langle r^2\rangle < 1$, the isolated chains extend $\sim \langle r^2\rangle^{1/2}$ into the solution, creating a layer with the density profile shown in Fig. 26a and a thickness of $L = n^{1/2}l$ for ideal chains and $L \sim n^{3/5}l$ in good solvents. When $\sigma\langle r^2\rangle > 1$ the coils overlap and the interactions will cause the chains to expand away from the surface into the bulk. The configurations of the individual molecules and the density profile within the layer (Fig. 26b) differ markedly from the dilute situation. When $\sigma l^2 \sim 1$ the molecules become fully stretched.

For $\sigma\langle r^2\rangle > 1$, the polymer chains interpenetrate, and segment densities become independent of lateral position and amenable to treatment by the SCF theory (Dolan and Edwards, 1974, 1975). The number of configurations of a

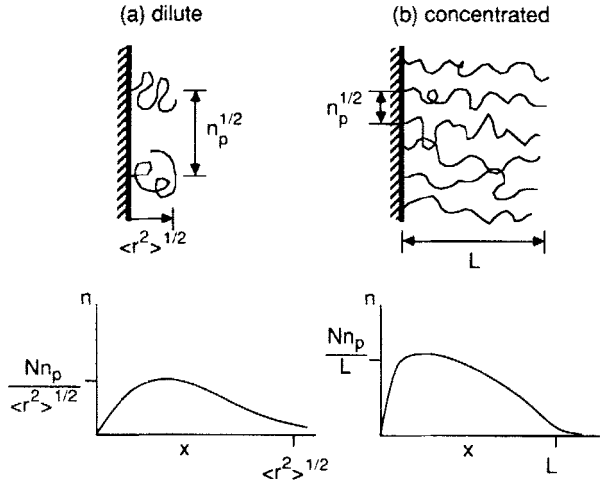

FIG. 26. Conformation of terminally anchored chains: (a) Isolated coils at low coverages (de Gennes, 1980); (b) high stretched chains at high coverages (Milner *et al.*, 1988). The distance between graph points scales as $\sigma^{-1/2}$.

chain of length s beginning at z' and ending at z, $G(z, z', s)$, is governed by Eq. (31) with $G(z, z', 0) = \delta(z - z')$ and

$$\rho(z) = \sigma \frac{\int_0^n G(z, 0, s) \int_0^\infty G(z, z'', n - s)\, dz''\, ds}{\int_0^\infty G(z'', 0, n)\, dz''}. \tag{104}$$

The boundary condition,

$$\frac{\partial G}{\partial s} = \frac{l}{2} \frac{\partial G}{\partial z} - \left[2 \exp\left(\frac{U}{kT} \right) - 1 \right] G \tag{105}$$

at $z = 0$, follows from Eq. (74). However, $\partial \ln G / \partial s \ll 1$ and $U/kT \ll 1$ near the interface, reducing this to

$$0 = \frac{l}{2} \frac{\partial G}{\partial z} - G, \tag{106}$$

which is equivalent to setting $G(-l/2) = 0$ or letting $G(0) = 0$ and considering the chains to be attached at $z' = l/2$.

For ideal conditions, i.e., $U = 0$, the solution to Eq. (31) (Dolan and Edwards, 1974),

$$G(z, z', s) = \left(\frac{3}{2\pi l^2 s} \right)^{1/2} \left\{ \exp\left(-\frac{3(z - z')^2}{2l^2 s} \right) - \exp\left(-\frac{3(z + z')^2}{2l^2 s} \right) \right\}, \tag{107}$$

corresponds to individual Gaussian chains anchored to the surface and

determines the mean square end-to-end distance and free energy of each chain as

$$\begin{aligned} \langle z^2 \rangle &= \tfrac{2}{3} nl^2 \\ \frac{A}{kT} &= \frac{1}{2} \ln \frac{2\pi n}{3}. \end{aligned} \tag{108}$$

Since $\langle z^2 \rangle = \langle r^2 \rangle / 3 = nl^2/3$ and $A/kT = 0$ for ideal chains in solution, the presence of the wall increases both $\langle z^2 \rangle$ and A/kT.

The effect of solvent quality on the thickness of the layer L and free energy of the individual chains is demonstrated by the work of Milner *et al.* (1988) and Halperin (1988). The result for the chain configurations comprises an asymptotic solution of Eq. (31) for highly stretched chains, i.e., $L \gg n^{1/2} l$, via the WKB approximation. This yields the end segment probability as

$$\frac{1}{W} G(z, 0, n) = \frac{\pi^2}{4} \frac{l^3}{n^3 v} z(L^2 - z^2)^{1/2} \tag{109}$$

for $0 \leq z \leq L$ and a SCF which varies quadratically with distance from the surface as

$$\begin{aligned} \frac{U}{kT} &= v\rho + \tfrac{1}{2} w\rho^2 \\ &= \frac{\pi^2}{8(nl)^2} (L^2 - z^2). \end{aligned} \tag{110}$$

Solving for $\rho(z)$ and then integrating the profile with the condition that

$$\int_0^L \rho(z)\, dz = n\sigma \tag{111}$$

determines the dimensionless layer thickness $\bar{L}$ through

$$\bar{v}^{-2} = \pm(1 + \bar{L}^2) \sin^{-1}\left(\frac{\bar{L}}{(1 + \bar{L}^2)^{1/2}} \right) - \bar{L} \tag{112}$$

with $\bar{L} = \pi w^{1/2} L / 2nvl$ and $\bar{v} = v(l/\pi w^{3/2}\sigma)^{1/2}$.

The numerical results for $\bar{L}$ in Fig. 27 illustrate the effect of solvent quality on the layer thickness. The limiting forms,

$$\begin{aligned} &\bar{v} \gg 0, \qquad L \sim \left(\frac{12v\sigma}{\pi^2 l} \right)^{1/3} nl \\ &\bar{v} \sim 0, \qquad L \sim \frac{2}{\pi} \left(\frac{2w^{1/2}\sigma}{l} \right)^{1/2} nl + \left(\frac{2}{\pi^2} \right) \left(\frac{v}{w^{1/2}} \right) nl \\ &\bar{v} \ll 0, \qquad L \sim -\frac{w\sigma}{vl} (nl) \end{aligned} \tag{113}$$

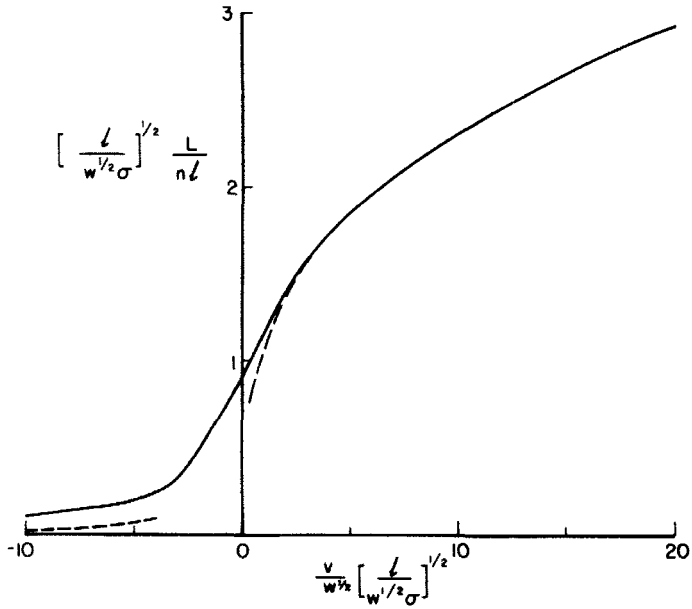

FIG. 27. Effect of solvent quality and graft density on layer thickness for terminally anchored chains from Eq. (112).

corresponding to the asymptotes in Fig. 27, provide additional insight. Note that $L \sim nl$ in all cases since the individual chains are highly stretched, but the layer thickness decreases with decreasing solvent quality or graft density. The sensitivity to the graft density, σ, increases as the solvent quality decreases. In the poor solvent case with $\bar{v} \ll 1$, the theory holds only for $-n^{1/2}w\sigma/vl \gg 1$.

The segment density profiles obtained from Eq. (110) have the limiting forms

$$\begin{aligned} \bar{v} \gg 1, \quad & \frac{\rho l}{\sigma} \sim \left(\frac{9\pi}{32}\right)^{1/3}\left(\frac{vl^2}{w^{3/2}\sigma^2}\right)^{1/2}\left(1-\frac{x^2}{L^2}\right) \\ \bar{v} \sim 0, \quad & \frac{\rho l}{\sigma} \sim \left(\frac{2l}{w^{1/2}\sigma}\right)^{1/2}\left(1-\frac{x^2}{L^2}\right)^{1/2} \\ \bar{v} \ll 1, \quad & \frac{\rho l}{\sigma} \sim -2\pi\frac{vl}{w\sigma} \end{aligned} \tag{114}$$

(Fig. 28). Clearly the profile becomes flatter with decreasing solvent quality. Note, however, that the self-consistent potential and the end-segment distributions still satisfy Eqs. (109) and (110).

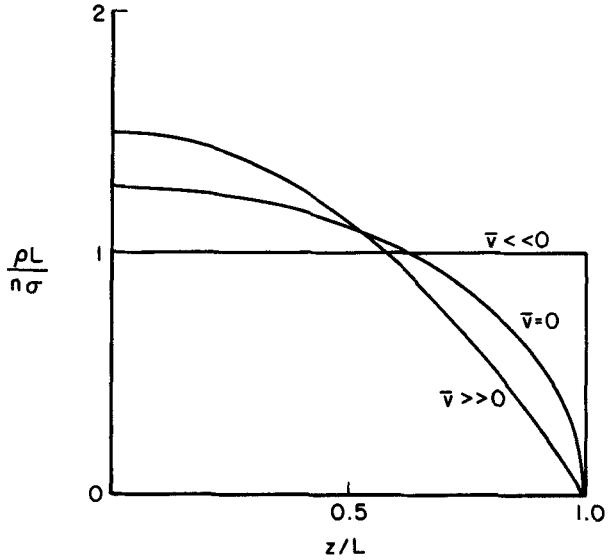

FIG. 28. *Effect of solvent quality on segment density profile for terminally anchored chains from Eq. (114).*

The predicted layer thicknesses resemble qualitatively those obtained for a step-function profile postulated by Alexander (1977) and de Gennes (1975). This mean-field approach approximates the free energy of the layer by

$$\frac{A}{kT} = \frac{3}{2}\left(\frac{L^2}{nl^2} + \frac{nl^2}{L^2} - 2\right) + \frac{nv\rho}{2} + \frac{nw\rho^2}{6}, \tag{115}$$

with constant segment density $\rho = n\sigma/L$. The bracketed term accounts for the elastic energy associated with compressing or extending the chains from the relaxed configuration, and the second and third terms represent the effects of two- and three-body segment–segment interactions. The equilibrium layer thickness then corresponds to the free energy for which the chemical potential of the solvent in the layer equals that in the bulk, or

$$\frac{\partial A}{\partial \rho} = -\frac{L^2}{n\sigma}\frac{\partial A}{\partial L} = 0.$$

Thus, the equilibrium layer thickness must satisfy

$$\left(\frac{L}{n^{1/2}l}\right)^3 - \left(1 + \frac{\phi_p^2}{9}\right)\frac{n^{1/2}l}{L} = \frac{n^{3/2}\sigma v}{6l}. \tag{116}$$

The dimensionless surface density, $\phi_p = n\sigma w^{1/2}/l$, is the volume fraction of

segments that would result from collapsing the chains into a layer of thickness l. The second parameter, $n^{3/2}\sigma v/l$, is the ratio of the excluded volume per chain ($n^2 v$) to the volume occupied by the chain at ideal conditions ($n^{1/2}l/\sigma$).

The limiting forms for the layer thickness, e.g.,

$$L \sim \left(\frac{v\sigma}{6l}\right)^{1/3} nl, \qquad \frac{n^{3/2}\sigma v}{l} \gg 1,$$

$$L \sim \left(\frac{w^{1/2}\sigma}{3l}\right)^{1/2} nl, \qquad \frac{n^{3/2}\sigma v}{l} \sim 0 \quad \text{and} \quad \phi_p \gg 1, \tag{117}$$

$$L \sim -\frac{2}{3}\left(\frac{w\sigma}{lv}\right) nl, \qquad \frac{n^{3/2}\sigma v}{l} \ll 1,$$

differ only in the numerical factors from Eq. (113). Thus, chains become highly stretched whenever either $n^{3/2}\sigma v/l$ or ϕ_p is large.

B. Interactions Between Layers

When two surfaces approach, the attached polymer layers first interact at separations h on the order of twice the layer thickness. The polymer–polymer and polymer–surface interactions alter the free energy by changing the volume available to an individual chain. For $v > 0$, interpenetration or compression of the two layers reduces the available volume and, hence, the number of configurations. The associated increase in free energy produces a repulsive force. However, with negative excluded volume, interpenetration increases the volume available per chain, thereby decreasing the free energy and causing an attraction. In both cases, reducing the separation to less than one layer thickness constrains the chains sufficiently to produce a strong repulsion.

The interaction potential equals the change in free energy per unit area, which is expressed according to Eq. (64) or alternatively as (Helfand, 1975a)

$$V = -2\sigma l^2 \ln W(h) - l^2 \int_0^h \left(\frac{1}{2}v\rho^2 + \frac{1}{3}w\rho^3\right) dz - \frac{l^2 A_\infty}{kT}, \tag{118}$$

with

$$W(h) = \int_0^h G(z, l/2, n)\, dz$$

and

$$A_\infty = \sigma kT \ln\left(2\pi\frac{n}{3}\right) + 2\sigma A_0\left(\frac{n^{3/2}\sigma v}{l}, \phi_p\right).$$

A_∞ is the free energy of the isolated layers with the first term comprising the ideal result and A_0 accounting for the effects of segment–segment interactions.

For ideal layers, solution of the SCF equation yields a small separation limit,

$$V(h) = \sigma l^2 \left[\frac{\pi^2 nl}{3h^2} + \ln\left(\frac{27h^2}{8\pi nl^2} \right) \right]. \tag{119}$$

The divergence of the potential as h^{-2} for $h \to 0$ arises from the compression of chains between the surfaces.

For dense layers in good solvents, the asymptotic theory of Milner *et al.* (1988) applies, but with $L = h/2$. Density profiles are truncated according to

$$\rho(x) = \frac{2n\sigma}{h} + \frac{\pi^2}{24v} \left[\left(\frac{h}{2nl} \right)^2 - 3\left(\frac{x}{nl} \right)^2 \right], \tag{120}$$

indicating that chains in the interacting layers do not interpenetrate, but are simply compressed. The interaction potential then follows, albeit indirectly, from Eq. (118), the density profile, the form of the self-consistent potential, and the end-segment density as

$$V(h) = n\sigma l^2 \left(\frac{\pi^2}{12} \right)^{1/3} \left(\frac{v\sigma}{l} \right)^{2/3} \left[\frac{2L}{h} + \left(\frac{h}{2L} \right)^2 - \frac{1}{5}\left(\frac{h}{2L} \right)^5 - \frac{9}{5} \right]. \tag{121}$$

For slight compression, this simplifies to

$$V(h) \sim 3n\sigma l^2 \left(\frac{\pi^2}{12} \right)^{1/3} \left(\frac{v\sigma}{l} \right)^{2/3} \left(1 - \frac{h}{2L} \right)^3. \tag{122}$$

In the same limit, the mean-field approach based on a step function profile yields

$$V(h) \sim 3^{4/3} n\sigma l^2 \left(\frac{v\sigma}{2l} \right)^{2/3} \left(1 - \frac{h}{2L} \right)^2. \tag{123}$$

Thus, the approaches concur on the scaling of the potential, $n\sigma(v\sigma/l)^{2/3}$, and the separation, $nl(v\sigma/l)^{1/3}$, and predict a strong repulsion for $h < 2L$; they differ, however, in the form of the separation dependence. Analogous treatments for semidilute concentrations within the layers differ only modestly from the preceding results (Milner, 1989).

The asymptotic approach has not yet been extended to interactions between stretched layers in theta and poor solvents, which control the incipient flocculation of polymerically-stabilized colloidal dispersions. Application of the mean-field theory to poor solvents produces an attractive minimum only for $-n^{1/2}v/w^{1/2} > n\sigma w^{1/2}/l$, when layers begin to interpenetrate rather than

simply compress as in good solvents (Russel *et al.*, 1989). This means denser layers provide greater stability, i.e., they require considerably worse than theta conditions for flocculation.

These potentials for interactions between flat plates provide the basis for addressing interactions between spheres of radius $a \gg L$ through the Derjaguin approximation

$$\frac{\Phi}{kT} = \frac{\pi a}{l^2} \int_{r-2a}^{\infty} V(h)\, dh.$$

For thicker layers, curvature effects become significant and must be treated explicitly (Witten and Pincus, 1986).

C. Experimental Results

Taunton *et al.* (1988) have measured forces between polystyrene layers in toluene, which are anchored to mica surfaces by small zwitterionic head

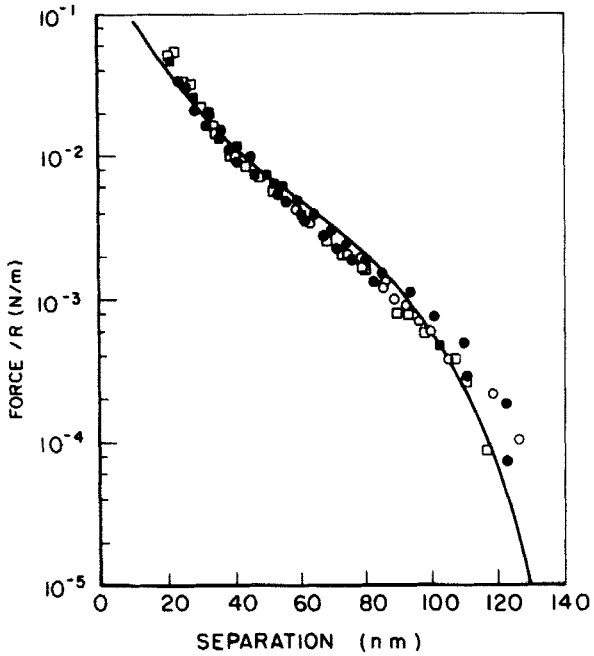

FIG. 29. Interaction potential as a function of separation for mica surfaces bearing terminally-anchored polystyrene chains with M = 131 kg/mol in toluene: Data points are taken from Taunton *et al.* (1988); the curve is from Eq. (121), with n = 265, l = 1.46 nm, $2L$ = 140 nm, $nl^2\sigma = 22$, and $v/l^3 = 0.06$.

groups. That the polystyrene chain does not adsorb and the anchoring by the polar group is irreversible were demonstrated in independent measurements, so the situation approximates that assumed for the theory.

The interaction in toluene at room temperature, a good solvent, is strongly repulsive at separations less than twice the apparent layer thickness (Fig. 29). Polystyrene has statistical segments with a molecular weight of 0.494 kg/mol and a length of 1.46 nm, indicating $n = 265$, $nl = 398$ nm, and $\langle r^2 \rangle^{1/2} =$ 24 nm. Thus, the apparent layer thickness of 60–70 nm detected in the experiment suggests highly stretched chains, presumably due to high graft densities. To test this quantitatively requires estimating σ and v/l^3 from the data. The solid curve in Fig. 29 results from choosing $L = 70$ nm and the prefactor in Eq. (121) as 1.14×10^{-3} N/m. With the good solvent limit for L from Eq. (113) this leads to $v/l^3 = 0.06$ and $nl^2\sigma = 22$, which are reasonable values.

Other experiments with block copolymers (Hadziioannou *et al.*, 1986; Tirrell *et al.*, 1987; Patel *et al.*, 1988; Ansarifar and Luckham, 1988) provide similar results in good solvents and strong, but shorter range repulsions at theta conditions. The behavior in poor solvents, i.e., the delineation between attractive and repulsive potentials, remains to be resolved.

V. Nonadsorbing Polymer

A. Depletion Layers

Dissolved, nonadsorbing polymer molecules must sacrifice configurational degrees of freedom to approach to surface closer than about one coil radius, an energetically unfavorable process in dilute solutions. Indeed, experiments confirm that a layer of thickness $L \sim \langle r^2 \rangle^{1/2}$ adjacent to any surface is depleted of segments (Aussere *et al.*, 1986).

The consequences for suspended particles can be understood from either a mechanical or a thermodynamic standpoint. A particle immersed in a polymer solution experiences an osmotic pressure acting normal to its surface. For an isolated particle, the integral of the pressure over the entire surface nets zero force. But when the depletion layers of two particles overlap, polymer will be excluded from a portion of the gap (Fig. 30). Consequently, the pressure due to the polymer solution becomes unbalanced, resulting in an attraction. The same conclusion follows from consideration of the Helmholtz free-energy. Overlap of the depletion layers reduces the total volume depleted of polymer, thereby diluting the bulk solution and decreasing the free energy.

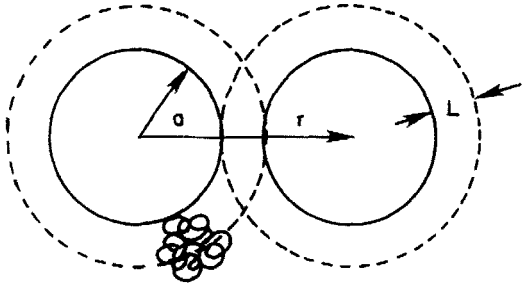

FIG. 30. Interaction between spheres of radius a at separation r showing overlap of depletion layers of thickness L.

The original geometrical analysis of Asakura and Oosawa (1954, 1958), generalized by Vrij (1976) and others, neglects the internal degrees of freedom of the polymer molecules to obtain simple, useful expressions for the interaction potential. The SCF theory reviewed here (Joanny *et al.*, 1979) demonstrates the validity of the simpler approaches.

The configuration density function G, governed by Eq. (31) with $G = 0$ at $z = 0, h$, is now related to the segment density through Eq. (92) with σ replaced by ρ, the average density of segments within the gap, such that

$$\int_0^h \rho(z)\,dz = h\rho. \tag{124}$$

Equilibrium with a bulk solution at segment density ρ_b requires the chemical potential for chains in the gap to equal that for the bulk, or

$$\rho = \rho_b W \exp\left(n v \rho_b + \frac{\partial \ln W}{\partial \ln \rho} + \frac{\partial}{\partial \rho}\int_v \tfrac{1}{2} v \rho^2 \frac{dV}{V}\right). \tag{125}$$

The solution for G, obtained by assuming a separable solution of the form in Eq. (82) (Gerber and Moore, 1977) to the nonlinear Eq. (31) and requiring $g = 0$ at $z = 0, h$ and

$$\int_0^h g^2(z)\,dz = 1, \tag{126}$$

can be expressed as a Jacobian elliptic function and then used to evaluate W and $\rho(z)$. For sufficiently small separations, $\rho(z) \sim 2\rho \sin^2(\pi z/h)$ and

$$W \sim \exp\left(-\frac{\pi^2 n l^2}{6h^2}\right), \tag{127}$$

so that application of the equilibrium condition in Eq. (125) determines

$$\rho \sim \rho_b \exp\left(n v \rho_b - \frac{\pi^2 n l^2}{6h^2}\right). \tag{128}$$

Thus, the segment density within the gap effectively vanishes when $h < \pi n^{1/2} l / [6(1 + n v \rho_b)]^{1/2}$. For theta conditions, this corresponds to $h < \pi \langle r^2 \rangle^{1/2}/6$ as suggested above. For good solvents with $n v \rho_b > 1$, the interactions in the bulk favor configurational changes near the interface, so chains remain in the gap until $h < \pi l (6 v \rho_b)^{1/2} = \xi$. These predictions pertain to the dilute and concentrated regimes in Fig. 3; the concentration dependence of the depletion layer thickness in the semidilute regime differs in the dependence of ξ on ρ_b (Joanny *et al.*, 1979).

In both theta and good solvents, the exclusion of chains from the gap when $h < 2L$, with L as the depletion layer thickness, allows the interaction potential to be written as

$$\begin{aligned} V(h) &= \frac{l^2}{kT}[A(h) - A(2L)] \\ &= -(2L - h)\frac{\Pi l^2}{kT}, \end{aligned} \tag{129}$$

with Π as the osmotic pressure of the bulk solution so that the force

$$\begin{aligned} F &= -\frac{kT}{l^2}\frac{dV}{dh} \\ &= -\Pi, \end{aligned}$$

conforms to the original results of Asakura and Oosawa (1954, 1958). Combining the mean-field expression for Π with Eq. (129), evaluated at $h = 0$, yields the minimum in the potential energy at contact as

$$V_{\min} = -\frac{\rho_b}{n}\left(1 + \frac{v\rho_b}{2}\right)\frac{\pi l^3}{[6(1/n + v\rho_b)]^{1/2}}. \tag{130}$$

Comparison of these potentials with those for the terminally anchored chains shows the interaction to be relatively weak. For example, experiments with polystyrene in cyclohexane, which does not adsorb on mica, yielded no detectable forces between mica surfaces because of the polymer (Luckham and Klein, 1985). Indeed, estimates of the potential from Eq. (130) at the experimental conditions fall several orders of magnitude below the detection limit for the instrument.

The simple form of the interaction potential,

$$V = -\frac{\Pi V_{\text{excl}}}{kT}, \tag{131}$$

with V_{excl} as the volume of overlap between the two depletion layers, permits straightforward generalization to other geometries (Vrij, 1976). For equal spheres of radius a at center-to-center separation r,

$$\Phi(r) = -\frac{4\pi}{3}(a+L)^3\left(1 - \frac{3r}{4(a+L)} + \frac{r^3}{16(a+L)^3}\right)\Pi \tag{132}$$

decreases monotonically from zero at $r = 2(a + L)$ to a minimum (Fig. 31),

$$\frac{\Phi_{\min}}{kT} = -\frac{4\pi L^3}{3}\left(1 + \frac{3a}{2L}\right)\frac{\Pi}{kT}, \tag{133}$$

at $r = 2a$. In ideal solutions with $a/L \gg 1$

$$\frac{\Phi_{\min}}{kt} \sim \frac{2\pi}{3} a l^2 \rho_b$$

becomes 0(1) for $\rho_b l^3 \sim l/a \ll 1$. Hence, while not measurable between macroscopic surfaces, the interaction is sufficiently strong to affect the phase behavior of colloidal dispersions.

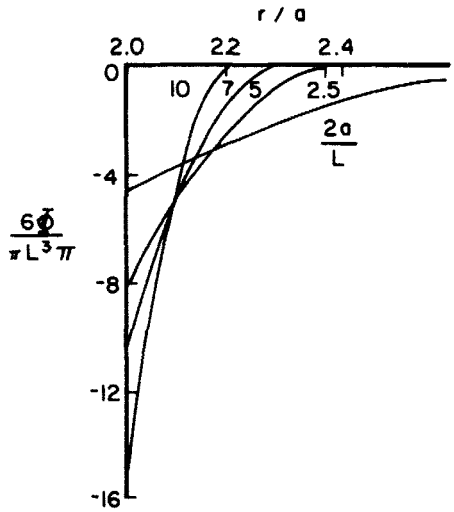

FIG. 31. Interaction potential between spheres of radius a with depletion layers of thickness L from Eq. (132) (Gast *et al.*, 1983b).

B. Effect of Terminally Anchored Chains

The presence of grafted polymer chains with molecular weight n_* alters both the depletion of the free polymer and the thickness of the grafted layer as described by de Gennes (1980) and Gast and Leibler (1986). Within the mean-field approach, the penetration of solution polymer into the grafted layer and the effect on the layer thickness are described by expressing the free-energy densities of the layer and the bulk solution as

$$\frac{A_*}{kT} = \frac{3\sigma}{2L}\frac{L^2}{n_* l^2} + \frac{1}{2}v(\rho_* + \rho)^2 + \frac{\rho}{n}\ln(l^3\rho)$$

and (134)

$$\frac{A}{kT} = \frac{1}{2}v\rho_b^2 + \frac{\rho_b}{n}\ln(l^3\rho_b),$$

with ρ_* and ρ as the segment densities for attached and free chains within the layer. Recall that the segment density and layer thickness for the grafted chains are related by $\rho_* L = n_*\sigma$. Equilibrium requires equal chemical potentials for the solvent and free polymer in the two regions or, equivalently, equal exchange potentials for the free polymer, i.e., $\partial A_*/\partial\rho = \partial A/\partial\rho_b$, and equal osmotic pressures, i.e.,

$$\rho_*\partial A_*/\partial\rho_* + \rho\partial A_*/\partial\rho - A_* = \rho_b\partial A/\partial\rho_b - A.$$

The form of the resulting equations identifies the three distinct regimes depicted in Fig. 32:

$$\begin{aligned}
&\rho_b < \left(\frac{6\sigma^2}{l^2 v}\right)^{1/3}, && \rho \sim \rho_b \exp\left[-\left(\frac{6v^2\sigma^2}{l^2}\right)^{1/3} n\right] \\
& && L \sim \left(\frac{v\sigma}{6l}\right)^{1/3} n_* l\left[1 - l^3\rho_b\left(\frac{v}{6l^3}\right)^{1/3}(l^2\sigma)^{2/3}\right] \\
&\left(\frac{6\sigma^2}{l^2 v}\right)^{1/3} < \rho_b < (3n)^{1/2}\frac{\sigma}{l}, && \rho \sim \rho_b \exp\left[-3n\left(\frac{\sigma}{l\rho_b}\right)^2\right] \\
& && L \sim \frac{n_*\sigma}{\rho_b}\left(1 + \frac{3n^2}{vl^2\rho_b^3}\right)^{-1} \\
&(3n)^{1/2}\frac{\sigma}{l} < \rho_b, && \rho \sim \rho_b\left[1 - (3n)^{1/2}\frac{\sigma}{l\rho_b}\right] \\
& && L \sim \frac{n_* l}{(3n)^{1/2}}.
\end{aligned} \tag{135}$$

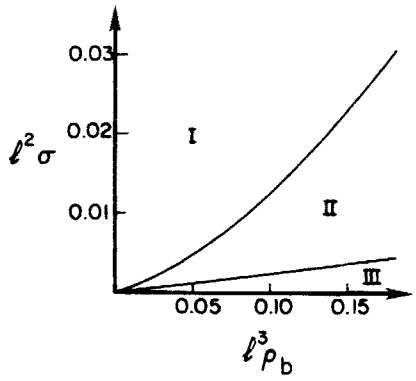

FIG. 32. Delineation of regimes for interaction between free polymer at bulk concentration $l^3\rho_b$ and terminally anchored chains of graft density $l^2\sigma$ for $n = 5000$, $p = 500$, and $v/l^3 = 1$ (Gast and Leibler, 1986): I, Negligible interpenetration and layer thickness unaffected by free polymer; II, slight interpenetration, but layer significantly compressed by free polymer; III, complete interpenetration and relaxed layer.

Thus, at low free-polymer concentrations, the penetration into the layer is exponentially small and the resulting contraction is negligible. However, when the bulk concentration exceeds the initial segment density within the layer, the bulk osmotic pressure causes significant contraction of the layer, though penetration remains small. Ultimately, at high concentrations, the layer relaxes to a thickness that is independent of both ρ_b and σ. The first two regimes are asserted to be the most important except, perhaps, for very low molecular-weight polymer in solution.

Detailed analysis, via the SCF theory, of the free polymer between two flat surfaces bearing grafted layers with constant segment density yielded profiles for ρ varying smoothly from ρ_b in the bulk to the asymptotic values cited above within the grafted layer (Gast and Leibler, 1986). The transition occurs within a region of dimension $l[1/6v\rho_*)^{1/2} + (6v\rho_b)^{1/2}]$ at the interface between the grafted layer and the solution. Thus, the depletion layer penetrates somewhat into the grafted layer, permitting the segment density at the interface to depart from zero. For example, in region II (Fig. 32).

$$n \sim \frac{1}{2}\rho_b\left(\frac{\rho_b}{\rho_*}\right)^{1/2}$$

at large surface-to-surface separations; the factor $(\rho_b/\rho_*)^{1/2}$ represents the ratio of the correlation length within the layer to that in the solution.

This diminution of the depletion layer reduces the attractive potential;

thus,

$$V_{\min} = -\frac{\pi}{2} l^3 \rho_b \left(\frac{v\rho_b}{6}\right)^{1/2} \left\{1 - \left[\frac{\rho_b}{(6\sigma^2/vl^2)^{1/3}}\right]^{1/2}\right\}, \tag{136}$$

in accordance with the earlier, qualitative arguments of de Gennes (1980). The prefactor in Eq. (136) corresponds to the attractive minimum in the absence of the grafted layer, but now $V_{\min} \to 0$ when $\rho_b \to (6\sigma^2/vl^2)^{1/3}$. One interesting feature of this result is that increasing the graft density increases the magnitude of the attraction, contrary to intuition. At separations less than $2L$, the interaction of the grafted layers produces the same strong repulsion described in the previous section.

VI. Macroscopic Consequences

A. Phase Separations

For colloidal systems, the homogeneous dispersed state becomes unstable when the attractive minimum in the interparticle potential exceeds a few kT. For $-5 \leq \Phi_{\min}/kT \leq -2$, dispersions of submicron particles separate on a reasonable time scale, i.e., a few days, into two coexisting equilibrium phases. With stronger attractions, equilibration becomes quite slow, requiring up to six months or a year. The nature and compositions of the phases depend on the range and magnitude of the attractive potential.

Phase separations induced by dissolved nonadsorbing polymer were recognized and exploited in the 1930s to concentrate, or cream, rubber latices (Napper, 1983, Sect. 15.2) and reappeared in the 1970s in the formulation of coatings (e.g., Sperry *et al.*, 1981). Experiments with a variety of dispersions—polymer latices, silica spheres, microemulsions, rodlike DNA—in aqueous solutions of nonionic polymers or polyelectrolytes and both ideal and nonideal solutions in organic solvents have clearly established the coexistence of equilibrium phases, one dense and one dilute in particles, above a critical polymer concentration that correlates with $-\Phi_{\min}/kT = 2 - 3$. Consequently, the critical polymer concentration decreases with increasing molecular weight or particle size in accordance with Eq. (132) (e.g., Cowell *et al.*, 1978; Vincent *et al.*, 1980; Sperry *et al.*, 1981; de Hek and Vrij, 1981).

Subsequently, more detailed studies have revealed two modes of phase behavior depending on the ratio of the sizes of the particle and the polymer (Gast *et al.*, 1983a,b, 1986; Sperry, 1984; Vincent, 1987). For example, electrostatically stabilized polystyrene latices in aqueous solutions of dextran exhibit a simple fluid–solid transition for $a/R_g = 6.9$, but they exhibit a more

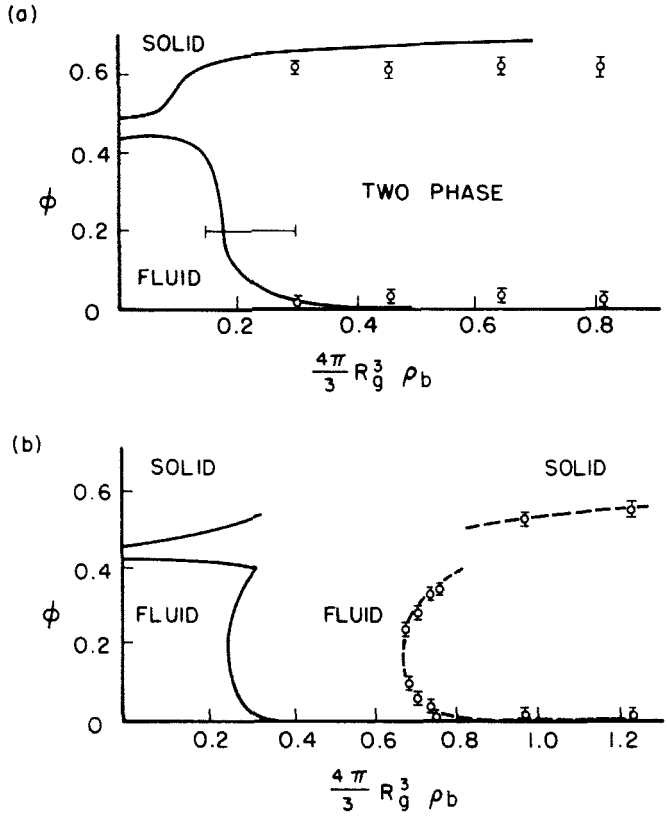

FIG. 33. Equilibrium phase behavior of polystyrene latices of radius a at volume fraction ϕ containing soluble dextran of radius of gyration R_g at fluid concentration ρ_b (Patel and Russel, 1989a). (a) $a/R_g = 6.9$: ⊼, measured compositions; ⊢⊣, bounds on transition; ——, predicted phase boundaries. (b) $a/R_g = 1.9$: ⊼, measured compositions; – – –, experimental phase boundary; ——, predicted phase boundary.

complex phase diagram with a fluid–fluid envelope, critical and triple points, and a fluid–solid region for $a/R_g = 1.9$ (Fig. 33) (Patel and Russel, 1989a). The solid phases display iridescence, characteristic of crystalline order, and the expected mechanical responses, i.e., yield stresses and finite low-frequency elasticity; the fluid phases are opaque and flow as Newtonian liquids in the low shear limit (Patel and Russel, 1989b).

At modest concentrations of free polymer, all dispersions behave generally as described above, independent of the mechanism stabilizing the particles in the absence of polymer, e.g., grafted polymer chains or electrostatic repulsion. However, with increasing polymer concentration, the correlation

length and, hence, the depletion layer thickness decrease, so the range and nature of the repulsion ultimately become important.

For particles stabilized with grafted polymer, generalization of the interaction potential in Eq. (136) to spheres via the Derjaguin approximation provides (Russel *et al.*, 1989)

$$\frac{\Phi_{\min}}{kT} = -\frac{\pi^3}{24} a l^2 \rho_b \left[1 - 0.74 \left(\frac{l v^{1/2} \rho_b^{3/2}}{\sigma} \right)^{1/3} \right]^2. \tag{137}$$

The second term in brackets reflects the penetration of free polymer into the grafted layer with increasing concentration and limits the maximum attraction to

$$\frac{\Phi_{\min}}{kT} = -\frac{\pi^3}{108} \frac{a}{l} \left(\frac{l^7 \sigma^2}{v} \right)^{1/3} \tag{138}$$

at $\rho_b = \frac{9}{4}(\sigma / l v^{1/2})^{2/3}$. Any smaller value can be achieved with either of two concentrations, e.g., for $a/l \gg 1$

$$l^3 \rho_b = -\frac{24}{\pi^3} \frac{l}{a} \frac{\Phi_{\min}}{kT}$$

or (139)

$$l^3 \rho_b = \frac{16}{9} \left(\frac{l^7 \sigma^2}{v} \right)^{1/3} \left[1 - \left(\frac{6l}{\pi^3 a} \right)^{1/2} \left(-\frac{\Phi_{\min}}{kT} \right)^{1/2} \left(\frac{l^7 \sigma^2}{v} \right)^{1/6} \right].$$

Edwards *et al.* (1984) performed experiments with silica spheres bearing a layer of grafted polystyrene chains in a solution of somewhat higher molecular-weight polystyrene in toluene. The stability boundaries depicted in Fig. 34 indicate aggregation, detected optically, over a finite range of polymer concentrations at volume fractions of particles ϕ exceeding a minimum value. Since the equilibrium ratio of doublets to singlets in a dilute dispersion should vary as

$$\phi \exp\left(-\frac{\Phi_{\min}}{kT} \right),$$

the attraction required to produce significant aggregation must increase with decreasing volume fraction. Thus, the potential described above leads to a stability boundary of exactly the form observed with the minimum volume fraction proportional to

$$\exp\left[-\frac{\pi^3}{108} \frac{a}{l} \left(\frac{l^7 \sigma^2}{v} \right)^{1/3} \right]$$

and the two branches of the curve related to the concentrations in Eq. (139).

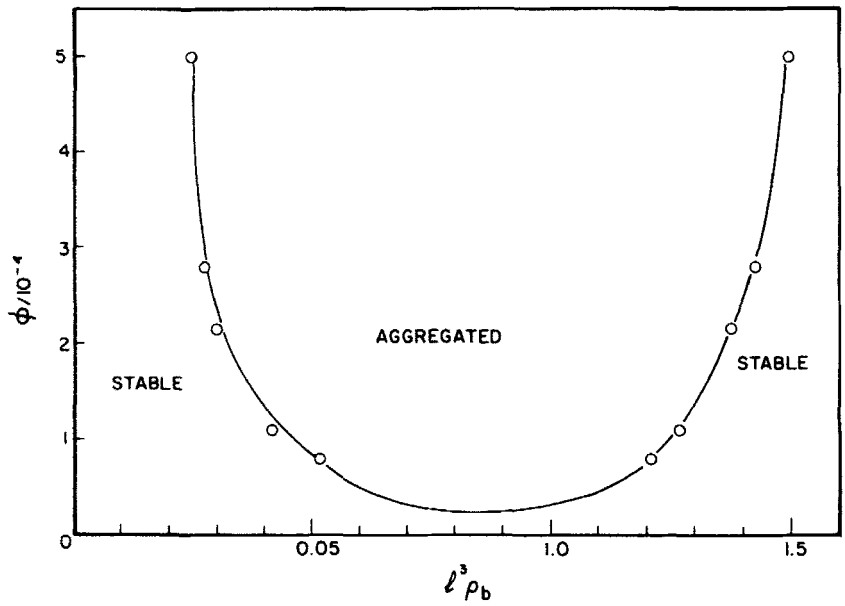

FIG. 34. Stability boundary for silica spheres (a = 115 nm) bearing grafted polystyrene chains (M = 7.5 kg/mol) in solution of polystyrene (M = 31 kg/mol) in toluene (Edwards *et al.*, 1984).

These results demonstrate that nonadsorbing polymer can induce phase separations in colloidal systems with the nature of the phases depending primarily on the ratio of the particle and polymer sizes. Since the strength of the attraction is not necessarily a monotonic function of the polymer concentration, e.g., because of penetration of the free polymer into a grafted layer, both destabilization and restabilization are possible.

B. POLYMERIC STABILIZATION

The interaction potentials described in previous sections for adsorbing homopolymer and terminally anchored layers in good solvents clearly indicate the ability of polymers to stabilize colloidal dispersions against flocculation due to van der Waals dispersion forces. Indeed, the practice preceeded the analyses by centuries in some cases and decades in others, since the use of adsorbing polymers dates to ancient times, and block copolymer stabilizers emerged from industrial laboratories in the 1960s (Napper, 1983).

Polymeric stabilization offers several advantages over the electrostatic

primary alternative:

(1) The absence of electroviscous effects,

(2) Stability in nonaqueous solvents with low dielectric constants and low surface charge densities,

(3) Robust stability over long periods of time and at high volume fractions, and

(4) Reversible flocculation if the solvent quality degrades.

Stability clearly requires a good solvent for the stabilizer and a repulsion of sufficiently long range to mask the dispersion forces, i.e., a minimum layer thickness. In addition, for adsorbing homopolymers, the interaction potentials are entirely repulsive only for strong adsorption at full coverage, Even then, though, the repulsion appears only when the long time-scale for desorption constrains polymer within the gap during interactions between particles. Otherwise, the greater free energy of the macromolecules squeezed between the surfaces drives a slow desorption, thereby reducing the repulsion. Indeed a slow flocculation, or aging, is possible in dispersions sufficiently concentrated to maintain the layers in contact. Hence, homopolymers are not the optimum stabilizers.

With chains anchored to the surface, either by a chemical grafting or an insoluble block, good solvent conditions always produce a repulsion. Consequently, copolymers, e.g., diblock, comb, or graft, tend to comprise the most effective stabilizers. Direct grafting to the particle is feasible but requires chemistry specific to the particle (e.g., Green *et al.*, 1987). Advances in synthetic polymer chemistry continue to increase the types of polymers available for this application (e.g., Reiss *et al.*, 1987).

The two primary features of the phenomena are the layer thickness necessary to provide stability and the conditions at which the dispersions flocculate. The first can be quantified by generalizing the potential for terminally anchored chains to interactions between spheres via the Derjaguin approximation, adding the attractive dispersion potential, and then assessing the layer thickness necessary to maintain $-\Phi_{min}/kT < 1 - 2$. To illustrate this, consider the small overlap limit of Eq. (122), which transforms into

$$\frac{\Phi}{kT} = \frac{\pi a}{l^2}\int_{r-2a}^{2L} V(h)\,dh$$

$$= \left(\frac{9\pi^5}{32}\right)^{1/3} n\sigma a L\left(\frac{v\sigma}{l}\right)^{2/3}\left(1 - \frac{r-2a}{2L}\right)^4 \qquad (140)$$

for equal spheres of radius a. A suitable approximation for the retarded dispersion potential between spheres with relatively thick polymer layers in

nonaqueous liquids is (Russel, *et al.*, 1989, sect. 9.2)

$$\frac{\Phi}{kT} = -\frac{2^{1/2}A_{\text{eff}}}{3\pi kT}\frac{\lambda}{n_0^2(\bar{n}_0^{-2}+n_0^2)^{1/2}}\frac{a}{(r-2a)^2}, \tag{141}$$

with A_{eff} as the nonretarded limit of the effective Hamaker constant, λ as the wavelength characteristic of the ultraviolet relaxation of the liquid, and n_0 and $\bar{n}_0$ as the low frequency limits of the refractive indices at visible wavelengths for the liquid and the particles, respectively.

Modest calculations demonstrate that the minimum occurs at

$$\frac{r-2a}{2L} \sim 1$$

if $\lambda/[L^3 n(v^2\sigma^5/l^2)^{1/3}] \ll 1$, which is invariably true. This leads to a minimum layer thickness of

$$\frac{L_{\text{min}}}{a} \sim \left[\frac{\lambda A_{\text{eff}}}{6\pi 2^{1/2}akTn_0^2(\bar{n}_0^{-2}+n_0^2)^{1/2}}\right]^{1/2} \tag{142}$$

and, along with Eq. (112), determines the requisite molecular weight. Since $A_{\text{eff}}/kT \sim 1-10$, n_0 and $\bar{n}_0 \sim 1.2$, and $\lambda \sim 0.1$ μm, the minimum layer thickness falls in the range $(0.05-0.20)a$.

The condition for incipient flocculation, i.e., the delineation between stable and unstable dispersions, generally corresponds to the theta condition for the stabilizer in solution. A large body of experimental data gathered by Napper and others (e.g., Napper, 1983) first established this correlation, and the theoretical predictions for the interaction potentials agree provided $nl^2\sigma \leq 1$.

At higher surface coverages, the mean-field treatment noted in Section IV indicates that worse than theta conditions are required before an attractive minimum appears in the potential. This phenomena has been observed and termed "enhanced steric stabilization" by Napper (1983). Recent experiments by Edwards *et al.* (1984) clearly show that grafting PDMS chains onto silica particles at $nl^2\sigma \sim 12-18$ extends the stable range substantially beyond theta conditions.

C. Polymeric Flocculation

Water soluble polymers serve widely as flocculants, particularly in the water treatment, paper making, and minerals industries. The objective generally is to destabilize dispersions and cause large, strong, and compact flocs to form quickly. The flocs are often removed subsequently by sedimentation or flotation. Polymers perform efficiently without introducing the salt needed to

suppress the electrostatic forces largely responsible for the stability of the dispersions (Rose and St. John, 1985). Polyelectrolytes, bearing multiple charges along their backbones or on side groups, provide enhanced solubility and promote adsorption onto particles of opposite charge. High molecular weights, $10-10^4$ kg/mol, tend to be preferred.

A combination of electrostatic and kinetic effects complicate the process, with no single mechanism appearing to control all systems of interest. Even interpretations based on the equilibrium interparticle potential present different possibilities (e.g., Vincent, 1974; Rose and St. John, 1985):

(1) *Charge neutralization.* Polyelectrolytes of opposite charge adsorb electrostatically, thereby neutralizing the surface charge and permitting dispersion forces to drive flocculation. Then the conditions for optimum flocculation should correlate with the point of zero charge for the particles.

(2) *Bridging flocculation.* Partial coverage of adsorbing nonionic polymer generally results in a strong attractive minimum in the pair potential, since individual macromolecules span the gap and attach to both particles. This implies optimum conditions for flocculation at surface coverages of about one half monolayer per surface.

Some suggestions concerning the conditions that specific mechanisms control emerge from the analyses of Section III. For example, lower molecular weight polymers adsorb with relatively flat conformations, making bridging across the electrical double layers unlikely; thus, charge neutralization might dominate in that limit. For higher molecular weights at moderate concentrations, the depth and position of the attractive minimum depend on the surface coverage (Fig. 17); hence, significant bridging should occur if the range exceeds twice the double layer thickness before the depth of the minimum becomes negligible, i.e., restabilization occurs. Conversion of the minimum, V_{min}, between flat surfaces to equal spheres via the Derjaguin approximation produces an attraction of roughly $aR_g V_{min}/l^2$. At the conditions of Fig. 25, $-aR_g V_{min}/l^2 \sim 1.5 - 14$ (with $a/l \sim 10^2$) for polymer concentrations of $l^3\rho_b < 10^{-3}$.

Experiments by Pelssers (1988) probe these issues for PEO adsorbed onto polystyrene at different surface coverages. At low molecular weights, the adsorption equilibrated under stable conditions before the ionic strength was raised to $10^{-2}M$ to initiate flocculation. The growth of small flocs was then detected with a novel scattering instrument. A distinct onset of flocculation appeared at a critical polymer dose (Fig. 35), presumably corresponding to the surface coverage at which the range of the attraction due to bridging exceeded twice the double layer thickness. Restabilization was not observed because of the limited surface coverage achievable with such low molecular weights.

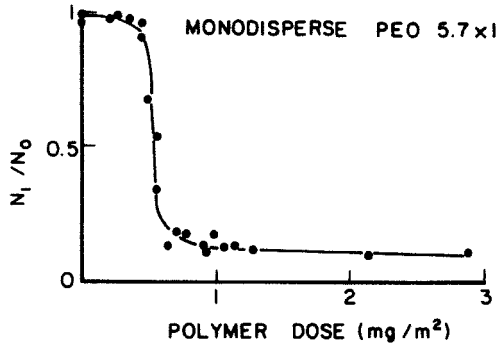

FIG. 35. Effect of the amount of PEO added on the fraction of individual polystyrene latex particles remaining (N_1/N_0) after 1.5 hours (Pelssers, 1988): M = 57 kg/mol, $2a$ = 0.7 μm, $\phi = 4 \times 10^{-4}$, $[KNO_3] = 10^{-2}$ M.

Kinetic measurements established binary collisions between unstable particles and flocs as the controlling process.

For higher molecular weights, however, the phenomena differs qualitatively in the dependence on time, initial number density of particles, and polymer dosage. Then the rate of polymer reconformation during the adsorption relative to the rate of particle collisions becomes a key consideration (Gregory, 1987). The data in Fig. 36 (Pelssers, 1988) reveal a transition from encounters of particles bearing equilibrium-adsorbed layers, at low particle number densities and long time-scales for collisions, to bridging by adsorbed polymer with dimensions comparable to the coil in solution at higher number densities

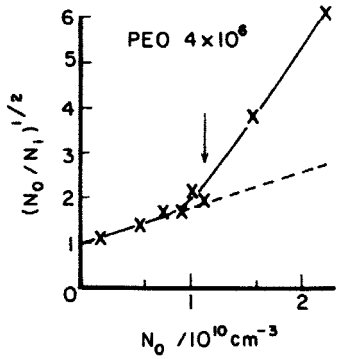

FIG. 36. Effect of the initial number density of polystyrene latices ($2a$ = 0.7 μm) on the fraction of singlets remaining 1.5 hours after the addition of PEO at 0.34 mg/m^2. The dashed line characterizes the doublet formation with relaxed chains and b indicates the transition to flocculation before reconformation (Pelssers, 1988).

and, hence, shorter collision times. Since the reconformation continues during the flocculation process, the rate decreases monotonically with time, in some cases arresting the process with flocs of finite size. Clearly the efficacy of higher molecular-weight polymers must arise at least in part from such kinetic effects.

For polyelectrolytes, analyses of equilibrium adsorption are only beginning to emerge. Muthukumar's (1987) treatment of a single polyelectrolyte chain interacting with a charged surface predicts adsorption with a mean square end-to-end distance of $O(\kappa^{-1})$ when

$$-\frac{lqq_s}{\varepsilon kT} > (l\kappa)^{11/5} n^{1/5}$$

with q, the charge per segment on the polymer; q_s the surface charge density; $\kappa^{-1} = (\varepsilon kT/e^2 I)^{1/2}$ (where I is ionic strength and e is electronic charge) the Debye length; and ε, the dielectric constant for the electrolyte solution. Hence, adsorption occurs only below a critical ionic strength. The consequences with respect to the mechanisms just cited and the interaction potentials between two surfaces remain to be explored.

Thus, the situation is currently clouded by an incomplete understanding of both the kinetic processes and the equilibrium behavior of polyelectrolytes. For specific systems, consistent correlations have been constructed, but a general understanding of the functioning of polymeric flocculants requires more extensive fundamental experiments and development of the equilibrium theory for polyelectrolytes.

D. Rheology

Several recent studies demonstrate convincingly the possibilities for adjusting the rheology of colloidal dispersions through the incorporation of polymer. Here we briefly review the effects of grafted polymer, adsorbing homopolymer, and nonadsorbing polymer. The literature abounds with other and more complicated phenomena.

A grafted layer of polymer of thickness L increases the effective size of a colloidal particle. In general, dispersions of these particles in good solvents behave as non-Newtonian fluids with low and high shear limiting relative viscosities (η_0 and η_∞), and a dimensionless critical stress ($a^3\sigma_c/kT$) that depends on the effective volume fraction $\phi_{\text{eff}} = (1 + L/a)^3\phi$. The viscosities diverge at volume fractions ϕ_{m0} and $\phi_{m\infty}$, respectively, with $\phi_{m0} < \phi_{m\infty}$; for $\phi_{m0} < \phi_{\text{eff}} < \phi_{m\infty}$, the dispersions yield and flow as pseudoplastic solids.

The data of Mewis *et al.* (1989) for poly(methyl methacrylate) spheres stabilized by poly(12-hydroxy stearic acid) and dispersed in decalin conform

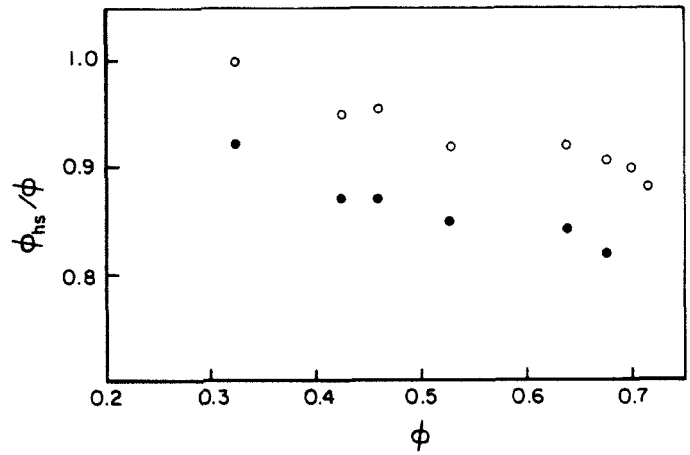

FIG. 37. The ratio of the equivalent hard sphere volume fraction φ_{hs} to the effective volume fraction ϕ based on the measured intrinsic viscosity as a function of ϕ for poly(methyl methacrylate) spheres with grafted poly(12-hydroxy stearic acid) layers such that $a/L = 4.7$ (Mewis *et al.*, 1989). Open and closed circles correspond to the low and high shear limits of suspension viscosity.

to results for hard spheres for $\phi_{eff} \leq 0.4$, although the critical stress is somewhat smaller. For $\phi_{eff} \geq 0.4$, however, the softness of the repulsion becomes evident. At rest, packing constraints cause some interpenetration of the layers and at high shear rates viscous forces drive the particles even closer together. Consequently, the ratio of the equivalent hard-sphere volume fraction, obtained by comparing the measured viscosities with those for hard spheres, to ϕ_{eff} decreases with increasing ϕ_{eff} and Pe (Fig. 37).

The grafted layer also affects two other features of the rheology. First, thicker polymer layers enhance the elasticity due to the longer range of the repulsion relative to the hard core size. Thus, samples formulated at $\phi_{eff} \geq \phi_{m0}$ possess easily measurable static elastic moduli. Second, the softer repulsion apparently suppresses the shear thickening observed at high volume fractions for the harder particles, in accordance with earlier measurements by Willey and Macosko (1978).

The situation with adsorbing homopolymer differs significantly because of ability of the polymer to either stabilize or bridge colloidal particles, depending on the characteristics of the polymer and particles in the quiescent state. In addition, shear can either induce bridging or breakup flocs formed by bridging. Experiments by Otsubo and co-workers (Otsubo and Umeya, 1983, 1984; Otsubo, 1986; Otsubo and Watanabe, 1987, 1988) with silica spheres in solutions of poly(acrylamide) in glycerin–water mixtures illustrate the effects of particle size and volume fraction, polymer molecular weight and concen-

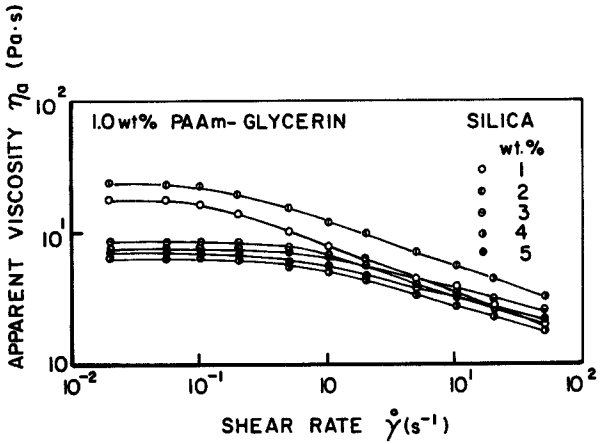

FIG. 38. Apparent viscosity of various dispersions of silica spheres ($2a = 20$ nm) in solutions of 1 wt% polyacrylamide ($M_w = 2 \times 10^3$ kg/mol) in glycerin (Otsubo and Umeya, 1984).

tration, solvent quality, and shear rate. Figs. 38 and 39 reflect the most striking features of the behavior.

In glycerin, the dispersion appears to be stable and behaves as a shear thinning fluid. However, the viscosity does not vary monotonically with silica concentration, instead decreasing initially before increasing at higher concentrations (Fig. 38). The phenomena reflect offsetting effects of adsorption, the reduction in the solution viscosity due to depletion of polymer

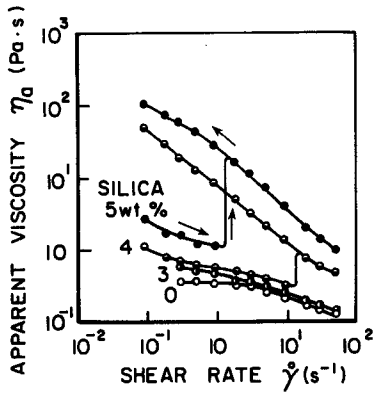

FIG. 39. Apparent viscosity of dispersions of silica ($2a = 2$ nm) in 0.5 wt% solutions of polyacrylamide ($M_w = 5.5 \times 10^3$ kg/mol) in 50/50 glycerin–water mixtures (Otsubo and Watanabe, 1987). Different symbols correspond to different weight percentages of silica.

and the increased hydrodynamic volume of the particles. The particles adsorb ~ 1.5 mg/m^2 of polymer on a surface area of 0.13 m^2/mg, so ~ 5 wt% silica substantially depletes the solution. At higher silica concentrations, interactions among the coated particles increase the viscosity, suggesting a layer thickness of ~ 10 nm, and lead to a dilatancy at higher shear rates. Thus, the coated particles behave as stable spheres at all shear rates.

Better solvents, e.g., glycerin–water mixtures, enhance the possibility of bridging, perhaps by reducing the surface coverage. The rheological behavior then becomes quite sensitive to those parameters controlling the surface coverage: The molecular weight and concentration of the polymer, the size and concentration of the particles, and the solvent quality (Fig. 39). At high surface coverages, i.e., large particles, low silica concentrations, or high polymer molecular weights, the systems flow as relatively low viscosity, stable dispersions. But at rather low coverages, arising for smaller particles, higher silica concentrations, or lower molecular weights, bridging produces very viscous, pseudoplastic materials. At intermediate coverages, an irreversible shear-induced transition occurs, transforming a low viscosity dispersion into a paste at a critical stress. While these interpretations are speculative, the dramatic effects warrant further study, perhaps with better characterized polymer and particles and more extensive measurements of the adsorption and the adsorbed layer thickness.

With nonadsorbing polymer, rheological effects of similar magnitude accompany the phase transitions described earlier (Patel and Russel, 1989a,b). Since macroscopic phase separation takes weeks or months, rheological measurements performed within a few days on samples formulated within the two-phase region, with $-\Phi_{min}/kT \sim 2 - 20$, detect a metastable structure that changes little over time. The systems respond as flocculated dispersions, but the microstructure recovers relatively quickly to a reproducible rest state after shear. Hence these weakly flocculated dispersions are quite tractable materials.

The steady shear viscosities in Fig. 40 demonstrate the primary features of the phenomena:

(1) A transition from fluid to solid in the mechanical response accompanying the frustrated fluid–solid phase transition,

(2) A yield stress that increases smoothly but dramatically with increasing polymer concentration, and

(3) A pronounced shear thinning of the fluid phase near or within the fluid–fluid region.

Linear viscoelastic measurements detect a low frequency plateau in the shear modulus whenever the yield stress appears. The magnitudes of both correlate

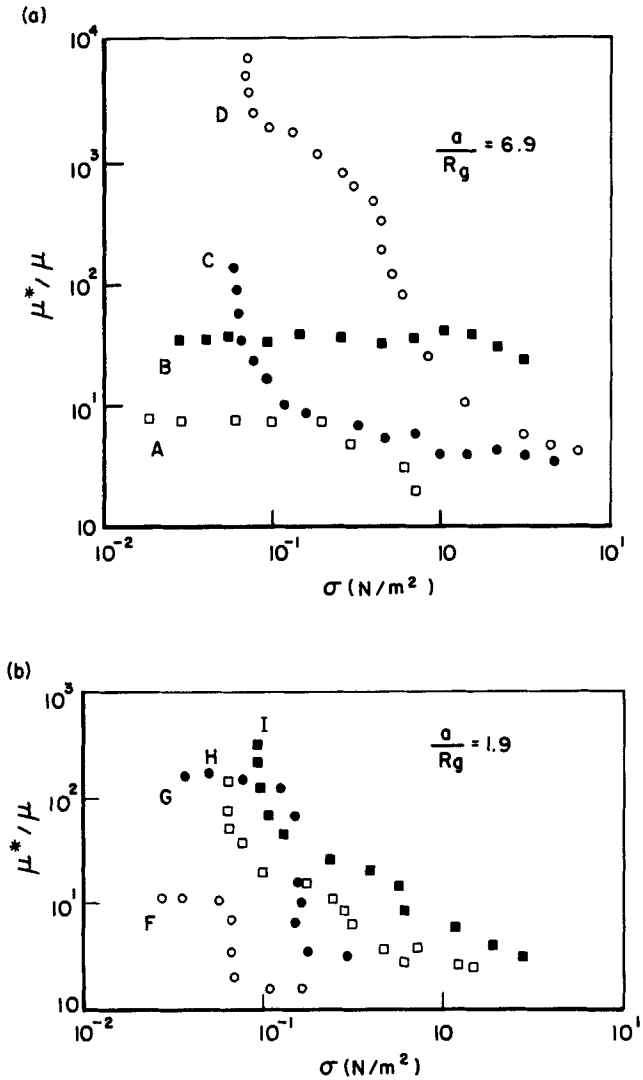

FIG. 40. Steady shear viscosities of aqueous dispersions of polystyrene latices in non-adsorbing dextran solutions (Patel and Russel, 1989b): (a) $a/r_g = 6.9$, $\phi = 0.20$. A, single phase, $4\pi R_g^3/3\rho_b = 0.15$; B, two-phase, $4\pi R_g^3/3\rho_b = 0.30$; C, two-phase, $4\pi R_g^3/3\rho_b = 0.45$; D, two-phase, $4\pi R_g^3/3\rho_b = 0.65$. (b) $a/R_g = 1.9$, $\phi = 0.10$. F, single phase, $4\pi R_g^3/\rho_b = 0.65$; G, fluid–fluid, $4\pi R_g^3/3\rho_b = 0.75$; H, fluid–solid, $4\pi R_g^3/3\rho_b = 0.95$; I, fluid–solid, $4\pi R_g^3/3\rho_b = 1.25$.

with characteristics of the interaction potential discussed in Section V, providing a convenient way of adjusting the rheology.

These examples serve to illustrate the ability of soluble polymer, interacting in a controlled fashion with colloidal particles, to transform both the equilibrium state and the mechanical properties of dispersions. All states are possible, from low viscosity fluids to pseudoplastic pastes with high yield stresses.

References

Alexander, S., *J. Phys. (Orsay, Fr.)* (1977).

Almog, Y., and Klein, J., *J. Colloid Interface Sci.* **106,** 33 (1985).

Anderson, J., and Kim, J. O., *J. Chem. Phys.* **86,** 5163 (1987).

Ansarifar, M. A., and Luckham, P. F., *Polymer* **29,** 329 (1988).

Asakura, S., and Oosawa, F., *J. Chem. Phys.* **22,** 1255 (1954).

Asakura, S., and Oosawa, F., *J. Polym. Sci.* **33.** 183 (1958).

Aussere, D., Hervet, H., and Rondalez, F., *Macromolecules* **19,** 85 (1986).

Auvray, L., and Cotton, J. P., *Macromolecules* **20,** 202 (1987).

Auvray, L., and de Gennes, P. G., *Europhys. Lett.* **2,** 647 (1986).

Baram, A., and Luban, M., *J. Phys. C* **12,** L659 (1979).

Bawendi, M. G., Freed, K. F., and Mohanty, U., *J. Chem. Phys.* **84,** 7036 (1986).

Baxter, R. J., *J. Chem. Phys.* **49,** 2770 (1969).

Billmeyer, F. W., "Textbook of Polymer Science." Wiley, New York, 1982.

Bovey, F. A., "Chain Structure and Conformation of Macromolecules." Academic Press. New York, 1982.

Brandrup, J., and Immergut, E. H., eds. *in* "Polymer Handbook," 2nd Ed. Wiley, New York, 1975.

Brebner, K. I., Chahal, R. S., and St-Pierre, L. E., *Polymer* **21,** 533 (1980a).

Brebner, K. I., Brown, G. R., Chahal, R. S., and St-Pierre, L. E., *Polymer* **22,** 56 (1980b).

Cahn, J., *J. Chem. Phys.* **66,** 3667 (1977).

Cahn, J., and Hilliard, J. E., *J. Chem. Phys.* **28,** 258 (1958).

Carnahan, N. F., and Starling K. E., *J, Chem. Phys.* **51,** 625 (1969).

Cebula, D., Thomas, R. K., Harris, N. M., Tabony, J., and White, J. W., *Faraday Discuss Chem. Soc.* **65,** 76 (1978).

Chandrasekhar, S., *Rev. Mod. Phys.* **15,** 1 (1943).

Charmet, J. C., and de Gennes, P. G., *J. Opt. Soc. Am.* **73,** 1773 (1983).

Cohen Stuart, M. A., Ph. D. Thesis, Agric. Univ., Wageningen, Netherlands, 1980.

Cohen Stuart, M. A., Fleer, G. J., and Scheutjens, J. M. H. M., *J. Colloid Interface Sci.* **97,** 515 (1984a).

Cohen Stuart, M. A., Fleer, G. J., and Scheutjens, J. M. H. M., *J. Colloid Interface Sci.* **97,** 526 (1984b).

Cohen Stuart, M. A., Waajen, F. H. F. H., Cosgrove, T., Vincent, B., and Crowley, T. L., *Macromolecules* **17,** 1825 (1984c).

Cohen Stuart, M. A., Cosgrove, T., and Vincent, B., *Adv. Colloid Interface Sci.* **24,** 143 (1986).

Cosgrove, T., Vincent, B., Crowley, T. L., and Cohen Stuart, M. A., *ACS Symp. Ser.* No. 240, 147 (1984).

Cosgrove, T., Heath, T. G., Ryan, K., and Crowley, T. L., *Macromolecules* **20,** 2879 (1987a).

Cosgrove, T., Heath, T. G., Ryan, K., and van Lent, B., *Polym. Commun.* **28,** 64 (1987b).

Cotton, J. P., Nierlich, M., Boue, F., Daoud, M., Farnoux, B., Jannink, G., Duplessix, G., and Picot, C., *J. Chem. Phys.* **65,** 1101 (1976).
Cowell, C., Li-In-On, R., and Vincent, B., *J. C. S. Faraday I* **74,** 337 (1978).
Croxton, C. A., *J. Phys. A* **12,** 2497 (1978).
Daoud, M., and Jannink, G., *J. Physc. (Orsay, Fr.)* **37,** 973 (1976).
Daoud, M., Cotton, J. P., Farnoux, B., Jannink, G., Sarma, G., Benoit. H., Duplessix, G., Picot, C., and de Gennes, P. G., *Macromolecules* **8,** 804 (1975).
de Gennes, P. G., *Rep. Prog. Phys.* **32,** 187 (1969).
de Gennes, P. G., *Phys. Lett. A* **38,** 339 (1972).
de Gennes, P. G., *J. Phys. (Orsay, Fr.)* **36,** L55 (1975).
de Gennes, P. G., "Scaling Concepts in Polymer Physics." Cornell Univ. Press, Ithaca, New York, 1979.
de Gennes, P. G., *Macromolecules* **13,** 1069 (1980).
de Gennes, P. G., *Macromolecules* **14,** 1637 (1981).
de Gennes, P. G., *Macromolecules* **15,** 492 (1982).
de Gennes, P. G., *Adv. Colloid Interface Sci.* **27,** 189 (1987).
de Gennes, P. G., and Pincus, P., *J. Phys., Lett. (Orsay, Fr.)* **44,** L241 (1983).
de Hek, H., and Vrij. A., *J. Colloid Interface Sci.* **84,** 409 (1981).
Des Cloizeaux, J., *J. Phys. (Orsay, Fr.)* **36,** 281 (1975).
Des Cloizeaux, J., *J. Phys., Lett. (Orsay, Fr.)* **41,** L151 (1980a).
Des Cloizeaux, J., *J. Phys. (Orsay, Fr.)* **41,** 749 (1980b).
Des Cloizeaux, J., *J. Phys. (Orsay, Fr.)* 761 (1980c).
Des Cloizeaux, J., *J. Phys. (Orsay, Fr.)* **42,** 635 (1981).
Dickman, R., and Hall, C. K., *J. Chem. Phys.* **85,** 4108 (1986).
DiMarzio, E. A., *J. Chem. Phys.* **42,** 2101 (1965).
DiMarzio, E. A., and McCrackin, F. L., *J. Chem. Phys.* **43,** 539 (1965).
DiMarzio, E. A., and Rubin, R. J., *J. Chem. Phys.* **55,** 4318 (1971).
Dolan, A. K., and Edwards, S. F., *Proc. R. Soc. London, Ser.* **A337,** 509 (1974).
Dolan, A. K., and Edwards, S. F., *Proc. R. Soc. London, Ser.* **A343,** 427 (1975).
Domb, C., *J. Chem. Phys.* **38,** 2957 (1963).
Domb, C., *Adv. Chem. Phys.* **15,** 229 (1969).
Douglas, J. F., Wang, S. Q., and Freed, K. F., *Macromolecules* **19,** 2207 (1986).
Douglas, J. F., Wang, S. Q., and Freed, K. F., *Macromolecules* **20,** 543 (1987).
Drude, P., *Ann. Phys.* **272,** 532 (1889a).
Drude, P., *Ann. Phys.* **272,** 865 (1889b).
Drude, P., *Ann. Phys.* **275,** 481 (1890).
Edwards, J., Lenon, S., Toussaint, A. F., and Vincent, B., *ACS Symp. Ser.* No. 240, 281 (1984).
Edwards, S. F., *Proc. Phys. Soc.* **85,** 613 (1965).
Edwards, S. F., *Proc. Phys. Soc.* **88,** 265 (1966).
Edwards, S. F., *J. Phys. A* **8,** 1670 (1975).
Edwards, S. F., and Jeffers, E. J., *J. C. S. Faraday II* **75,** 1020 (1979).
Edwards, S. F., and Singh, P., *J. C. S. Faraday II* **75,** 1001 (1979).
Eirich, F. R., *J. Colloid Interface Sci.* **58,** 423 (1977).
Eisenriegler, E., *J. Chem. Phys.* **79,** 1052 (1983).
Eisenriegler, E., *J. Chem. Phys.* **81,** 4666 (1984).
Eisenriegler, E., *J. Chem. Phys.* **82,** 1032 (1985).
Eisenriegler, E., Kremer, K., and Binder, K., *J. Chem. Phys.* **77,** 6296 (1982).
Evans, E., *Macromolecules*, **22,** 2277 (1989).
Fleer, G. J., *in* "Reagents in Mineral Technology" (P. Somasundaran and B. M. Moudgil, eds.). Dekker, New York, 1988.

Fleer, G. J., and Lyklema, J., *in* "Adsorption from Solution at the Solid/Liquid Interface" (G. D. Parfitt and C. H. Rochester, eds.). Academic Press, New York, 1983.
Fleer, G. J., and Scheutjens, J. M. H. M., *J. Colloid Interface Sci.* **16,** 341 (1982a).
Fleer, G. J., and Scheutjens, J. M. H. M., *J. Colloid Interface Sci.* **16,** 361 (1982b).
Fleer, G. J., and Scheutjens, J. M. H. M., *J. Colloid Interface Sci.* **111,** 504 (1986).
Fleer, G. J., Cohen Stuart, M. A., and Scheutjens, J. M. H. M., *Colloids Surf.* **31,** 1 (1988).
Flory, P. J., *J. Chem. Phys.* **10,** 51 (1942).
Flory, P. J., "Principles of Polymer Chemistry." Cornell Univ. Press, Ithaca, New York, 1953.
Flory, P. J., "Statistical Mechanics of Chain Molecules." Wiley (Interscience), New York, 1969.
Flory, P. J., *Discuss Faraday Soc.* **49,** 7 (1970).
Forsman, W. C., ed., "Polymers in Solution." Plenum, New York, 1986.
Freed, K. F., *Adv. Chem. Phys.* **22,** 1 (1972).
Freed, K. F., *J. Phys. A* **18,** 871 (1985).
Freed, K. F., "Renormalization Group Theory of Macromolecules." Wiley (Interscience), New York, 1987.
Frisch, H. L., *J. Phys. Chem.* **59,** 633 (1955).
Frisch, H. L., and Simha, R., *J. Phys. Chem.* **58,** 507 (1954).
Frisch, H. L., and Simha, R., *J. Chem. Phys.* **24,** 652 (1956).
Frisch, H. L., and Simha, R., *J. Chem. Phys.* **27,** 702 (1957).
Frisch, H. L., Simha, R., and Eirich, F. R., *J. Chem. Phys.* **21,** 365 (1953).
Gast, A. P., *Proc. NATO ASI* Ser., Ser. E, Strasbourg, France, 1990.
Gast, A. P., and Leibler, L., *Macromolecules* **19,** 686 (1986).
Gast, A. P., Hall, C. K., and Russel, W. B., *J. Colloid Interface Sci.* **96,** 251 (1983a).
Gast, A. P., Hall, C. K., and Russel, W. B., *Faraday Discuss* **76,** 189 (1983b).
Gast, A. P., Russel, W. B., and Hall, C. K., *J. Colloid Interface Sci.* **109,** 161 (1986).
Gerber, P. R., and Moore, M. A., *Macromolecules* **10,** 476 (1977).
Green, M., Kramer, T., Parish, M., Fox, J., Lalanandham, R., Rhine, W., Barclay, S., Calvert, P., and Bowen, H. K., *Adv. Ceram.* **21,** 449 (1987).
Gregory, J., *Colloids Surf.* **31,** 231 (1987).
Hadziioannou, G., Patel, S., Granick, S., and Tirrell, M., *J. Am. Chem. Soc.* **108,** 2869 (1986).
Halperin, A., *J. Phys. (Orsay, Fr.)* **49,** 547 (1988).
Helfand, E., *J. Chem. Phys.* **63,** 2192 (1975a).
Helfand, E., *Macromolecules* **8,** 307 (1975b).
Helfand, E., *J. Chem. Phys.* **62,** 999 (1975c).
Helfand, E., *Macromolecules* **9,** 307 (1976).
Helfand, E., and Sapse, A. M., *J. Chem. Phys.* **62,** 1327 (1975).
Helfand, E., and Sapse, A. M., *J. Polym. Sci., Polym. Symp.* **54,** 289 (1976).
Helfand, E., and Wasserman, Z., *Macromolecules* **9,** 879 (1976).
Hesselink, F. T., *J. Phys. Chem.* **73,** 3488 (1969).
Hesselink, F. T., *J. Phys. Chem.* **75,** 65 (1971).
Hoeve, C. A. J., *J. Chem. Phys.* **43,** 3007 (1965).
Hoeve, C. A. J., *J. Chem. Phys.* **44,** 1505 (1966).
Hoeve, C. A. J., DiMarzio, E. A., and Peyser, P., *J. Chem. Phys.* **42,** 2558 (1965).
Hong, K. M., and Noolandi, J., *Macromolecules* **14,** 727 (1981).
Huggins, M. L., *Ann. N.Y. Acad. Sci.* **41,** 1 (1942).
Ishinabe, T., *J. Chem. Phys.* **76,** 5589 (1982).
Israelachvili, J. N., Tandon, R. K., and White, L. R., *J. Colloid Interface Sci.* **78,** 430 (1980).
Israelachvili, J. N., Tirrell, M., Klein, J., and Almog, Y., *Macromolecules* **17,** 204 (1984).
Jenckel, E., and Rumbach, B., *Z. Elektrochem.* **55,** 612 (1951).
Joanny, J. J., Leibler, L., and de Gennes, P. G., *J. Polym. Sci., Polym. Phys. Ed.* **17,** 1073 (1979).
Jones, I. S., and Richmond, P. J., *J. C. S. Faraday II* **73,** 1062 (1977).

Kato, T., Nakamura, K., Kawaguchi, M., and Takahashi, A., *Polym. J.* **13,** 1037 (1981).
Kawaguchi, M., Hayakawa, K., and Takahashi, A., *Polym. J.* **12,** 265 (1980).
Kawaguchi, M., Hayakawa, K., and Takahashi, A., *Macromolecules* **16,** 631 (1983).
Killmann, E., and Bergmann, M., *Colloid Polym. Sci.* **263,** 381 (1985).
Killmann, E., Eisenlauer, J., and Korn, M., *J. Polym. Sci., Polym. Symp.* **61,** 413 (1977).
Klein, J., *Adv. Colloid Interface Sci.* **16,** 101 (1982).
Klein, J., *J. C. S. Faraday I* **79,** 99 (1983).
Klein, J., and Luckham, P. F., *Nature (London)* **308,** 836 (1984a).
Klein, J., and Luckham, P. F., *Macromolecules* **17,** 1041 (1984b).
Kosmas, M., and Freed, K. F., *J. Chem. Phys.* **69,** 3647 (1978).
Kurata, M., "Thermodynamics of Polymer Solutions." Harwood, New York, 1982.
Levine, S., Thomlinson, M. M., and Robinson, R., *Faraday Discuss Chem. Soc.* **65,** 202 (1978).
Lifshitz, I. M., Grosberg, A. Y., and Khokhlov, A. R., *Rev. Mod. Phys.* **50,** 683 (1978).
Luckham, P. F., and Klein, J., *Macromolecules* **18,** 721 (1985).
Ma, S., "Modern Theory of Critical Phenomena." Benjamin, Reading, Massachusetts, 1976.
McCrackin, F. L., and Colson, J. P., *NBS Misc. Publ. (U.S.)* No. 256, 61 (1964).
McQuarrie, D. A., "Statistical Mechanics." Harper, New York, 1976.
Marques, C., Joanny, J. F., and Leibler, L., *Macromolecules* **21,** 1051 (1988).
Mewis, J., Frith, W., Strivens, T. A., and Russel, W. B., *AIChE J.* **35,** 415 (1989).
Milner, S. T., Witten, T. A., and Cates, M. E., *Europhys. Lett.* **5,** 413 (1988).
Milner, S. T., *Europhys. Lett.* **7,** 695 (1988).
Moore, M. A., *J. Phys. A* **10,** 305 (1977a).
Moore, M. A., *J. Phys. (Orsay, Fr.)* **38,** 265 (1977b).
Moore, M. A., and Al-Noaimi, G. F., *J. Phys. (Orsay, Fr.)* **39,** 1015 (1978).
Munch, M. R., and Gast, A. P., *Macromolecules* **21,** 1360, 1366 (1988).
Muthukumar, M., *J. Chem. Phys.* **86,** 7230 (1987).
Muthukumar, M., and Edwards, S. F., *J. Chem. Phys.* **76,** 2720 (1982).
Napper, D. H., "Polymeric Stabilization, of Colloidal, Dispersions." Academic Press, New York, 1983.
Nemirovsky, A. M., and Freed, K. F., *J. Chem. Phys.* **83,** 4166 (1985).
Noda, I., Kato, N., Kitano, T., and Nagasawa, M., *Macromolecules* **14,** 668 (1981).
Ohta, T., and Oono, Y., *Phys. Lett. A* **89,** 460 (1982).
Okamoto, H., *J. Chem. Phys.* **64,** 2686 (1975).
Oono, Y., and Freed, K. F., *J. Chem. Phys.* **75,** 993 (1981).
Oono, Y., Ohta, T., and Freed, K. F., *J. Chem. Phys.* **74,** 6458 (1981).
Otsubo, Y., *J. Colloid Interface Sci.* **112,** 380 (1986).
Otsubo, Y., and Umeya, K., *J. Colloid Interface Sci.* **95,** 279 (1983).
Otsubo, Y., and Umeya, K., *J. Rheol.* **28,** 95 (1984).
Otsubo, Y., and Watanabe, K., *J. Non-Newtonian Fluid Mech.* **24,** 265 (1987).
Otsubo, Y., and Watanabe, K., *J. Colloid Interface Sci.* **122,** 346 (1988).
Patel, P. D., and Russel, W. B., *J. Colloid Interface Sci.* **131,** 192 (1989a).
Patel, P. D., and Russel, W. B., *J. Colloid Interface Sci.* **131,** 201 (1989b).
Patel, S., Tirrell, M., and Hadziioannou, G., *Colloids Surf.* **31,** 157 (1988).
Pelssers, E., Ph.D. Thesis, Agric. Univ., Wageningen, Netherlands, 1988.
Ploehn, H. J., Ph.D. Thesis, Princeton Univ., Princeton, New Jersey, 1988.
Ploehn, H. J., and Russel, W. B., *Macromolecules* **22,** 266 (1989).
Ploehn, H. J., Russel, W. B., and Hall, C. K., *Macromolecules* **21,** 1075 (1988).
Prigogine, I., "The Molecular Theory of Solutions." North-Holland Publ., Amsterdam, 1957.
Reiss, G., Bahadur, P., and Hurtvez, G., *Encycl. Polym. Sci. Eng.* **2,** 324 (1987).
Roe, R. J., *J. Chem. Phys.* **43,** 1591 (1965).
Roe, R. J., *J. Chem. Phys.* **44,** 4264 (1966).

Roe, R. J., *J. Chem. Phys.* **60,** 4192 (1974).
Rose, G. R., and St. John, M. R., *Encycl. Polym. Sci. Eng.* **7,** 211 (1985).
Rubin, R. J., *J. Chem. Phys.* **43,** 2392 (1965).
Russel, W. B., "The Dynamics of Colloidal, Systems." Univ. of Wisconsin Press, Madison, 1987.
Russel, W. B., Saville, D. A., and Schowalter, W. R., "Colloidal Dispersions." Cambridge Univ. Press, London, 1989.
Sanchez, I. C., and Lacombe, R. H., *Macromolecules* **11,** 1145 (1978).
Schaefer, D. W., *Polymer* **25,** 387 (1984).
Scheutjens, J. M. H. M., and Fleer, G. J., *J. Phys. Chem.* **83,** 1619 (1979).
Scheutjens, J. M. H. M., and Fleer, G. J., *J. Phys. Chem.* **84,** 178 (1980).
Scheutjens, J. M. H. M., and Fleer, G. J., *Macromolecules* **18,** 1882 (1985).
Scheutjens, J. M. H. M., Fleer, G. J., and Cohen Stuart, M. A., *Colloids Surf.* **21,** 285 (1986).
Silberberg, A., *J. Phys. Chem.* **66,** 1872 (1962a).
Silberberg, A., *J. Phys. Chem.* **66,** 1884 (1962b).
Silberberg, A., *J. Chem. Phys.* **46,** 1105 (1967).
Silberberg, A., *J. Chem. Phys.* **48,** 2835 (1968).
Silbergberg, A., *Pure Appl. Chem.* **26,** 583 (1971).
Simha, R., Frisch, H. L., and Eirich, F. R., *J. Phys. Chem.* **57,** 584 (1953).
Sperry, P. R., *J. Colloid Interface Sci.* **99,** 97 (1984).
Sperry, P. R., Hopfenberg, H. B., and Thomas, N. L., *J. Colloid Interface Sci.* **82,** 62 (1981).
Sperry, P. R., Thibeault, J. C., and Kostanek, E. C., *Adv. Coatings Sci. Technol.* **9,** 1 (1987).
Stanley, H. E., "Introduction to Phase Transitions and Critical Phenomena." Oxford Univ. Press (Clarendon), London and New York, 1971.
Stromberg, R. R., *In* "Treatise on Adhesion and Adhesives" (R. Patrick, ed.), Vol. 1, Chap. 3. Dekker, New York, 1967.
Stromberg, R. R., Passaglia, E., and Tutas, D. J., *J. Res. Natl. Bur. Stand., Sect. A* **67A,** 431 (1963).
Tabor, D., and Winterton, R. H. S., *Proc. R. Soc. London, Ser. A* **312,** 435 (1969).
Tadros, T. F., *In* "The Effect of Polymers on Dispersion Properties" (T. F. Tadros, ed.), pp. 1–38. Academic Press, London, 1982.
Tadros, T. F., *In* "Polymer Colloids" (R. Buscall, T. Corner, and J. F. Stageman, eds.), pp. 105–139. Elsevier, London, 1985.
Takahashi, A., and Kawaguchi, M., *Adv. Polym. Sci.* **46,** 1 (1982).
Takahashi, A., Kawaguchi, M., Hirota, H., and Kato, T., *Macromolecules* **13,** 884 (1980).
Taunton, H. J., Toprakcioglu, C., Fetters, L. J., and Klein, J., *Nature (London)* **332,** 712 (1988).
Tirrell, M., Patel, S., and Hadziioannou, G., *Proc. Natl. Acad. Sci. U.S.A.* **84,** 4725 (1987).
van der Beek, G. P., and Cohen Stuart, M. A., *J. Phys. (Orsay, Fr.)* **49,** 1449 (1988).
vander Linden, C., and van Leemput, R., *J. Interface Sci.* **67,** 48 (1978).
van Kampen, N. G., "Stochastic Processes in Physics and Chemistry." North-Holland Publ., Amsterdam, 1981.
Vincent, B., *Adv. Colloid Iinterface Sci.* **4,** 193 (1974).
Vincent, B., *Chem. Eng. Sci.* **42,** 779 (1987).
Vincent, B., Luckham, P. F., and Waite, F. A., *J. Colloid Interface Sci.* **73,** 508 (1980).
Vrij, A., *Pure Appl. Chem.* **48,** 471 (1976).
Weber, T. A., and Helfand, E., *Macromolecules* **9,** 311 (1976).
Weiss, G. H., and Rubin, R. J., *Adv. Chem. Phys.* **52,** 363 (1983).
Widow, B., *Physica A (Amsterdam)* **95A,** 1 (1979).
Willey, S. J., and Macosko, C. W., *J. Rheol.* **22,** 525 (1978).
Wiltzius, P., Haller, H. R., Cannell, D. S., and Schaefer, D. W., *Phys. Rev. Lett.* **51,** 1183 (1983).
Witten, T. A., and Pincus, P. A., *Macromolecules* **19,** 2509 (1986).
Yamakawa, H., "Modern Theory of Polymer Solutions." Harper, New York, 1971.
Ziman, J. M., "Models of Disorder." Cambridge Univ. Press, London, 1979.